NON LINEAR VISCOELASTICITY AND EXTENSIONAL VISCOSITY OF LINEAR MALEATED POLYPROPYLENE-CLAY NANOCOMPOSITES

By

Tanmay Janardan Pathak

A DISSERTATION

Submitted to
Michigan State University
in partial fulfillment of the requirements
for the degree of

Chemical Engineering - Doctor of Philosophy

2014

ABSTRACT

NON LINEAR VISCOELASTICITY AND EXTENSIONAL VISCOSITY OF LINEAR MALEATED POLYPROPYLENE-CLAY NANCOMPOSITES

By

Tanmay Janardan Pathak

Strain hardening of polymer melts in elongational flow is important for a variety of polymer processing operations such as thermoforming, foaming and blow molding. As such the measurement of transient extensional viscosity becomes important to understand the elongational behavior of the polymeric materials. It is well known that linear polypropylene; a widely used commodity polymer; does not strain harden in melt extensional flow and there arises a need to structurally modify this polymer so as to achieve strain hardening.

In the present work, the effect of dispersing two different organoclays in linear maleated polypropylene on the transient uniaxial extensional viscosity and shear viscoelasticity (linear and nonlinear) has been investigated. The matrix polymer was a linear random copolymer of propylene and ethylene grafted with maleic anhydride (PP-g-MA). Two different grades of nanoclay organically modified with different ionic surfactants were used as fillers. The extensional rheology was carried out at different strain rates, on an Extensional Viscosity Fixture (EVF) mounted on a TA-ARES rheometer. The neat PP-g-MA matrix did not show any strain hardening at different extensional strain rates whereas the nanocomposites with different organoclays showed different extents of strain hardening. Strain hardening was quantified by calculating the ratio of transient extensional viscosity to the viscosity obtained from linear viscoelastic envelope, called as the strain hardening parameter (χ) which was around 3 at lower strain rates for one of the nanocomposite with 5wt% clay loading. Linear and non-linear shear

rheology of these nanocomposites was also investigated to understand the reinforcement effects upon filler additions in the polymer matrix and to get an insight on the nanocomposite structure. From the combined observations in linear and nonlinear shear rheology along with nonlinear extensional rheology we were able to conclude that the polymer matrix chains physically coupled (mainly by hydrogen bonding) to the nanoclays and these particle attached polymer chains formed hindered chain entanglements with the free matrix chains. The formation of such entangled structure led to improvements in the reinforcement levels as well as strain hardening behavior in uniaxial extensional flow. The second part of this study is focused on understanding the effects of filler loadings on the strain hardening and non-linear viscoelasticity of these nanocomposites. This study showed that there lies an optimum level of nanoclay loading (2 vol%) with an effective aspect ratio and specific surface area that are necessary to form hindered chain entanglements necessary for strain hardening. For composites with higher nanoclay loadings, the strain hardening diminishes with decreasing effective aspect ratios.

Dedicated to my parents:

Dr. Janardan M. Pathak
&
Mrs. Bindu J. Pathak

ACKNOWLEDGMENTS

I take this opportunity to sincerely thank Dr K. Jayaraman who is not only my doctoral guide but also has been a mentor throughout my Ph.D. work and stay at MSU. He has provided continuous support through these years and has always been available to clarify my queries. I have been able to build a strong understanding of the fundamental concepts in the research work with his help. I have been very fortunate in having a guide and a mentor like Dr. Jay. I also take this opportunity to thank my committee members Dr. Baker, Dr. Lee, Dr. Drzal and Dr. Hawley for serving on my committee and providing valuable guidance.

I thank my parents and take pride in this moment to acknowledge their continuous and immense support and encouragement throughout my Ph.D. I have always sought inspiration and patience in my doctoral research from my father Dr. Janardan Pathak and would like to thank my mother Mrs. Bindu Pathak for her courage, sacrifice, and unconditional love. Without their support, this task would not have been possible. I also thank my whole family without whose support this would have been a daunting task.

I would like to express my deepest gratitude to my fellow colleagues, who helped me learn the research techniques and skills in my Ph.D. I would especially like to thank Sharad, Giri, John, Amit, Katie, Rahul, Susan, Madhu, Hemant, Devesh and Shreya. Finally yet significantly, I would also like to acknowledge my closest buddies Nikunj, Malini, Madhuri, Akshay, Hemant, Ritesh, Keyur, Dhruvi, Devang Arpi, Ashutosh, Priya, and a special thanks to Saurabh and Anamika for being my extended family at MSU.

TABLE OF CONTENTS

LIST OF TABLES

LIST OF FIGURES

INTRODUCTION

CHAPTER 1

1.1 BACKGROUND

Recently, the polymer layered silicate nanocomposites have been widely developed for various applications in automotive industries, for food packaging films, etc. In the packaging industry polymer composites have gained importance because of their improved barrier properties as well as flame retardancy [1-6]. In the automotive industry polymer nanocomposites are preferred widely to make automotive bumpers, car interiors such as dash board panels, hard and soft instrument panels, trims etc. because of their low density, light weight and mold ability as compared to traditional micro composite systems and metal parts. For such applications the nanocomposites are processed through various processes such as extrusion foaming, thermoforming, blow molding, etc. where high melt strength of the polymer nanocomposite system is preferred. The study of the extensional flow behavior of these polymer nanocomposite melts is therefore very important for such processes.

Thermoplastic polymer-layered silicate nanocomposites first came into light in the mid 1990's after the initial research work done by Toyota researchers on nylon/clay nanocomposites [7,8]. Since then there has been considerable research interest in making these nanocomposites more viable for the processing industry. The addition of small amount of high aspect ratio (of the order of ~200) nanoclay platelets to polymer matrix, through melt mixing, leads to significant improvements in the polymer/clay nanocomposite properties such as stiffness, tensile strength, barrier properties as well as melt strength [9-12]. Polypropylene (PP) which is a commodity

polymer has been widely investigated to make its nanocomposites with clay. PP being non polar needs to be functionalized with maleic anhydride to form maleated PP so as to wet the clay surface more readily and mix properly for making the nanocomposites . Okada and co-workers were the first to make nanocomposites out of PP, maleated PP and clay [13-15]. They dissolved the functionalized polyolefin oligomer with clay in toluene such that the polymer intercalates in the clay galleries. The toluene was then evaporated and the intercalated mix was melt blended with the bulk PP. The functionalized polymers that facilitate the interactions between the clay particles and the bulk PP matrix are generally called as compatibilizers. Literature also reports the mixing of all three, the compatibilizer, the clay as well as the bulk polymer by directly melt mixing them [15, 16]. The presence of a compatibilizer with a polar functional group facilitates the delamination of the clay platelets and eases the dispersion of the non polar polymer chains in the clay galleries has been shown for a wide range of polymers [17-22]. Hence in the present study maleated polypropylene is used as the entire polymer matrix to which montmorillonite clay is added. The primary objective in using the maleated PP alone was to understand the kind of interactions between the polymer and clay particles and to avoid the complexity of adding a third phase which would have been non functionalized bulk polypropylene. It has been established in literature that functionalization of polypropylene with maleic anhydride leads to its chain scissions [23] which reduces the molecular weight. A maleated polypropylene {Exxelor PO 1015} was therefore chosen in this study which has a fairly decent amount of maleic anyhride functionality (0.4 wt%) and a molecular weight (M_w) of around 180,000 and to this a montmorillonite clay was added.

Montmorillonite is a widely used layered silicate for enhancing the properties of polymer composites. The clay in its natural form has layered platelets which form stacks. The clay

platelet has a thickness of around 1nm and a length dimension of around 100-300 nm thereby giving a high aspect ratios particle and also an interlayer spacing of around 1nm. They provide a surface area of around 700 m^2/g [24, 25]. The layered sheets in montmorillonite clay have an excess negative charge which is neutralized by highly charged inorganic cations such as Na^+ and Ca^{2+} present in a hydrated form in the interlayers of untreated clay [1, 26]. The hydration spheres of these inorganic cations form unfavorable organophobic conditions for adsorption of organic polymer molecules between the interlayer. Also, the removal of water of hydration of these cations leads to collapsing of the interlayer spacing thereby preventing the entrance of the organic polymer chains between the interlayer spacing and exfoliation of clay in polymer matrix. The clay surface is therefore treated so as to make the clay interlayer region organophilic and make the adsorption of organic polymer molecules between the clay platelets easier [11, 27-31]. The polymer chains can then enter the clay galleries between two subsequent clay layers and separate them causing exfoliation of clay in the polymer. The cation exchange capacity of clay is very important in determining the effectiveness with which it can be treated with organophilic surfactants and also the level of exfoliation that can be achieved when mixed with a polymer. There has been a lot of work done and reported in literature on achieving exfoliation of fillers in polymer matrices by either using different minerals, varying the cation exchange capacity, surfactant chemistry as well as reacting the polymer precursor first with the clay and then polymerizing [27-37].

It is well reported in literature so as to make the clay interlayer region organophilic, it is first intercalated with surfactants which have long chain alkyl ammonium ions, wherein the ion is tethered to the clay surface and the alkyl tails swell the clay improving its dispersion in the

polymer. This surface treatment of clay is done by exchanging the hydrated cations with quaternary organo-ammonium salts or with primary amines having hydrocarbon groups attached to them, thereby creating organophilic condition in the clay interlayer region. Heinz and co-workers [38] have investigated the structure and dynamics of alkyl-ammonium modified clays having different cation exchange capacity, different head groups (quaternary : NMe_3^+ -R and primary: NH_3^+ -R), as well as different alkyl chain lengths (C_4 to C_{22}). They have also studied the effect of these variables on the cleavage energy required to delaminate the clay platelets to achieve exfoliation [39].

In the present study, organoclays with two different surfactant chemistries are used for making the PP – clay nanocomposites. One grade of montmorillonite clay has a primary amine ion surfactant with a single alkyl (C_{18}) tail and another one has a quaternary ammonium ion surfactant with two alkyl (C_{18}) tails in the clay interlayer galleries. Heinz et al. [38] have commented on the structure and conformation of these surfactants in the interlayer galleries. According to them, both the surfactant head groups are attached to the clay face ionically, however the primary amine ion surfactant head can have three additional hydrogen bonds (N-H---O-Si). As such this surfactant with a C-18 tail is hydrogen bonded more tightly to the clay surface and tends to orient itself perpendicular to the clay surface. The quaternary ammonium ion surfactant with two C-18 tails has larger head group size, flexibly bonded and is more mobile in the interlayer galleries; it also packs to a greater extent in the interlayer galleries.

These organoclays were melt mixed at different loadings with linear maleated polypropylene and different nanocomposites were made, in the current study. These

nanocomposites were tested for nonlinear, uniaxial extensional melt viscosity transients to check if the addition of the organically modified nanoclay imparted any melt strength to the non strain hardening linear polypropylene matrix. Also, the effect of increasing the test temperature and clay loadings on the melt strength of these nanocomposites has been investigated. To further probe into the non-linear extensional behavior of the nanocomposites, linear as well as non-linear shear rheology was used as an investigative tool.

As mentioned earlier, polymeric materials, blends and composites are used in a wide range of daily applications and products and this demand is ever increasing. For the manufacturing of these daily commodities, the polymers need to be processed through different processes such as thermoforming, blow molding, foaming, etc. The polymeric materials while undergoing through these processes experience mainly extensional and shear flow. Also these processes require the material to be processed at higher temperatures and show good melt strength so that the final product shows good properties. For this reason, it becomes imperative to study the transient extensional behavior and melt strength of the polymers, polymer blends and polymer composites. There is an abundance of literature on the extensional flow behavior of different polymeric blends, crystalline polymers, amorphous polymers, food items, polymer composites etc [40-67]. As early as 1977, Agrawal et.al [40] worked with several different polymer melts and measured their shear and extensional flow. Wagner [41] measured the uniaxial, biaxial and ellipsoidal extensions on a polyisobutylene melt and compared the data to predictions from Doi-Edwards Model. He found out that the model needed more modifications to accurately predict the transient extensional data. Wilson and Baird [43] worked with thermotropic liquid crystalline polymer melts and measured their transient extensional viscosity. They found out that the extensional data followed linear viscoelastic behavior at low strains and

showed mild strain hardening with increasing strains. Elongational flow behavior has also been investigated for daily use items such as viscoelastic liquid foods [45], ceramics [51], and polymeric blends such as LLDPE/LDPE [47, 55] as well polymeric composites [48,54,61,67,68].

It however is necessary to understand the relevance between the transient elongation measurements and the actual industrial processes in which the materials experience such elongational flows. Micic and Bhattacharya [47, 55] have shown in their work on LLDPE/LDPE blends, the relevance between the shear and elongational measurements and film blowing process. Foaming is another process where in the transient extensional measurements can give insight on how the material will foam. Bhattacharya and co-workers [67] as well as Jayaraman.K and Chaudhury.A [68] have shown that polypropylene nanocomposites that show better strain hardening also foam well. These foams in general show closed foam cells as well as a higher cell density and lower bulk density. Foaming studies and their relation to strain hardening behavior in polypropylenes has also been shown by Spitael and Macosko [69] as well as Munstedt et.al [70]. Previously, measurements of transient uniaxial extensional viscosity [69-72] and of melt strength [73, 74] of pure polymer melts and their blends have been done to understand their strain hardening behavior. In the current research study, we focus on the "strain hardening" behavior of linear polypropylene and polypropylene nanocomposites that is observed in uniaxial extensional flow. In particular, a rise in polymer melt viscosity (above the linear viscoelastic limit) with increasing Hencky strain is called as "strain hardening" and it is desirable to a certain extent for processing operations. Linear polypropylene, however, does not display any strain hardening and therefore it becomes necessary to modify the molecular structure or incorporate components in the linear polypropylene so as to achieve strain hardening in melt extensional flow.

Sugimoto and coworkers have shown that linear polypropylene on its own does not display any strain hardening. However they were able to show strain hardening in polypropylene which was modified either by introducing branched molecular structure through irradiation or by adding di-2-ethylhexyl peroxy dicarbonate (EHPC) treated polymer [75]. By irradiation or by adding the EHPC polymer they were able to obtain high melt strength PP with long chain branches which showed improved strain hardening behavior. Similar observations of good strain hardening by long chain branches have been reported elsewhere [77, 78]. In another research study Sugimoto and co-workers were able to achieve good strain hardening in linear PP by adding a small amount of uhmw–PE to linear PP [76]. In that study, they used a Meissner type rheometer to measure the uniaxial and biaxial extension of the modified PP blend and found out that this modified PP having long chain PE showed enhanced strain hardening beyond a critical strain. Similar extensional flow studies on blends of polymers have been done by Yamaguchi et.al [79-81]. They modified linear polypropylene by adding a small amount of a crosslinked terpolymer {gEHDM} characterized as gel just beyond the sol-gel transition point and the blend showed improved strain hardening behavior. They suggested that with appropriate cross link density the stretching of trapped chains between the crosslinking points were responsible for the strain hardening and an increase in the crosslinking density leads to suppression of the strain hardening behavior. Strain hardening of crosslinked polymers such as poly methyl (methacryalate) has also been reported in literature by Takahashi.M and Ogura [82] and for sparsely crosslinked PDMS by Takahasi.H and Watanabe [83]. They both have reported that with appropriate cross link density, good amount of strain hardening can be achieved in polymeric systems and that excessive cross link density can hinder the strain hardening property.

A similar analogy has been drawn in the current work involving nanocomposites having physical crosslinks between polymer chains and organically modified nanoclay particles.

The extensional flow of composites with micron and nano sized fillers has also been investigated and reported in literature. Micro composites with different sizes, shapes and aspect ratios were made and tested for extensional flow by Takahashi et al. [84] and Le Meins et al [85]. Takahashi used microscale fillers such as mica, talc, glass beads and glass flakes in a low density polyethylene matrix, whereas Le Meins et al. suspended monodisperse polystyrene spheres in polyisobutylene liquid. They found that the strain hardening goes down with filler addition and even more so with high aspect ratio particles such as fibers. They also observed that the formation of aggregates led to a decrease in strain hardening behavior. Similar observations of decreasing strain hardening have also been reported by Bhattacharya and coworkers [66, 86]. In one of his studies he has mixed talc with polypropylene and found out that the melt strength and drawability of these composites goes down with filler loadings. In his other work, he mixed nanoclay to ethylene vinyl acetate copolymer (EVA) and found that the strain hardening of the nanocomposites matches with that of the unfilled EVA beyond a certain strain. The drop in the strain hardening for filled EVA systems beyond a certain strain was attributed to the restructuring of the clay platelets in a way that slows down the strain hardening. There have been couple reports, however, with nylon 6 [87] and maleated polypropylene [88] composites wherein the strain hardening improved slightly upon addition of nano size filler particles having high aspect ratio. Seong and coworkers [87] dispersed Closite nanoclay in Polyamide 6 matrix and observed that with well dispersed systems there was an improvement in the storage modulus, viscosity as well as the strain hardening behavior in extension. Okamoto et al. [88, 89] dispersed treated montmorillonite clay in maleated polypropylene and investigated the strain hardening as

well rheopexy features of the nanocomposites. They observed an improvement in the strain hardening behavior of these nanocomposites and attributed it to the perpendicular alignment of the clay platelets to flow direction, forming a "house of cards" structure. They made similar observations in polylactide-layered silicate nanocomposites [90].

There have been several attempts and many theories that are used in literature to explain the possible causes of strain hardening behavior in different systems such as polymer melts, polymer blends and polymer composites. Sugimoto et al. [76] and Wagner et al. [91] have observed that larger relaxation times lead to greater extents of strain hardening. Larger relaxation times would be associated with stronger entanglements. In general the presence of entanglement structure within the polymer causes a slow relaxation of the polymer chains upon deformation and longer the relaxation time scale greater is the lift off in extensional viscosity which is nothing but strain hardening in melt extension. Several authors have made attempts to predict the extensional behavior and strain hardening based on shear viscoelastic data. Measurement of shear viscoelastic data both in linear and non-linear shear rheology is very important to understand the flow behavior and the molecular structure of the polymeric system. Especially in polymeric composite systems, non-linear shear rheology along with shear viscoelastic data can give useful insight of the reinforcements brought about by fillers.

It is well know that addition of filler particles in a polymer leads to greater modulus values and more elastic behavior in shear thereby showing greater reinforcement. It is reported in literature that at higher filler loadings, improvement in the reinforcement levels is a result of filler network formation and filler agglomeration [92-94]. Also in non-linear shear, with increasing strain the network formation breaks down causing a drop in the measured modulus values which is called as the "Payne effect". However the mechanisms behind these

reinforcements and nonlinearity with increasing strain, at lower filler loadings, are still an area of considerable research. Sternstein and co-workers have tried to understand these mechanisms by which the nano-scale fillers promote both reinforcement and nonlinear viscoelastic behavior in polymer melts [95, 96]. They have worked with fumed silica fillers, at various loadings, having different surface treatments and poly (vinyl acetate) matrix with different molecular weights and explored the nonlinear vsicoelasticity of these nanocomposites. They have proposed that the reinforcement and nonlinear viscoelastic behavior of the nano filled polymers is a result of "trapped entanglements" which occur because of interactions between the filler and the polymer chains at the filler-polymer interface. Also, when large strain amplitudes are applied, these trapped entanglements are lost because of the debonding of polymers chains from the filler surface which results in overall relaxation of the matrix entanglement structure. This loss of entanglement structure causes non linearity in the viscoelastic behavior of the nanocomposites [95].

Cassagnau and Melis [97] have worked with fumed silica composites with different polymer systems such as PP, PS and EVA and carried subsequent strain sweep tests and time sweep tests to understand the non-linear viscoelastic behavior of these composites and modulus recovery kinetics. Contrary to Sternstein's work, they proposed that the non-linear behavior of the filled polymer composites can be associated with both mechanisms of chain disentanglements and breakdown of filler network depending on filler concentration and amplitude deformation. With the actual mechanisms, that cause improved reinforcements, non-linearity in shear and improved strain hardening behavior, still being obscure or unclear for polymeric composites, it becomes necessary to explore the correlation if any between these three measurements for the polypropylene-layered silicate nanocomposites made in this study.

1.2 RESEARCH OBJECTIVES

The present study revolves around several objectives that need to be achieved in order to obtain better melt strength and strain hardening in linear polypropylene system and understand the possible mechanism behind it. One of the primary objectives, therefore, is to achieve the strain hardening by incorporating inorganic filler in the linear polypropylene system and testing these nanocomposites for nonlinear, uniaxial extensional melt viscosity transients. This research is also motivated by the need for a better understanding of the interactions between the polymer matrix and the nano-filler which is montmorillonite clay with different surfactant treatment in the interlayer galleries. Also for this purpose maleated polypropylene alone was used as the entire matrix because in bulk polypropylene composites, the maleated PP acts as a functionalized compatibilizer and serves to provide favorable interactions at the clay faces. In addition to measuring transient extensional behavior, linear and non-linear shear viscoelasticity is also investigated for these nanocomposites to better understand the reinforcement mechanisms and get an insight of the possible polymer – filler structure. While investigating the structure – property relationships for the nanocomposites, there are several factors that are varied to understand their effects on the morphology as well as the melt extensional and shear rheology.

The different research objectives thus aimed to be explored though this study includes:

1) Preparation and characterization of polypropylene-layered silicate nanocomposites with different organoclays. These nanocomposites will be tested for their strain hardening property in melt extension as well viscoelasticity.

2) Investigation of the effects of varying surfactant treatment in clay interlayer galleries and aspect ratios on the nanoclay dispersion, thermal stability, linear and non-linear shear rheology

and uniaxial elongational flow of nanocomposites. This is mainly done in the first part of the research wherein two different organically modified nanoclays are incorporated in the linear maleated polypropylene matrix. The final motive behind this study is to understand the possible mechanisms and molecular interactions that would help improve the measured reinforcement and strain hardening properties as compared to the neat polymer matrix.

3) Investigation of the effects of increasing the clay loading on the level of reinforcement and strain hardening in these nanocomposites. This is an important part of the second phase of this research. It aims at understanding the effects of varying the filler volume fractions dispersed in the matrix. A similar set of experiments as done in the first part are done for the nanocomposites with different nanoclay loadings. Once again this study focuses on combining the observations made in shear and elongational flows to get an idea about the possible structural arrangements of the layered silicates and polymer chains and the interactions between them.

4) Investigation of the effects of increasing the test temperature on the level of strain hardening in these nanocomposites. This is also a part of the second phase of the research work where in the strain hardening parameters will be calculated for the nanocomposite and compared at different extensional test temperatures.

EXPERIMETAL TECHNIQUES FOR PREPARATION AND CHARACTERIZATION OF NANOCOMPOSITES

CHAPTER 2

2.1 MATERIALS

The matrix material used in the present study was a functionalized polypropylene having maleic anhydride as the functional group and was obtained from ExxonMobil under the trade name of Exxelor PO 1015. The amount of maleic anhydride grafted on to the linear polypropylene was about 0.4 wt%. This maleated polypropylene (PP-g-MA) had a molecular weight of about 70,000. Maleated polypropylene is generally used as a compatibilizer in making bulk polypropylene clay nanocomposites so as to effect the exfoliation of clay. The choice of using a maleated polypropylene as the whole matrix was specifically made to understand the polymer filler interactions while observing the melt strength properties of these nanocomposites.

Two different clays were used in preparing the nanocomposites: A) Nanomer I.30P which had a primary ammonium ion surfactant with a single alkyl tail in the galleries and; B) Nanomer I.44P which had quaternary ammonium ion surfactant with two C-18 tails. These clays were obtained from Nanocor.

2.2 COMPOUNDING OF NANOCOMPOSITES

The nanocomposites for this study are all compounded using a batch melt mixing technique. This technique was used to provide enough shear and residence time for good mixing, to have lesser contamination and also to minimize the degradation of maleated polypropylene. A

mixing bowl with 75cc volume and two Banbury impellers from CW Brabender Instruments, Inc was used for this purpose. Previous studies involving preparation of polymer nanocomposites have used small scale batch mixers like the Banbury [22, 98-100] and Gelimat [101] with shear rates around $200s^{-1}$ and mixing time between 5 to 10mins. The mixing bowl was purged with nitrogen during mixing so as to minimize polymer degradation. Park [102] and coworkers have also used nitrogen purge during mixing of polypropylene nanocomposites.

The first step before melt mixing maleated polypropylene pellets and clay powder was to dry them overnight in a vacuum oven at 80°C and 20 mm Hg vacuum. This was done to ensure that moisture does not degrade the polymer nanocomposites while mixing. The dried materials were then shaken vigorously in a bag for about 2 minutes to have a homogenized powder-pellet mixture. This mixture was then melt blended in a pre-heated at a temperature of 165°C at 150 rpm for 10 minutes. The mixing speed was determined by the maximum speed on the mixers drive such that maximum possible shear is imparted into the material and 10 minutes of mixing time is sufficient to ensure the complete melting and mixing of polymer pellets with the nanoclay powder. The mixing speed and time on Banbury mixer for compounding polypropylene clay nanocomposites have been optimized through previous work in our lab. The mixing temperature of 165°C was chosen to be well above the melting point of the maleated polypropylene as has been observed through DSC scans, run on the pellets. Figure 2.1 shows representative DSC scans run on the nanocomposites which show that the melting transition for the materials is around 145°C. A high mixing temperature also provides enough polymer melt viscosity necessary to generate shear stresses that are sufficient to separate the clay platelets and obtain complete mixing. One batch of the mixer amounted to 47 grams of the compound. The compounded material was then removed from the mixing bowl and impeller screws with the help of a brass

scraper to form small clumps. These clumps were then directly used to make samples through compression molding, for rheological analysis as well as X-ray diffraction measurements.

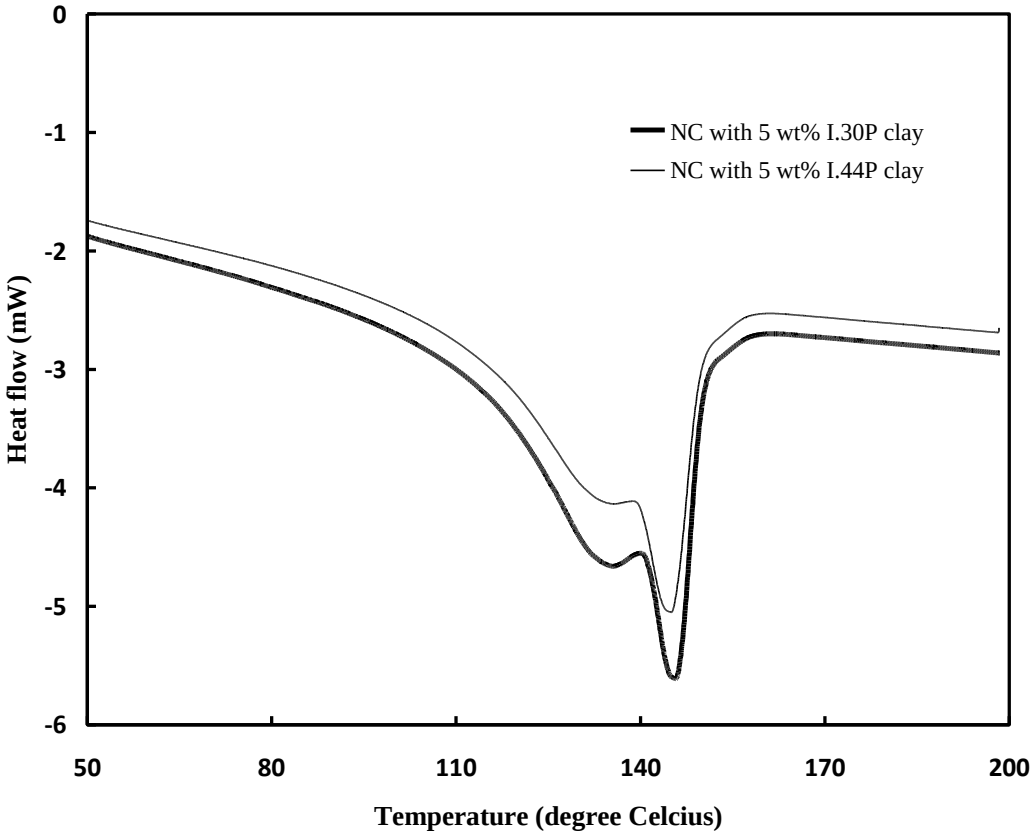

Figure 2.1. Representative DSC scans for melting transitions of maleated polypropylene nanocomposites: (▬) Nanocomposite with 5 wt% of I.30P clay, (—) Nanocomposite with 5 wt% of I.44P clay.

2.3 COMPRESSION MOLDING

2.3.1 Shear Rheology and XRD samples

The compression molding of shear rheology and XRD samples was done in Wabash Compression Molder at a temperature of 175°C, which is well above the melting transition of the

nanocomposites. A mold with 4 square cavities was used for the compression molding procedure. Small clumps of compounded nanocomposite material were directly placed in these cavities, the weight of which was calculated on the basis of volume of one mold cavity times the density of the material taken as 0.9 g/cc. The thickness of the cavity was about 1 mm. The mold filled with the material was covered on both sides with polyimide release films and this was then put in between 2 thick steel plates. This whole mold assembly was then placed in between the pre heated compression molder platens and the clumps of nanocomposites were allowed to melt completely such that there was no gap left between the mold and the steel plates. After this the platens were closed and initially a low pressure of about 2 tons was applied for 5minutes. This was followed by the next step wherein the tonnage pressure was increased to 10 tons and kept there for another 5 minutes. At the end of this, valves of cooling water to the platens were opened so as to cool down the whole assembly to room temperature at the 10 ton pressure. Once the room temperature was reached the pressure was released and the mold assembly was taken out of the compression molder. Samples obtained from the 4 cavities were then used for XRD and shear rheology characterization. For shear rheology, 40 mm diameter disks were cut out from the square samples and used for characterization.

2.3.2 Elongational Rheology samples

The procedure used for compression molding samples for elongational rheology is different from that used for shear rheology samples. A 20-specimen mold was used for compression molding samples that were 18mm long, 10mm wide and 0.7mm thick for the elongational theology tests. Once again required weight of the nanocomposite was calculated on the basis of volume of a single cavity times total number of the cavities times the density of the material (0.9 g/cc). The mold was covered with polyimide release films and then placed between

two thick steel plates. This mold assembly was then transferred between the compression molder platens preheated to 175°C. Initially, the clumps of nanocomposite were allowed to melt down completely into the mold. The tonnage pressure used for compression molding elongational rheology samples was different than that for shear rheology samples. The first step required closing the platens such that a 0 ton pressure was applied to the mold assembly for 5 minutes. After this the tonnage pressure was increased to 5 tons for additional 5 minutes. The platens were then cooled to room temperature using cooling water and the samples were gently removed from the mold.

2.4 X RAY DIFFRACTION

All the nanoclays were investigated for their interlayer spacing using X-ray diffraction (XRD) patters. XRD was also used to investigate the extent of intercalation or exfoliation of clay in the nanocomposites depending on the shoulder observed in their XRD pattern. X ray diffraction is a method of determining the arrangement of atoms in crystals by diffracting an X-ray beam through the crystal. The atoms that are spaced in a regular order within a crystal act as scattering sites for the X-ray beam which has a wavelength equal to the inter atomic distance in a crystal. In 1912, W.H. Bragg and W.L. Bragg expressed the necessary conditions for diffraction as the mathematical form given in Equation 2.1.

$$n\lambda = 2d\sin\theta \quad \text{..... (2.1)}$$

Equation 2.1 is the expression for the Bragg Law of diffraction where ‘n’ is the order of reflection, ‘λ’ is the wavelength of the beam, ‘d’ represents the spacing between atoms or planes and ‘θ’is the diffraction angle. The first order reflection was considered for the work done here [103]. Montmorillonite clay, in its natural form has an interlayer basal spacing of around 0.95 nm

[104]. The addition of octadecyl ammonium surfactants with primary and quaternary onium ion surfactant heads increases this interlayer basal spacing. The basal spacing for the organoclay I.30P having a primary onium ion surfactant increases to about 2.2 nm whereas the spacing for I.44P organoclay with quarternary onium ion surfactant increases to 2.59 nm. For maleated polypropylene, the X-ray peak is obtained at a 2θ value of about 14 degrees.

The X-ray diffractometer used for the present study was a Rigaku Rotaflex Ru-200BH X-ray diffractometer, which is equipped with a Ni-filtered Cu Kα radiation source and operated at 45 kV and 100 mA. The sample is scanned over a 2θ range of 0.5^o to 15^o at a rate of 0.5^o/min and measurements are recorded at equal increments of 0.01^o. The low end of the scanning range is defined by the smallest angle the wide-angle instrument can scan whereas the high end of the scanning range is chosen so that the first diffraction peak for the maleated polypropylene matrix occurring at about 14^o 2θ is observed. The powder x-ray diffraction of the clays is carried out by compacting the clay in a 1"-1" cavity on a glass slide. For all the nanocomposites, compression-molded disks were used which were first pasted onto glass slides to provide enough rigidity to the samples. This would allow us to obtain enough diffraction intensities with the x-ray beam.

The scanning speed of 0.5 degrees/minute was chosen to obtain high resolution diffraction. . The speed of the detector is important because a high scanning speed may not register small variations in the diffraction intensity, which may be essential for testing in the lower range of 2θ values. For the same reasons, a smaller sampling interval of 0.01^o was chosen over the entire range of 2θ values. Also, the X ray diffraction machine has four diffraction slits; one between the x-ray source (diffraction slit) and the sample; two after the sample on the goniometer and the last slit is on the detector. To obtain low angle diffraction data, a small diffraction slit of $1/6^o$ was chosen for the first 2 slits which conventionally have the same width.

The other 2 slits do not have to be of the same width and on the basis of previous work done in our lab on polypropylene –clay nanocomposites, a slit size of 0.3^{o} was chosen for them.

2.5 THERMOGRAVIMETRIC ANALYSIS

Thermo gravimetric analysis was carried out on the pure organoclays, neat matrix as well as the nanocomposites to determine the amount of surfactant in the organoclay and also the total clay content in the nanocomposites. The TGA measurements also gave an idea about the thermal stability of the nanocomposites. TGA is a technique used to determine changes in weight with respect to changes in temperature. TGA is commonly used to determine the material characteristics of different polymers, their decomposition temperatures and also the amount of organic and inorganic components in a system.

The Thermo gravimetric analyzer used in the present study was a TA instrument TGA Q500 with a low mass furnace, ultra-sensitive thermo balance and an efficient purge gas system. A high precision platinum pan was used to measure the percentage weight change with respect to change in temperature for the different materials. The platinum pan was first tarred to remove any offset with respect to weight. The pan was then loaded with approximately 10 mg of the different materials each time to measure their weight changes. A high resolution temperature ramp was used at a rate of 10°C / min from 4°C to 600°C on the different materials. The high resolution TGA procedure allows greater accuracy since the temperature changes slowly when the weight loss increases. An inert atmosphere was created by purging nitrogen gas in the electrically heated oven equipped with a high precision thermocouple to measure the accurate temperature.

The TGA measurements on the pure organoclays revealed that the I.44P clay had about 30% of the quaternary ammonium ion surfactant whereas the I.30P clay had 23% of the primary amine surfactant. The TGA measurements also indicated that the thermal stability of the nanocomposites increased by around 50°C to 55°C as compared to neat PP-g-MA matrix at about 10% of the weight loss.

2.6 RHEOLOGY

Rheology, the study of flow and deformation [105], is an important tool for investigating the micro structural changes occurring in polymer nanocomposites upon deformation. Based on the applied deformation, rheological measurements help to determine the linear as well as non-linear viscoelastic properties such as viscosity, modulus etc. by using rheometers. Rheometers can be classified into different categories depending on what material functions they are used to determine. The first basic division is by kinematics: Shear versus Extension [105]. They can be also classified based on the type of strain applied viz., small strains, large strains, steady strains. The present work focuses on both the shear as well as extensional rheology on the polypropylene-layered silicate nanocomposites. At smaller strains or strain rates both shear and extensional measurements give the same material function which is the linear viscoealstic limit of time dependent viscosity.

$$\lim_{\dot{\gamma}\to 0}\eta^{+}(t,\dot{\gamma}) = \lim_{\dot{\varepsilon}\to 0}\mu_1^{+}(t,\dot{\varepsilon}) = \eta(t) \qquad \text{..... (2.2)}$$

However at long times or very large strains, $\eta^{+}(t,\dot{\gamma})$ becomes a function of shear rate only. Between these two limits extensional behavior for a material maybe different form the shear behavior and it depends on time and strain or strain rate. The following sections describe in

detail the various viscoelastic properties measured on these nanocomposites through shear and extensional rheology.

*2.6.*1 *Shear Rheology*

Shear rheology was used here to investigate the linear viscoelastic response of the polypropylene clay nanocomposites. Shear rheometers can be classified based on the flow that is used to generate the shear on the material, viz., “drag flow” and “pressure driven flow”. In drag flows shear is generated between a moving and a fixed surface whereas in pressure driven flows the shear is generated by a pressure difference across a channel. For the present work a parallel plate geometry was used in which shear is generated on the material between a moving plate and a parallel fixed plate. The parallel disk geometry is shown in figure 2.2.

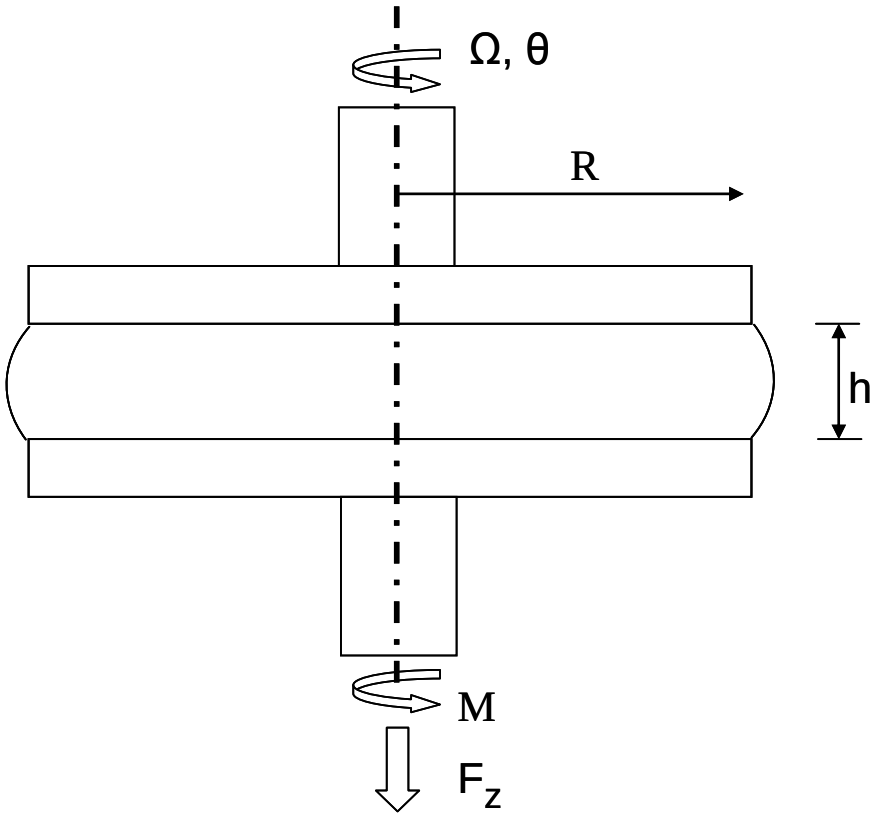

Figure 2.2. Schematic of a parallel plate rheometer.

Based on the assumptions of [105]:

1. Steady, laminar, isothermal flow
2. $\nu_\theta(r,z)$ only, $\nu_r = \nu_z = 0$
3. Negligible body forces
4. Cylindrical edge

The equations of motion for parallel plate geometry with radial co-ordinates become:

$$\theta: \quad \frac{\partial \tau_{\theta z}}{\partial z} = 0 \qquad (2.3)$$

$$z: \quad \frac{\partial \tau_{zz}}{\partial z} = 0 \qquad (2.4)$$

$$r: \quad \frac{1}{r}\frac{\partial}{\partial r}(r\tau_{rr}) - \frac{\tau_{\theta\theta}}{r} = -\rho\frac{\upsilon_\theta^2}{r} \qquad (2.5)$$

The above equations can be solved by assuming a condition of no slip at plate surfaces and the shear stress can be related to the torque observed on the plate by:

$$\tau_{12}(R) = \frac{M}{2\pi R^3}\left[3 + \frac{d\ \ln M}{d\ \ln \dot{\gamma}_R}\right] \qquad (2.6)$$

This shear stress data can be then used to calculate the linear viscoelastic properties such as the viscoelastic modulus. By applying small amplitude oscillatory strains one can obtain oscillatory stress data which can be mathematically expressed as:

$$\gamma = \gamma_0 \sin\omega t \qquad (2.7)$$

$$\tau = \tau_0 \sin(\omega t + \delta) \text{ .....(2.8)}$$

This oscillatory stress data can be decomposed into an in phase elastic component with strain wave and 90° out of phase viscous component. Based on these two components two different dynamic moduli can be obtained: the elastic component called as the "storage modulus" (G') and the viscous component called as the "loss modulus" (G"). The equations for the storage, loss and complex modulus are given below:

$$G' = \frac{\tau_0^{'}}{\gamma_0} \text{ ....(2.9)}$$

$$G'' = \frac{\tau_0^{''}}{\gamma_0} \text{ ....(2.10)}$$

$$G^* = G' + iG'' \text{ .... (2.11)}$$

A complex viscosity is defined in a similar manner and its magnitude is given as:

$$\left|\eta^*\right| = (\eta'^2 + \eta''^2)^{1/2} = \left[\left(\frac{G''}{\omega}\right)^2 + \left(\frac{G'}{\omega}\right)^2\right]^{1/2} = \frac{\left|G^*\right|}{\omega} \quad \text{..... (2.12)}$$

Based on these equations, the different material functions for the various nanocomposites were determined which were useful in gaining an insight into the material micro structure.

Parallel plate geometry on a TA Instruments AR2000 rheometer was used to perform the oscillatory shear measurements. The linear viscoelastic regime was determined by first running a strain sweep test on the nanocomposites. In a strain sweep test the strains are varied on the material by keeping a fixed frequency and observing the various viscoelastic properties (G', η') as a function of strain. The strain at which these properties show a change indicates that beyond

this strain value the non-linear region starts. A strain value of 0.5% was well within the viscoelastic regime for these nanocomposites and all the linear viscoelastic properties were obtained at this strain. The strain sweep tests were also used for probing into the non-linear viscoelasticity of the nanocomposites. To obtain torque values much greater than the lower bound of torque values for the AR 2000 rheometer, 40 mm diameter disk geometry was used instead of 25mm diameter disk geometry. To probe into the structure of the nanocomposites, lower strains are used because it has been shown previously that large amplitude oscillatory strains align the nanoparticles [106, 107]. A frequency range of 0.01 to 100 ω (rad/s) at 0.5% strain amplitude was chosen to perform the frequency sweep tests and the linear viscoelastic data was measured over this entire range. A time sweep was also carried out on these nanocomposites on the 40 mm parallel plate geometry for about 1 hour to check for the stability of modulus for these nanocomposites with respect to time.

For the non-linear shear rheology three subsequent strain sweep tests were run to observe the drop in storage and loss modulus values. The strain amplitude varied from 0.1% to 100% and the consequent storage and loss moduli were recorded. To understand the recovery kinetics of the modulus values of the nanocomposites, a time sweep was run at low strain amplitude and fixed frequency immediately after running a strain sweep test. The delay between the first point of the time sweep test and the last strain amplitude point in strain sweep was 10 sec. A continuous purge of nitrogen was supplied during all these tests to avoid thermal degradation.

2.6.2 *Extensional Rheology*

In the early 1900's, Trouton carefully tested different viscous sample at slow extensional deformation rates and found that the viscosity measured in uniaxial extension is three time the

shear viscosity for Newtonian fluid. This was the start of the extensional rheometry field; however it significantly advanced only after the 1970's. Extensional rheology is very sensitive to structural changes and plays a significant role in many processing operations such as thermoforming, blow molding, fiber spinning and foaming. This is because the polymer chains and asymmetric particles get oriented along the extensional flow which bears a significant effect on the final product properties [105]. However, it is very difficult to generate reliable extensional flow data because of the shear stresses generated at stationary boundaries. Therefore utmost care needs to be taken while measuring extensional flow properties of a material.

In the present work, simple uniaxial extension has been used to obtain the extensional rheology data. The test samples are pulled between rotating clamps, a design developed by Meissner [108] and further improved by him and his coworkers [109-111]. In this design one end of the sample is fixed and the free end being wrapped around a rotating rod [112-118]. The apparatus or the fixture used in this work is called as the "Elongational Viscosity Fixture" (EVF) that can be mounted onto a TA ARES rheometer. The design of EVF is based on the original Meissner concept, however, instead of the rotary clamps, two cylinders are used to wind up the sample; one cylinder is rotating while the other is stationary and measuring the force. The schematic of the elongational viscosity fixture is shown in figure 2.3. The rotating cylinder moves on a circular orbit around the force- measuring cylinder while rotating around its own axis at the same time and this helps in winding up the sample equally on both sides. The rotation of the cylinder is made by the ARES actuator. The advantage with this design is that the stationary cylinder measuring the force is fixed in space and as such can be decoupled with the torque transducer of the ARES instrument. Since the force measurement is decoupled from all the

moving parts, factor such as friction and inertia do not contribute to the force signal giving pure extensional force.

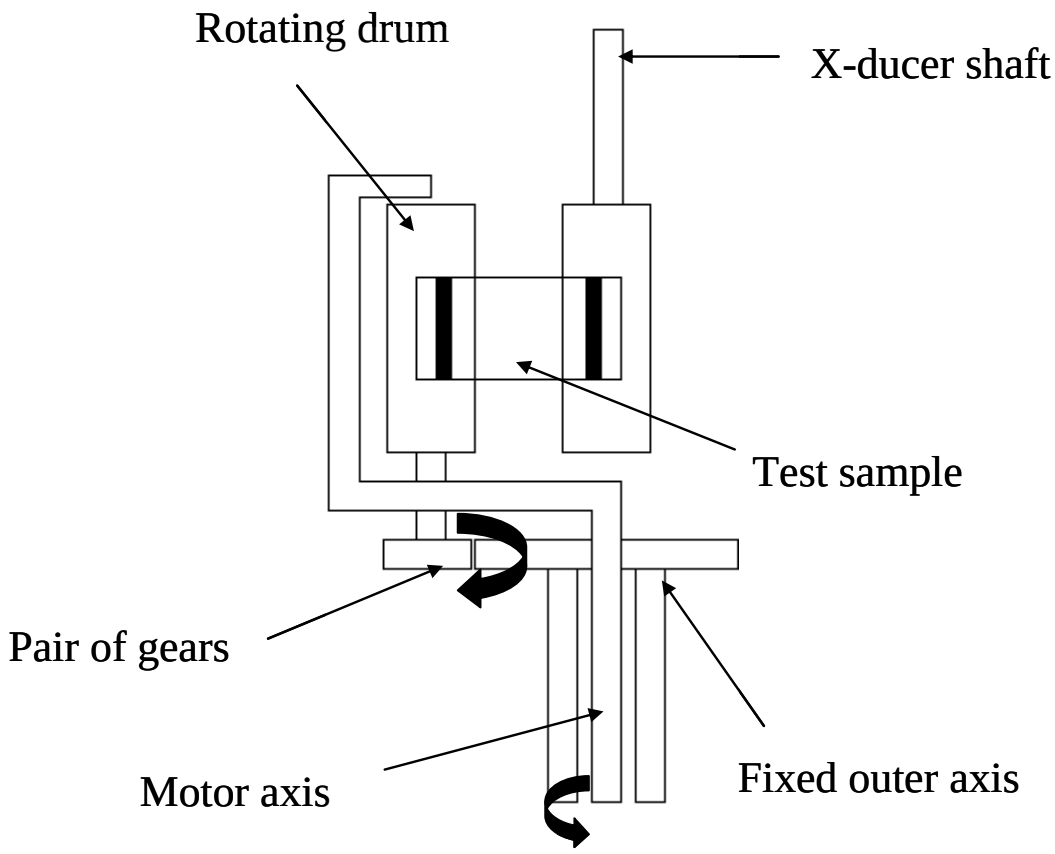

Figure 2.3. Schematic of an Elongational Viscosity Fixture (EVF).

Based on the torque measured the following working equations help in calculating the extensional viscosity of the material tested on EVF. The extensional strain rate is given as

$$\dot{\varepsilon} = \frac{d}{dt}\varepsilon_H = \frac{\Omega(t).D_d}{L_s} \quad \text{..... (2.13)}$$

Where, $\dot{\varepsilon}$ is the extensional strain rate, ε_H is the Hencky strain, Ω (t) is the motor speed, D_d is the drum diameter of cylinder and L_S is the sample length. The time required for performing uniaxial extension on a sample can be calculated on the basis of the Hencky strain to which the sample has to be stretched and the extensional strain rate.

$$t = \frac{\varepsilon_H}{\dot{\varepsilon}} \quad \text{..... (2.14)}$$

The extensional stress is calculated from the extensional force measured on EVF divided by the area of the sample A_S.

$$\sigma_E(t) = \frac{F_s(t)}{A_s(t)} \quad \text{..... (2.15)}$$

Based on this extensional stress and the extensional strain rate, the uniaxial extensional viscosity of the samples can be given by the following equation:

$$\eta_E(t) = \frac{\sigma_E(t)}{\frac{d}{dt}\varepsilon_H} \quad \text{..... (2.16)}$$

In the EVF the motor and transducer axis are aligned and the actual center to center distance between the rotating and stationary drum on the EVF is 12.7 mm. This means that the initial sample length is taken as 12.7 mm. A fixed hollow shaft having one end attached as a spur gear on top of the rotating drum and the other end mounted on the motor shaft imparts spin to the rotating drum. The diameters of the two drums are 10.3 mm and the clearing distance is 2.4 mm.

The whole EVF assembly fits into the conventionally heated ARES oven. Once the desired test temperature is reached the sample is clipped between the two cylinders. The transient uniaxial extensional viscosity of the nanocomposites as well as the pure maleated polypropylene matrix was measured at strain rates ranging from $0.1s^{-1}$ to $2s^{-1}$ up to a Hencky strain of 3. The test temperature for the matrix was taken as 150°C which was well above its melting point. However the different polypropylene clay nanocomposites were measured at two different test temperatures of 155° C and 160° C. These temperatures were well beyond the melting transition for these nanocomposites. Due to the small sample size and the fast heating rate of the ARES oven, the waiting time after loading the sample could be reduced to less than three minutes, thus preventing creep in the sample. During the measurement itself, the gravitational force does not contribute significantly. The test samples were examined after completion of the test and if any necking was noted in the stretched portion in the middle, the test was rejected.

RHEOLOGY OF MALEATED LINEAR POLYPROPYLENE-CLAY NANOCOMPOSITES VARYING THE CLAY ASPECT RATIO AND ORGANIC CONTENT

CHAPTER 3

3.1 INTRODUCTION

Polymer-layered silicate nanocomposites have gained considerable research interest in recent years, after the initial research work done by Toyota researchers on nylon/clay nanocomposites [7,8]. The addition of small amount of high aspect ratio (of the order of ~200) nanoclay platelets to polymer matrix, through melt mixing, leads to significant improvements in the polymer/clay nanocomposite properties such as stiffness, tensile strength, barrier properties, reduction in flammability, etc. [9-12]. Polypropylene (PP) which is a commodity polymer has been widely investigated to make its nanocomposites with clay. PP being non polar needs to be functionalized with maleic anhydride to form maleated PP so as to wet the clay surface more readily and mix properly for making the nanocomposites . Okada and coworkers were the first to make nanocomposites out of PP, maleated PP and clay [13-15]. These polymer clay nanocomposites are characterized by structural as well rheological techniques depending on the kind of industrial process they need to be developed for.

Recently, the polymer- layered silicate nanocomposites have been widely developed for various applications in automotive industries, for food packaging films, etc. For such applications the nanocomposites are processed through various processes such as extrusion foaming, thermoforming, blow molding, compression molding etc. The study of the extensional flow behavior of these polymer nanocomposite melts is very important for such processes and as

such the measurements of transient uniaxial extensional viscosity for polymer melts become imperative. Several researchers have measured the transient uniaxial extensional viscosity [69-72] and melt strength [73, 74] of pure polymer melts and their blends to understand their stain hardening behavior. In particular, a rise in polymer melt viscosity (above the linear viscoelastic limit) with increasing Hencky strain is called as "strain hardening" and is desirable to a certain extent for above mentioned processes.

Sugimoto and coworkers have shown that linear polypropylene on its own does not display any strain hardening. However they were able to show strain hardening in PP which was modified either by introducing branched molecular structure through irradiation [75] or by adding a small amount of uhmw–PE to linear PP [76]. The extensional flow of composites with micron size fillers has also been investigated with different sizes, shapes and aspect ratios by Takahashi et al. [84] and Le Meins et al [85]. Takahashi used microscale fillers such as mica, talc, glass beads and glass flakes in a low density polyethylene matrix, whereas Le Meins et al. suspended monodisperse polystyrene spheres in polyisobutylene liquid. They found that the strain hardening goes down with filler addition and even more so with high aspect ratio particles such as fibers. They also observed that the formation of aggregates led to a decrease in strain hardening behavior. Although similar observations of decreasing strain hardening have also been reported on nanocomposites by several authors including Bhattacharya and coworkers [66, 86], there have been two reports with nylon 6 [87] and maleated polypropylene [88] nanocomposites wherein the strain hardening improved slightly. Seong and coworkers [87] dispersed Closite nanoclay in Polyamide 6 matrix and observed that with well dispersed systems there was an improvement in the storage modulus, viscosity as well as the strain hardening behavior in extension. Okamoto et al. [88] dispersed treated montmorillonite clay in maleated polypropylene

and investigated the strain hardening as well rheopexy features of the nanocomposites. However, there have been no reports which show a thorough investigation of the strain hardening behavior of linear maleated polypropylene and layered silicate nanocomposite melts with respect to varying organic surfactant content in the nanoclays as well different effective aspect ratios of the nanoclays. Also, finding a possible correlation between the effects of varying aspect ratio and organic content in the filler and the linear as well as nonlinear shear viscoelastic behavior of the nanocomposites leaves us with a scope of research work that is done in the present study.

The system of interest here is linear polypropylene grafted with maleic anhydride, also called as linear maleated polypropylene (PP-g-MA), used as the matrix. The primary objective in choosing just the functionalized (maleated) polypropylene as the complete matrix was to understand the kind of interactions taking place between the maleic anhydride group on the polymer chains and the -OH groups on the clay edges, that may aid in achieving strain hardening in the nanocomposites. The addition of linear bulk polypropylene would add a third phase making the system more complex. Hence just the linear maleated polypropylene copolymer (with ethylene) was chosen as the matrix to which layered silicates (Montmorillonite clay) having varying aspect ratios and different surfactant treatments were added as the filler.

The layered sheets in montmorillonite clay have an excess negative charge which is neutralized by highly charged inorganic cations such as Na^{+} and Ca^{2+} present in a hydrated form in the interlayers of untreated clay [1, 26]. The hydration spheres of these inorganic cations form unfavorable organophobic conditions for adsorption of organic polymer molecules between the interlayer. Also, the removal of water of hydration of these cations leads to collapsing of the interlayer spacing thereby preventing the entrance of the organic polymer chains between the

interlayer spacing and exfoliation of clay in polymer matrix. The clay surface is therefore treated so as to make the clay interlayer region organophilic and make the adsorption of organic polymer molecules between the clay platelets easier. The polymer chains can then enter the clay galleries between two subsequent clay layers and separate them causing exfoliation of clay in the polymer. The surface treatment of clay is done by exchanging the hydrated cations with quaternary organo-ammonium salts or with primary amines having hydrocarbon groups attached to them, thereby creating organophilic condition in the clay interlayer region. In the present study, two different montmorillonite clays, organically modified by incorporating primary amine surfactant in one and quaternary ammonium ion surfactant in other are used. These surfactants are present in the clay interlayer galleries. The organoclays were melt-mixed with linear polypropylene and different nanocomposites were made. These nanocomposites were tested for nonlinear, uniaxial extensional melt viscosity transients to check if the addition of the organically modified nanoclay imparted any strain hardening to the non-strain hardening PP matrix. Also, linear and nonlinear shear rheology was used to further probe into the structure of the nanocomposites and understand the shear and extensional behavior.

In general, the addition of nanofiller to polymeric systems leads to improvements in the reinforcement and various physical properties of the polymer. Sternstein et.al, [95, 96] proposed different mechanisms to explain the reinforcements observed in silica-filled poly (vinyl acetate) [PVAc] matrix at low filler loadings in linear and nonlinear viscoelastic properties. They proposed that the possible reinforcements in the nanofilled polymer melt may be due to the trapped or hindered chain entanglements formed between the bulk PVAc chains and the chains that are physically attached to the filler surfaces. A similar observation of increase in reinforcement as well as strain hardening was previously made by Yamaguchi and coworkers

[79-81] with blends of linear and cross linked polymers. They observed that the addition of a small amount of cross linked terpolymer (gEHDM) characterized as gel just beyond the sol-gel transition point to a linear polypropylene improved the strain hardening behavior of the blend greatly. They suggested that with appropriate cross link density the stretching of trapped chains between the crosslinking points were responsible for the strain hardening and an increase in the crosslinking density leads to suppression of the strain hardening behavior. Cassagnau and Melis [97] studied the nonlinear viscoelastic behavior and modulus recovery in silica filled polymers and showed that in physically crosslinked composites the complex shear modulus is perfectly recoverable as shown through subsequent strain sweeps and time sweeps.

In the current study, both nonlinear extension and linear and nonlinear shear rheology are used as investigative tools to understand the effects of nanoclay addition in linear maleated polypropylene. An increase in reinforcement and strain hardening in the nanocomposites has been explained by the possible formation of hindered chain entanglements between particle attached polymer chains and free polymer chains.

3.2 EXPERIMENTAL METHODS

3.2.1 Materials

The matrix material is maleated polypropylene (PP-g-MA) (Exxelor PO1015) with 0.4 wt% maleic anhydride and a molecular weight of 180,000. (ζ =0.9 g/cc). It is important to choose a PP-g-MA having a high molecular weight and substantial polymer chain length necessary for the formation of hindered chain entanglements. Exxelor PO1015 was chosen amongst several other PP-g-MA's (Honeywell AC 950 and AC 1325) to fit the criteria for this study. The melt mass flow rate (MFR) of Exxelor PO1015 is 150g /10 min at 230°C under a load

of 2.16 kg and it melts at 145°C. It is a random copolymer of propylene and ethylene which is the reason for its low melting point. The organoclay used for preparing the nanocomposites was (a) Nanocor I.30P which had a primary amine surfactant with single alkyl tail and (b) Nanocor I.44P which had quaternary ammonium ion surfactant with two C-18 tails.

3.2.2 *Compounding*

PP-g-MA and clay were dried overnight at 100°C and 20 mm Hg vacuum in a vacuum oven and then compounded with maleated polypropylene at 165° C and at 150 rpm for 10 minutes in a Banbury mixer; this was done under nitrogen to avoid thermal degradation. One batch of the mixer amounted to 47 grams of compound. The compounded material was removed from the mixer with a brass scraper and ground up with a mini granulator. The granules were further compression molded to desired thicknesses for different shear and extensional tests.

3.3 CHARACTERIZATION TECHNIQUES

3.3.1 DSC and TGA Measurements

The melting temperature of the nanocomposite pellets as well as the neat polymer was obtained using DSC runs on a TA DSC instrument. The melting point of neat PP-g-MA was 145°C while the nanocomposites melted around 146.5°C. Hence compounding was carried out at 165°C and compression molding was carried out at 175°C which is well above the melting points of these nanocomposites. Thermo gravimetric Analysis was carried out on the pure clay, neat matrix as well the nanocomposites on a TA Q500 TGA instrument from 4°C to 600°C through a high resolution temperature ramp of 10°C / min. The weight loss from TGA revealed that the pure I.30P clay had lesser amount of organic surfactant than the I.44P clay.

3.3.2 X ray Diffraction Measurement

All the clays and nanocomposites were analyzed using X-ray diffraction patterns. The characterization of the structure by XRD was performed on the compression-molded disks with a Rigaku Rotaflex Ru-200BH X-ray diffractometer, which is equipped with a Ni-filtered Cu K α radiation source and operated at 45 kV and 100 mA. The sample was scanned over a 2θ range of 0.5° to 10° at a rate of 0.5°/min and measurements were recorded at equal increments of 0.01°.

3.3.3 Extensional Viscosity Measurements

An extensional viscosity fixture (EVF) mounted on a TA-ARES rheometer was used to record the transient uniaxial extensional viscosity at strain rates ranging from $0.1s^{-1}$ to $2s^{-1}$ up to a Hencky strain of 3. A 20-specimen mold was used for compression molding samples 18mm long, 10mm wide and 0.7mm thick for the EVF tests. Test specimens were molded at 175° C and the mold was cooled slowly using cooling water under a pressure of 5 tons. This ensured stress free and relaxed homogenous samples with minimum dimensional variation. The molded specimens were dried overnight before performing the extensional tests at 155° C. The test samples were examined after completion of the test and if any necking was noted in the stretched portion in the middle, the test was rejected.

3.3.4 Shear Rheology

Parallel plate geometry on a TA Instruments AR2000 rheometer was used to perform frequency sweep tests on these nanocomposites in the linear viscoelastic region. The diameter of the parallel plates was 40 mm and a frequency range of 0.01 to 100 ω (rad/s) at 0.5% strain

amplitude was chosen to perform these tests. The corresponding storage modulus and complex shear viscosity were noted over the entire frequency range. The strain amplitude was chosen such that it was in the linear viscoelastic region and this was found out by running strain sweep tests at 1 rad/s on the nanocomposites. A time sweep was also carried out on these nanocomposites on the 40 mm parallel plate geometry for about 1 hour to check for the stability of modulus for these nanocomposites with respect to time. Subsequent strain sweep tests were used for probing into the nonlinear viscoelasticity of the nanocomposites. Also, a time sweep was run immediately after a strain sweep to get an estimate of the recovery time of complex shear modulus. A continuous purge of nitrogen was supplied during these tests to avoid thermal degradation.

3.4 RESULTS AND DISCUSSIONS

3.4.1 Effect of nanoclay dispersion and stability in nanocomposites

Organoclays with different surfactant chemistries are used for making the PP – clay nanocomposites. One grade of montmorillonite clay has a primary onium ion surfactant (NH_3^+ head group with single C-18 tail) and another one has a quaternary onium ion surfactant ($N^+(CH_3)_2$ with two C-18 tails) in the clay interlayer galleries. Heinz et al. [29] have commented on the structure and conformation of these surfactants in the interlayer galleries. The primary onium ion surfactant with a C-18 tail is hydrogen bonded more tightly to the clay surface and tends to orient itself perpendicular to the clay surface. The quaternary onium ion surfactant with two C-18 tails is more mobile in the interlayer galleries; it also packs to a greater extent in the interlayer galleries. The extent of surfactant packing can be judged from the X-ray diffraction patterns of the different organoclays, presented in Figure 3.1.

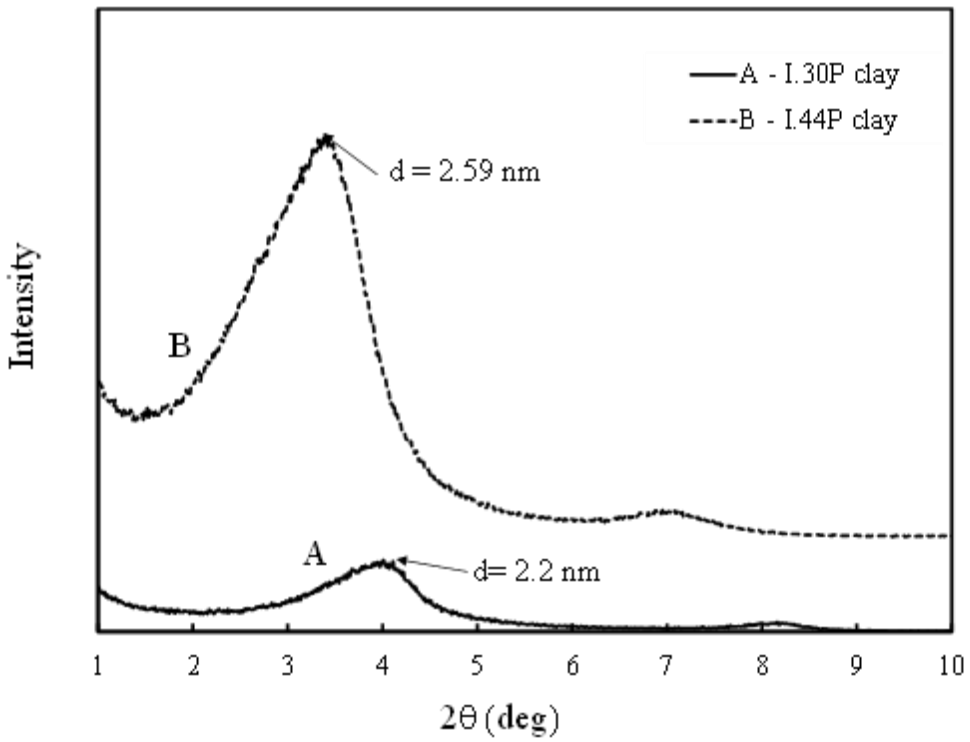

Figure 3.1. X-ray diffraction of organoclay: a) I.30 P clay (clay A), b) I.44 P clay (clay B)

It can be seen that the basal spacing for I.30P clay (2.2 nm) is smaller as compared to that of I.44P clay (2.59 nm). We infer that the greater basal spacing of the I.44P clay is mainly because of the greater extent of surfactant packing in its interlayer galleries.

XRD patterns for the different nanocomposites made with 5 wt% of the clays are presented in Figure 3.2. It can be seen that the composites with I.30 P clay (PPNC-A5) and with I.44 P clay (PPNC-B5) do not show distinct peaks indicating a good level of dispersion of clay platelets in the polymer matrix. The presence of a broader shoulder, instead of sharp peak in XRD suggests that there must be some intercalated clay structure present in these nanocomposites. This is more so evident with PPNC–B5 as compared to PPNC-A5.

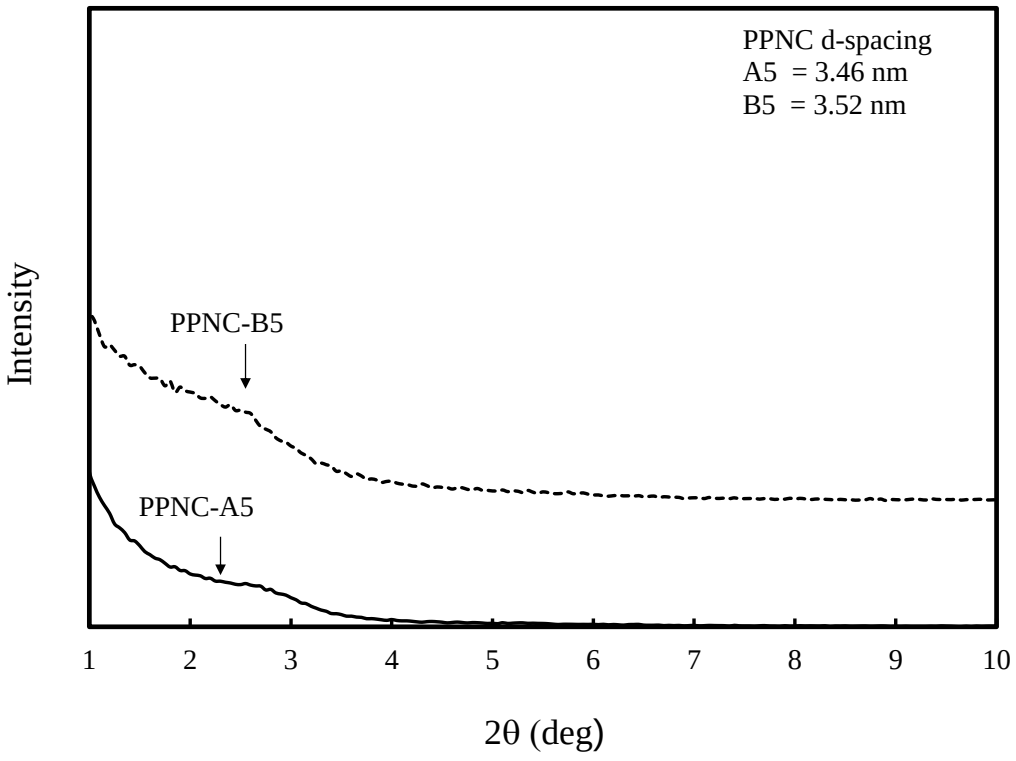

Figure 3.2. X-ray diffraction of composites: a) A5 nanocomposite, b) B5 nanocomposite.

Thermo gravimetric Analysis on the pure clay further confirmed the XRD observations and proved from the ash content calculations that I.30P clay had lesser organic content in the interlayer galleries than the I.44P clay. Figure 3.3 shows the weight percentage lost with increase in temperature for the neat matrix and nanocomposites. The dispersion of clay in the matrix increased the thermal stability of the composites by almost 50°C-60°C. The onset of decomposition for neat matrix begins around 330°C whereas for the nanocomposites it is 390°C. The amount of clay dispersed in the nanocomposites was calculated from the char yield at 600°C and was about 5.1% for PPNC A5 nanocomposite and 4.7% for PPNC B5 nanocomposite. The shear and extensional rheology tests were carried out at a temperature which is well within the stability limits of the clay and the matrix polymer.

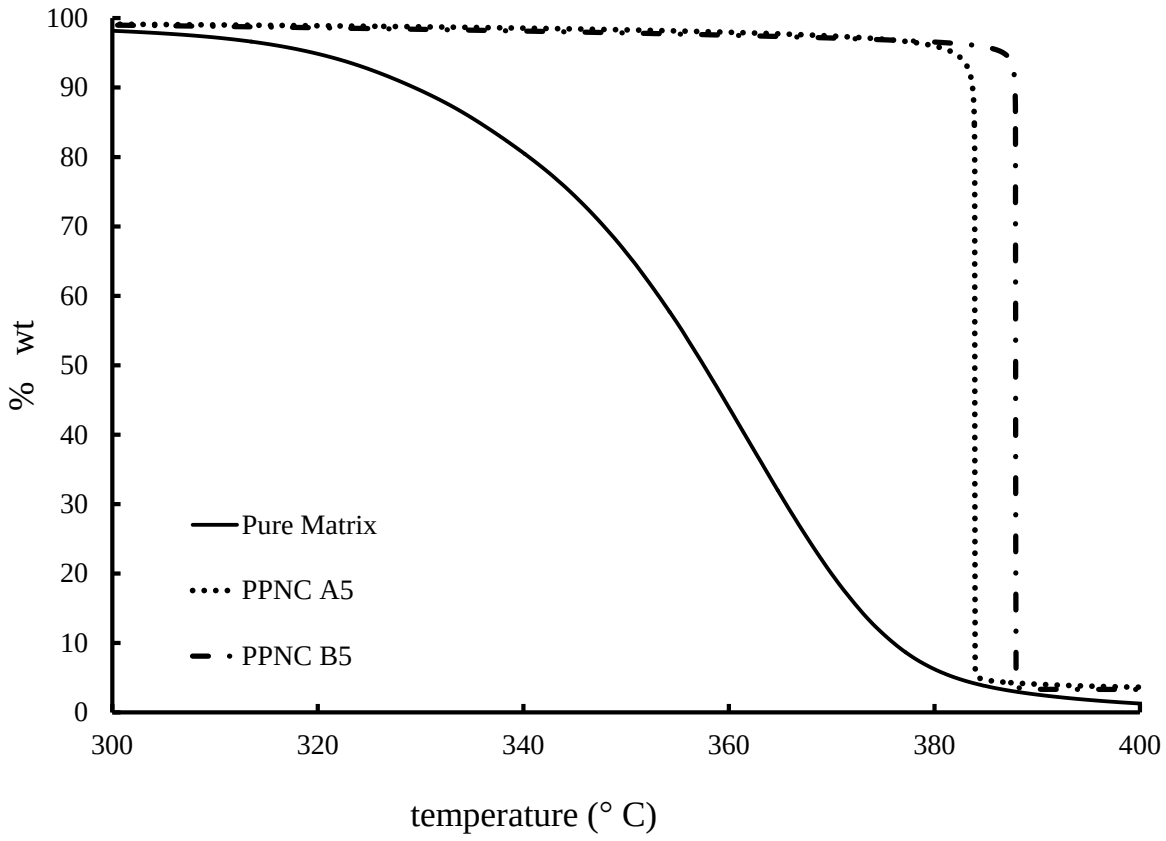

Figure 3.3. Thermo gravimetric Analysis (TGA) curves obtained for neat matrix, A5 and B5 nanocomposites at 10°C / min up to 600°C.

The stability of the modulus of maleated polypropylene matrix and the nanocomposites with the 5wt% of the organoclays was also checked with the help of a time sweep. The time sweep was carried out for about one hour and at 1 rad/s frequency and 0.5% strain amplitude. It can be seen from Figure 3.4, that the modulus of the matrix and the nanocomposite was stable and did not fluctuate over the time period of the test. The strain amplitude chosen was obtained by running strain sweep tests on the nanocomposites at 1rad/s frequency and was found to be well within the linear viscoelastic regime.

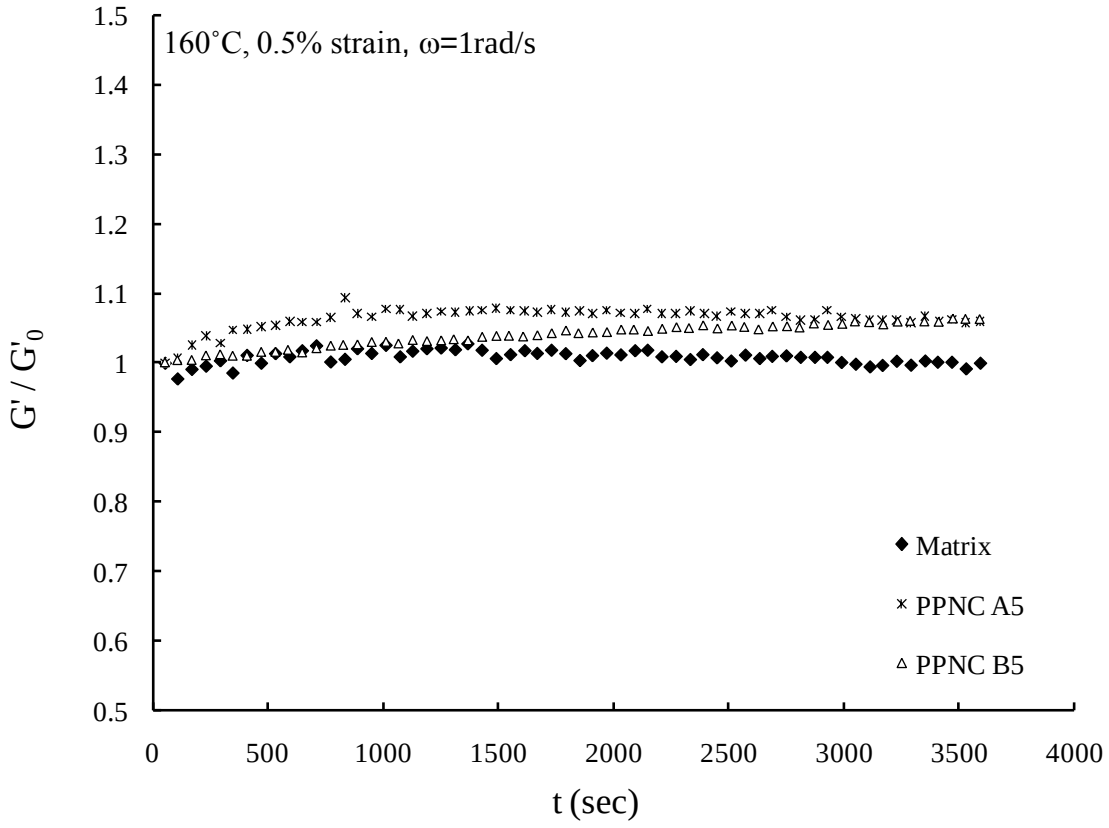

Figure 3.4. Time Sweep test: Change in normalized Storage modulus curves with respect to time for the neat matrix (●), A5 nanocomposite (*) and B5 nanocomposite (Δ)

3.4.2 Oscillatory Shear rheology

3.4.2.1 Linear Viscoelastic Measurements

The frequency sweep measurements done by parallel plate oscillatory shear rheology yielded results of the dynamic modulus and dynamic viscosity of the nanocomposites. A comparison of the dynamic viscosities for the two composites as well as the base polymer matrix is shown in Figure 3.5.

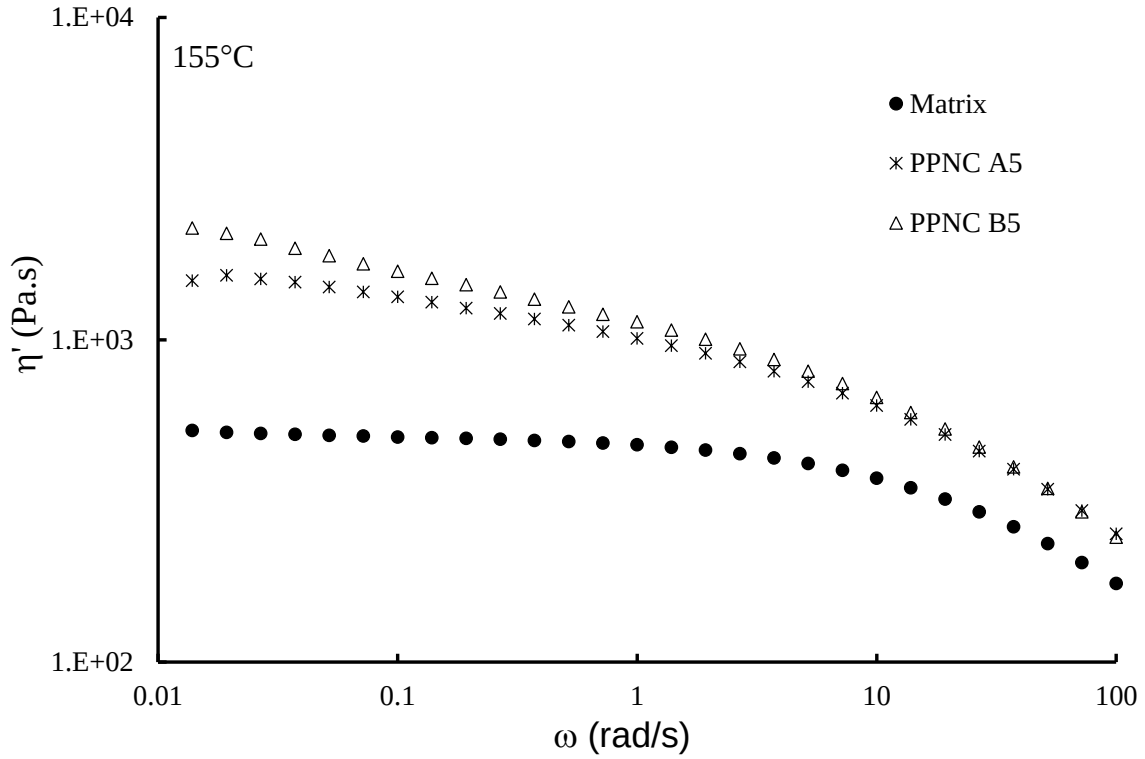

Figure 3.5. Dynamic viscosity curves for the neat matrix (●), A5 nanocomposite (*) and B5 nanocomposite (Δ).

The dynamic viscosity for the pure matrix is fairly constant at lower values of the frequency and much lower than that of the nanocomposites exhibiting a pseudo-Newtonian behavior. However, the dynamic viscosity increases significantly upon addition of a small amount of nanoclay to the pure matrix. The comparison between the dynamic viscosities of the two composites shows that PPNC B5 (5wt% I.44P clay) does not show a complete leveling off at lower frequencies, in the given frequency range, indicating a more elastic response in this nanocomposite.

In order to gain more physical insight, the nanocomposite melt viscosity relative to that of the matrix was correlated with the help of the Pierce-Maron empirical model, equation (3.1)

which applies to concentrated suspensions. Carreau and co-workers [125] used the same equation and correlated the complex viscosity data of PET nanocomposites at higher frequencies to volume fraction of the clay platelets in order to determine the extent of polymer matrix degradation upon compounding the nanocomposites. In this work, the dynamic viscosity data in the low frequency region were used instead of the complex viscosity. In the low frequency region, the dynamic storage modulus is quite sensitive to the particle-particle interactions which are not accounted for in the Pierce-Maron equation given below. Hence, we have used dynamic viscosity data for our calculations. .

$$\frac{\eta'}{\eta'_{matrix}} = \left(1 - \frac{\phi}{\phi_M}\right)^{-2} \quad \text{..... (3.1)}$$

where, η' is the dynamic viscosity of the nanocomposite and η'_{matrix} is that for the linear maleated polypropylene matrix, ϕ is the volume fraction of nanoclay (including surfactant) and ϕ_M is the maximum packing volume fraction. The maximum packing volume fraction can be related to the average ratio a of diameter D to thickness t for the nanolayers as done by Sun et.al [126] and Wan et.al [127] in their work on nanoclay filled composites and shown in Equation 3.2;

$$\phi_M = \frac{3.55}{a} \quad \text{.....(3.2)}$$

In this work, Equation (3.1) was used first estimate the maximum packing fraction ϕ_M, of the nanoclay in the composites with the two different clays: I.30 P and I.44P at 5wt% loading. Equation (3.2) was used next to determine the effective aspect ratio of the different nanoclays.

These calculations showed that the effective aspect ratio for the I.30P clay was around 56 and that of I.44P clay was 68, which is significantly higher.

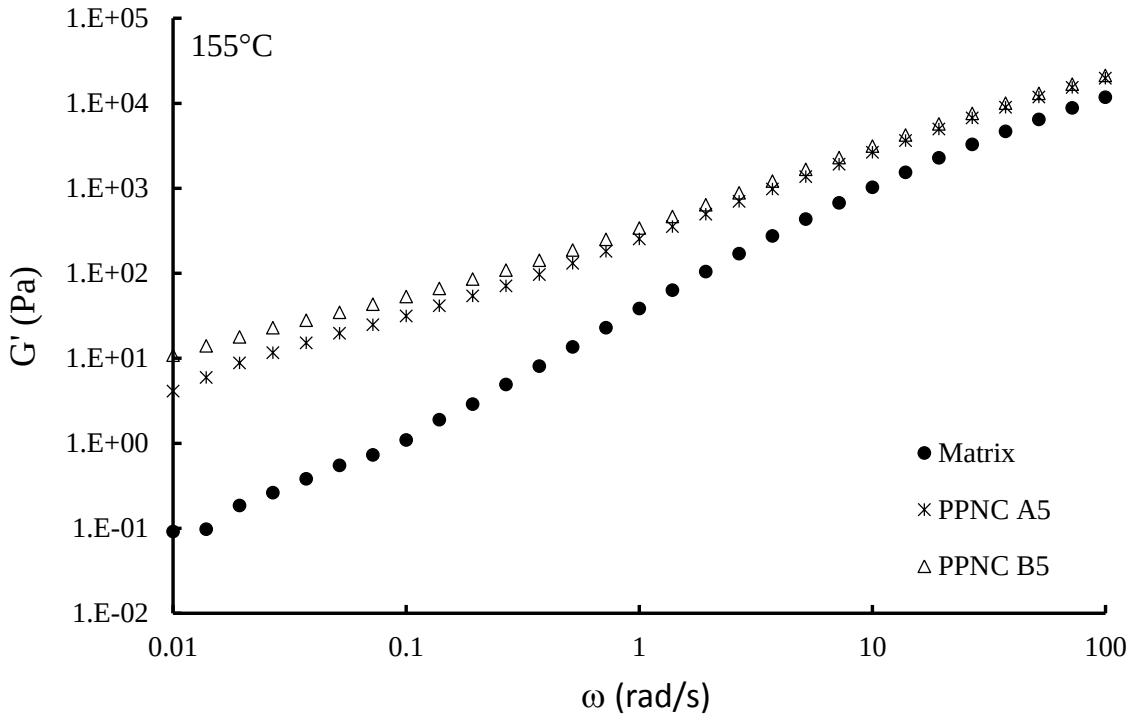

Figure 3.6. Dynamic Storage Modulus curves for the neat matrix (●), A5 nanocomposite (*) and B5 nanocomposite (Δ).

The dynamic modulus curves for the two nanocomposites are presented along with that for the polymer matrix in Figure 3.6, The dynamic modulus curve for the B5 nanocomposite (with I.44P) is greater than that of the A5 nanocomposite (with I.30P) and also shows an approach to a plateau like region at low frequencies. The low frequency storage modulus of nanocomposites is raised above the matrix values because of the filler network formed by particle-particle interactions [97]. Higher aspect ratio particles present more surface area per unit volume for such interactions and strengthen the filler network leading to a greater increase in low

frequency storage modulus of the B5 nanocomposite. So the comparison of the storage modulus curves is consistent with estimated trends in aspect ratio from dynamic viscosity data. The low frequency "plateau" or increase in storage modulus may arise in general from two contributions: (1) a filler particle network formed by van der Waals forces and, (2) entanglements between free polymer chains and particle attached polymer chains. The second factor involves the volume fraction of chains attached to particles which can also be increased by increasing aspect ratio of the nanolayers.

3.4.2.3 Non-Linear Viscoelastic Measurements

It is widely understood that higher levels of reinforcement observed upon addition of filler particles in a polymer are a result of filler network formation and filler agglomeration [92-94]. However the mechanisms behind these reinforcements and nonlinearity with increasing strain, at lower filler loadings, are still an area of considerable research. Sternstein and coworkers have tried to understand these mechanisms by which the nano-scale fillers promote both reinforcement and nonlinear viscoelastic behavior in polymer melts [95, 96]. They have worked with fumed silica fillers, at various loadings, having different surface treatments and poly (vinyl acetate) matrix with different molecular weights and explored the nonlinear viscoelasticity of these nanocomposites. They also proposed that the reinforcement and nonlinear viscoelastic behavior of the nano filled polymers is a result of "trapped entanglements" which occur because of interactions between the filler and the polymer chains at the filler-polymer interface. The polymer chains attach to the filler surface through polymer filler interactions thereby causing physical cross links. These polymer chains in turn entangle with the surrounding polymer chains causing trapped or hindered chain entanglements. Thus trapping of polymer chain loops at the filler surface lead to an increase in the entanglement density and this increase leads to overall

stiffening of the matrix. Also, when large strain amplitudes are applied, these entanglements are lost because of the debonding of polymers chains from the filler surface which results in overall relaxation of the matrix entanglement structure. This loss of entanglement structure causes non linearity in the viscoelastic behavior of the nanocomposites [95]. Cassagnau and Melis [97] have also worked with fumed silica composites with different polymer systems such as PP, PS and EVA and carried subsequent strain sweep tests and time sweep tests to understand the nonlinear viscoelastic behavior of these composites and modulus recovery kinetics.

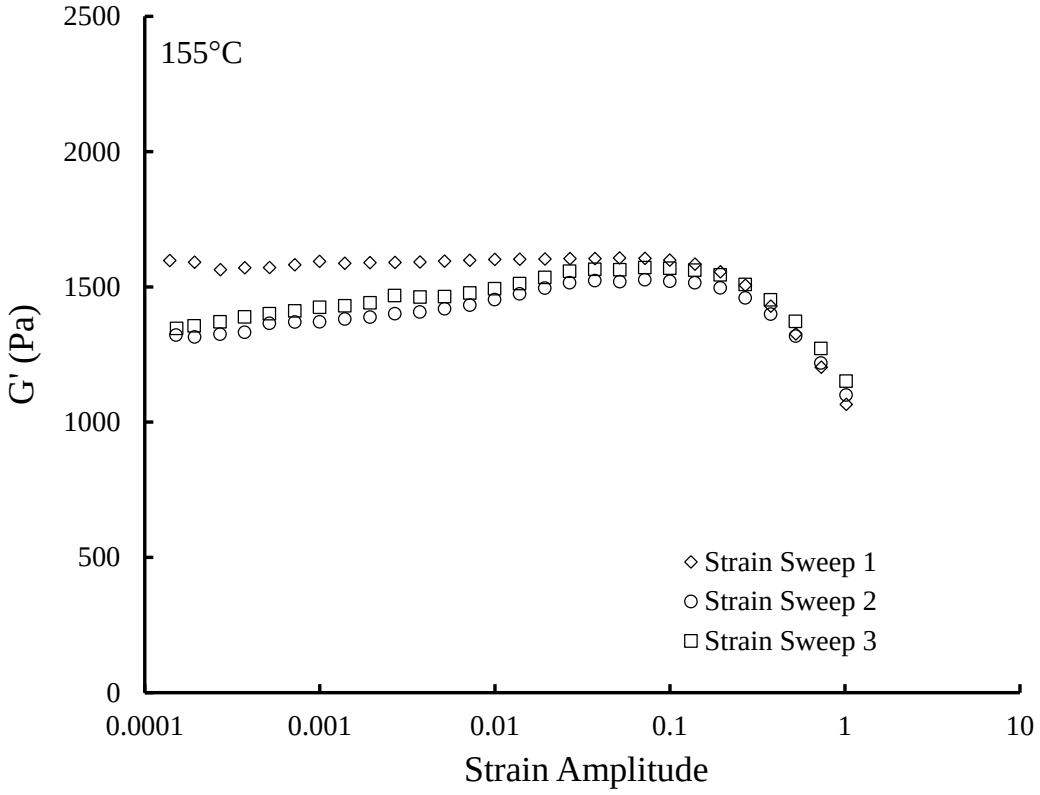

Figure 3.7. Subsequent strain sweep tests. Variation of storage modulus with strain amplitude for A5 nanocomposite at 155°C and 1 Hz.

In the present work, to understand the possible causes of the reinforcements as well as recovery kinetics of storage modulus from nonlinearity of the polypropylene-layered silicate nanocomposites, the nanocomposites were tested for their nonlinear viscoelastic behavior. This was achieved by performing subsequent strain sweep tests on the nanocomposites at a test temperature of 155°C and a frequency of 1 Hz. The strain amplitude varied from 0.1% to 100% and the consequent storage and loss moduli were recorded. Figures 3.7 and 3.8 show the storage modulus over three subsequent strain sweep measurements for PPNC A5 and PPNC B5 nanocomposites respectively, over the entire strain amplitude range. It can be seen for both PPNC A5 and PPNC B5 that mostly all the dynamic stress softening happens in the first strain sweep and very less in the subsequent strain sweep

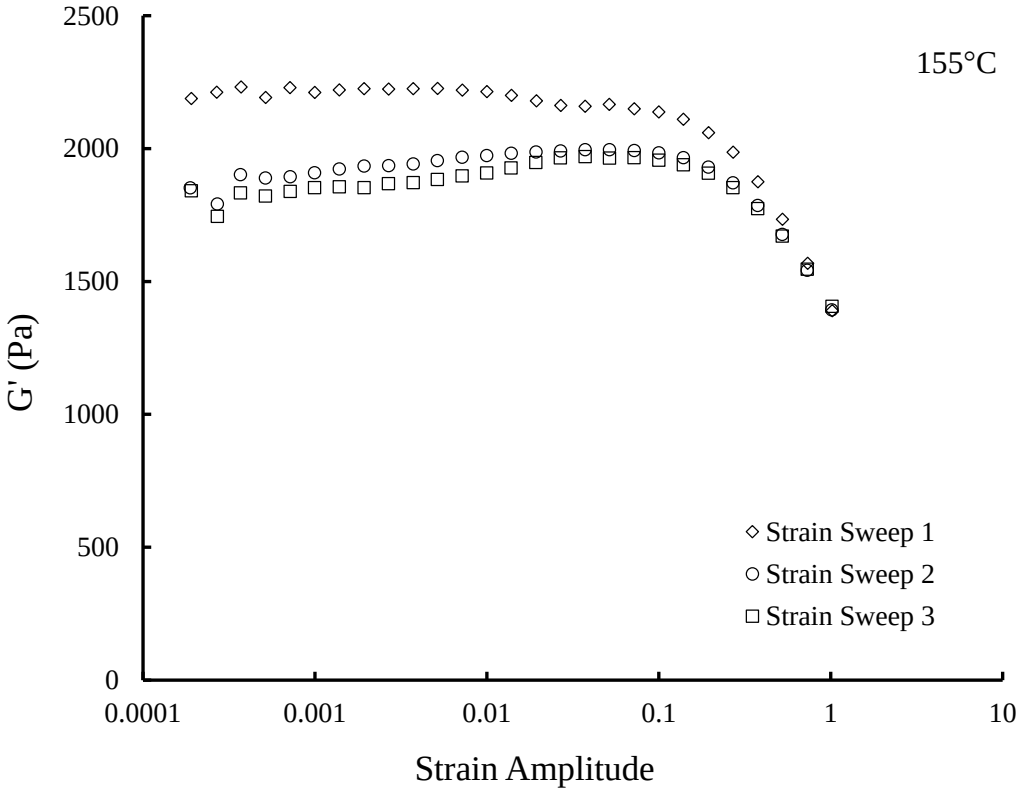

Figure 3. 8.Subsequent strain sweep tests. Variation of storage modulus with strain amplitude for B5 nanocomposite at 155°C and 1 Hz.

In addition to this, PPNC B5 nanocomposite shows a two stage drop in the storage modulus with increasing strain which highlights the breakup of two structures—the particle network followed by the hindered chain entanglement network involving attached chains.

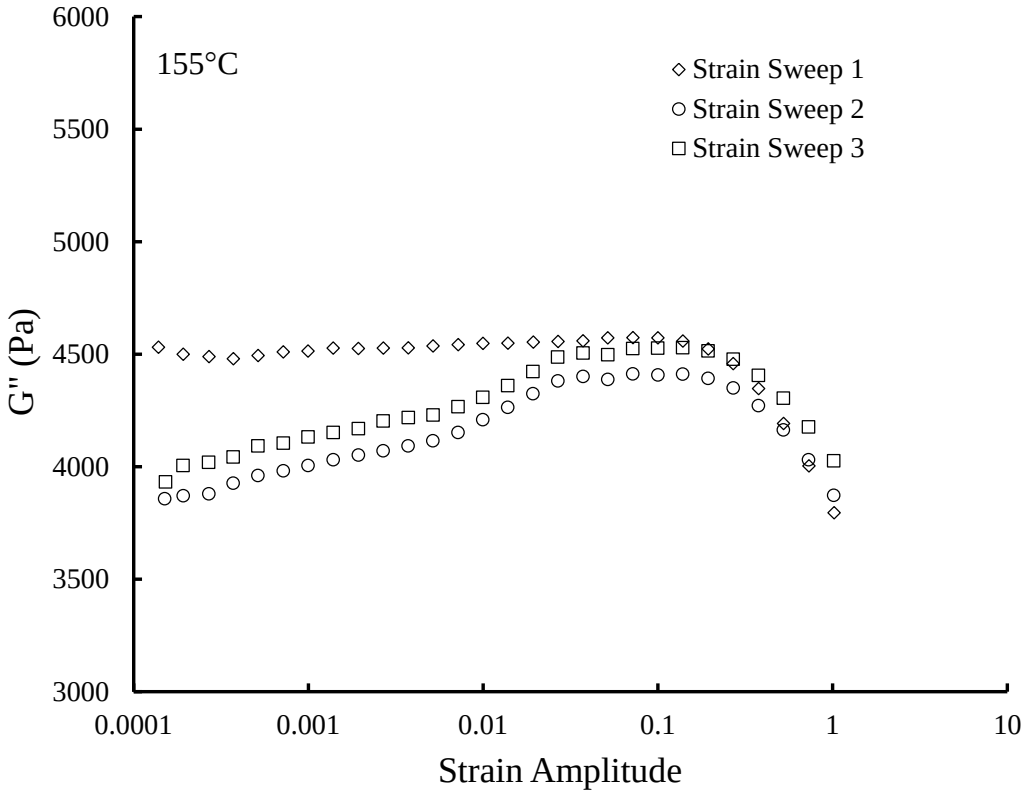

Figure 3.9. Subsequent strain sweep tests. Variation of loss modulus with strain amplitude for A5 nanocomposite at 155°C and 1 Hz.

A similar behavior is observed in the loss modulus of the two composites over the subsequent strain sweeps as shown in Figures 3.9 and 3.10. The two stage drop is more prominent in the loss modulus curve for PPNC B5 nanocomposite, further confirming the existence and breakup of the particle network followed by that of hindered chain entanglement network.

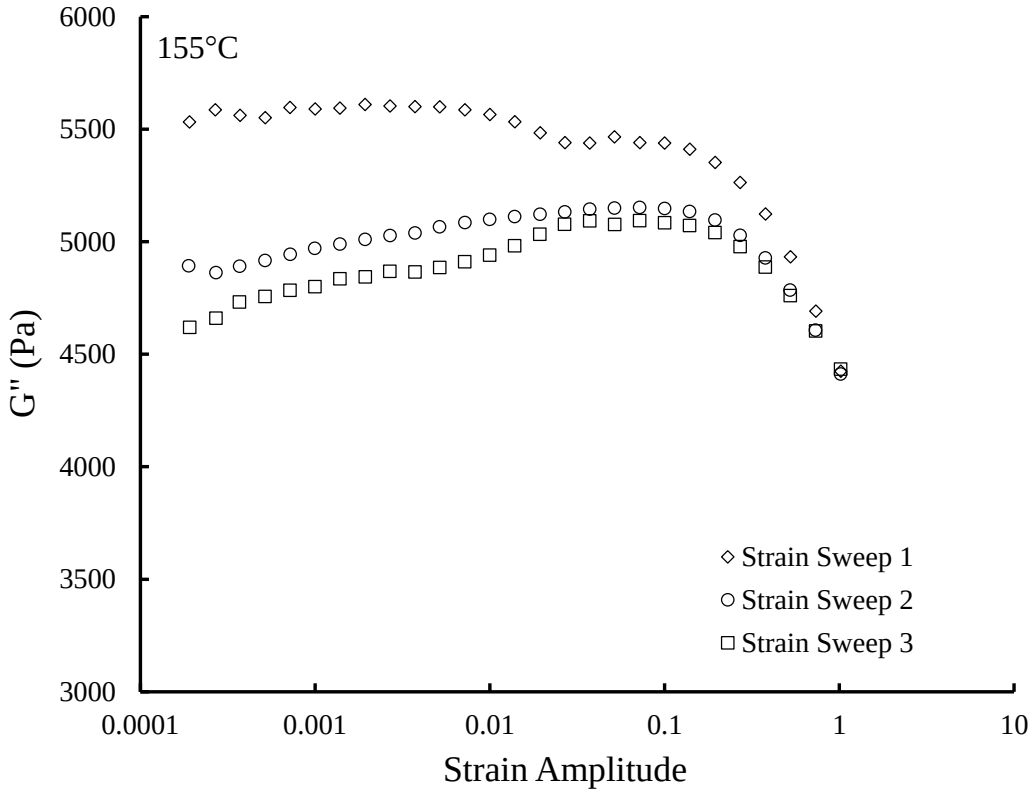

Figure 3. 10. Subsequent strain sweep tests. Variation of loss modulus with strain amplitude for B5 nanocomposite at 155°C and 1 Hz.

The modulus recovery between subsequent strain sweeps happens quicker in the PPNC A5 nanocomposite since the actual drop in modulus is not as great as the PPNC B5 composite. To get a more clear idea about the complex modulus recovery kinetics from nonlinearity, a time sweep experiment was run at lower strain amplitude (in linear viscoelastic region) immediately after a strain sweep experiment. Figure 3.11 shows the recovery kinetics of the storage modulus for both the nanocomposites. It can be clearly seen here that PPNC A5 composite shows a faster recovery as compared to PPNC B5. Also it can be seen from the time sweep experiment that the storage modulus keeps increasing even beyond the initial modulus that was measured before the strain sweep experiment.

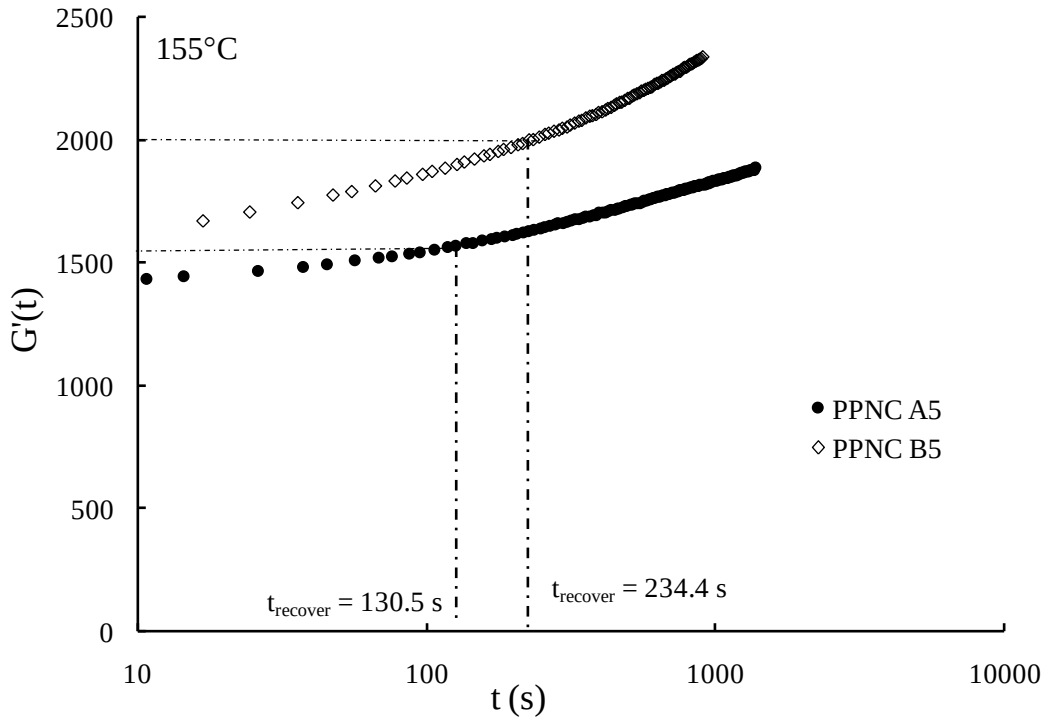

Figure 3.11. Storage modulus recovery versus time ($\omega = 1$Hz and $\gamma = 0.5\%$). A5 and B5 nanocomposites at 155°C. G' (t) is the storage modulus value as obtained from time sweep test which is done immediately after one strain sweep.

This could imply that the strain sweep experiment acts as a trigger in deforming the entanglement structure such that it requires much more time to reach an equilibrium state and have a leveled out modulus value. A similar recovery behavior is seen for the loss modulus of these composites (Figure 3.12), although the rate of recovery for loss modulus (G'') is lesser than that for storage modulus (G').

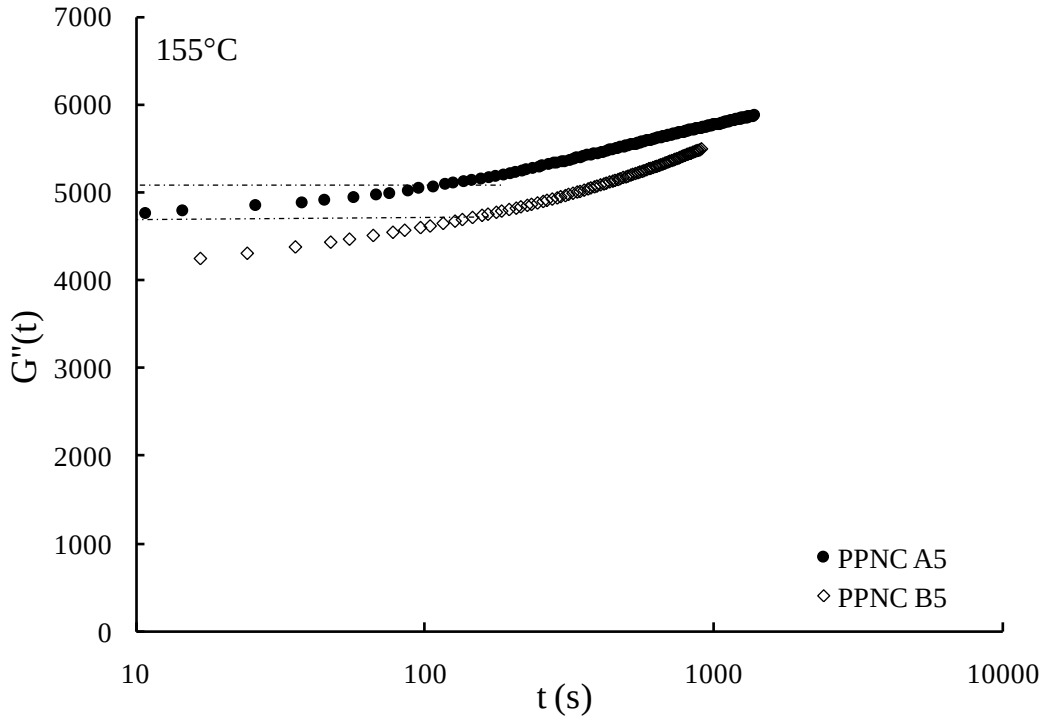

Figure 3.12. Loss modulus recovery versus time (ω = 1Hz and γ = 0.5%). A5 and B5 nanocomposites at 155°C. G'' (t) is the Loss modulus value as obtained from time sweep test which is done immediately after one strain sweep.

This is further evident from the loss factor values when plotted against the recovery time. Sternstein et.al [96] have shown trends in loss factor recovery for composites having fillers with different surface treatment by plotting the ratio of loss factor observed during the recovery time sweep to that observed in the linear viscoelastic region of the strain sweep experiment. Such a plot is shown in Figure 3.13. It can be seen through this plot that the loss factor values for PPNC B5 are greater than that of PPNC A5 indicating that the rate at which storage modulus is recovered is greater in PPNC B5 case. However, since the drop in the storage modulus value

after first time sweep was greater in case of PPNC B5, it takes more time to reach that initial value.

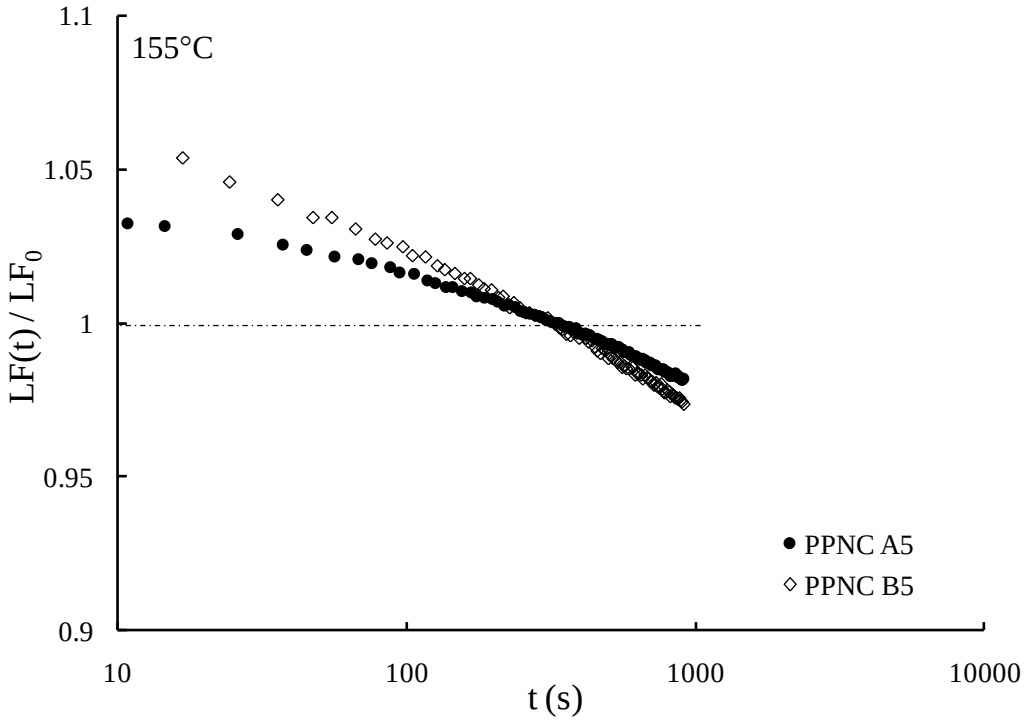

Figure 3.13. Rate of Recovery of the loss factor after initial strain sweep for PPNC A5 and PPNC B5. The Loss Factor LF (t) is that obtained from the time sweep test and LF_0 is the plateau value of loss factor obtained from initial strain sweep test.

This effect of non-linearity is further investigated in uniaxial extension by performing transient extensional viscosity measurements on the nanocomposites at different test temperatures.

3.4.3 Uniaxial Extensional Rheology

3.4.3.3 Effect of filler addition

The transient extensional viscosity curve $\eta_E^+(t)$ for the neat matrix was obtained by stretching it in an uniaxial direction at a temperature well above its melting point, as shown in Figure 3.14.

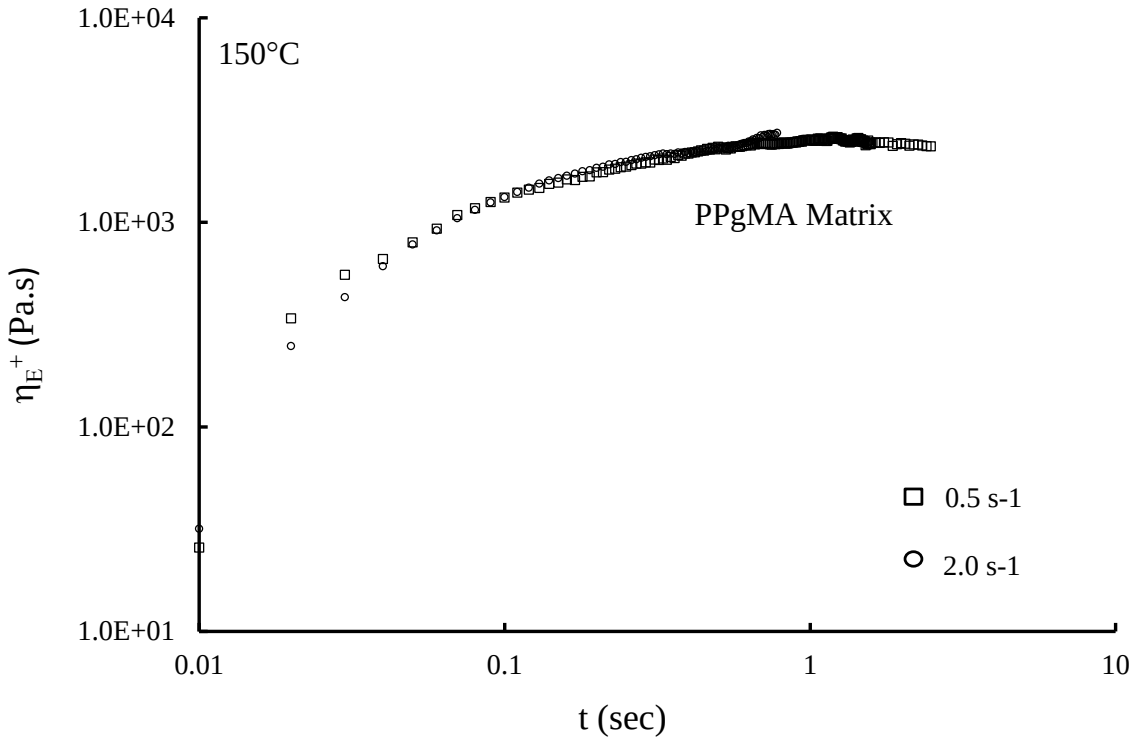

Figure 3.14. Transient extensional viscosity curve for maleated polypropylene matrix.

It can be clearly seen that the neat matrix doesn't show any strain hardening characteristic for the different extensional strain rates. However by the addition of just 5 wt% of nanoclay in the polymer matrix significant amount of strain hardening is observed for the nanocomposites with different clays as seen in Figure 3.15.

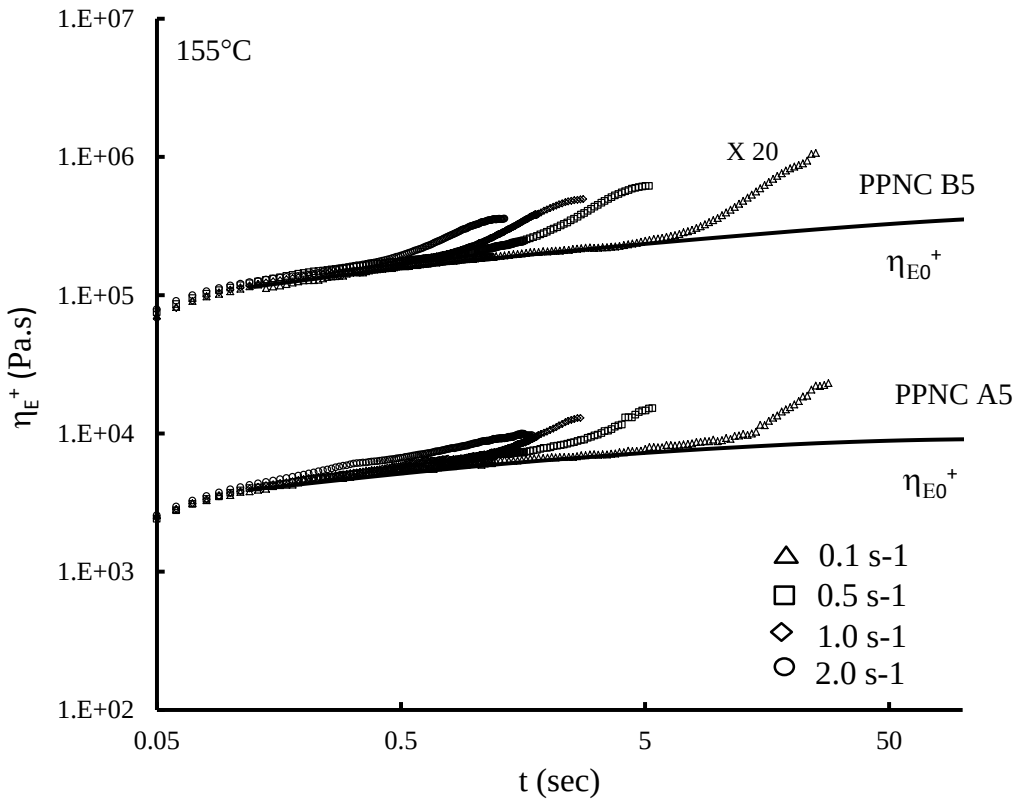

Figure 3.15. Transient extensional viscosity curve for nanocomposites A5 and B5 at 155° C and four extensional strain rates: $0.1s^{-1}$ (Δ), $0.5s^{-1}$(□), $1s^{-1}$(◊) and $2s^{-1}$(○).

In general, with any additive that causes strain hardening, Sugimoto et al. [76] and Wagner et al. [91] have observed that larger relaxation times lead to greater extents of strain hardening. Larger relaxation times would be associated with stronger entanglements. The maleated polypropylene chains that are physically attached at the ends to the clay edges would entangle with the bulk polymer chains thereby forming hindered chain entanglements. The increase in entanglements would in turn cause the polymer chains to relax slowly upon stretching thereby increasing the relaxation times. This kind of strain hardening behavior observed in maleated polypropylene – layered silicate nanocomposites is similar to that reported for polymer blends containing small amount of chemically cross linked polymer chains. Yamaguchi and

Miyata [79, 80] blended small amounts of cross linked terpolymer (gEHDM) characterized as gel just beyond the sol-gel transition point to a linear polypropylene. They observed that for systems with appropriate cross link density the stretching of trapped or hindered chains between the crosslinking points were responsible for the improved strain hardening behavior. Also, an increase in the crosslinking density leads to suppression of the strain hardening behavior. Yamaguchi and Suzuki [81] have similar reports wherein they blended small amounts of cross linked linear low density polyethylene to bulk linear low density polyethylene and the blends showed enhanced strain hardening behavior. It was reported that the cross linked polymer chains formed trapped or hindered chain entanglements with the bulk chain segments between the cross links which lead to improvement in the strain hardening of these blends.

3.4.3.2 Effect of surfactant head group and effective aspect ratio

Figure 3.15 shows a comparison between the transient extensional viscosity curves $\eta_E^+(t)$ for the nanocomposites PPNC A5 and PPNC B5 at four different strain rates and at a test temperature of 155˚C. The test temperature chosen is well above the melting point of the nanocomposites. It has been well know through literature that transient extensional viscosity measurements are difficult to obtain and therefore care should be taken while performing the EVF tests so that the test sample does not sag or neck during the test. Also, a relatively lower molecular weight, a low melting point and a high melt flow rate (150 g/10min @ 230°C/2.16 kg) of the maleated polypropylene matrix did not allow us to go to higher test temperatures on the extensional viscosity fixture. The comparison of the extensional viscosity transients show that the viscosity curve rose more sharply from the base viscoelastic envelope $3\eta_0^+(t)$ for nanocomposite PPNC B5 at each strain rate than the nanocomposite PPNC A5.

Quantitative comparison of the extents of strain hardening may be obtained by evaluating a strain hardening ratio χ which increases with increasing strain.

$$\chi = \frac{\eta_E^+(\dot{\varepsilon}, t)}{\eta_{E0}^+} \quad \text{..... (3.2)}$$

Where, η_E^+ is the transient extensional viscosity and η_{E0}^+ is the base viscoelastic envelope. There are in general couple different methods to obtain the linear viscoelastic envelope: (a) by measuring or calculating from the relaxation spectrum a linear zero shear viscosity growth curve, or (b) by extrapolating the linear part of the extensional viscosity curve. Unlike homogenous polymer melts, for nanocomposite systems it is observed that there is an offset between the base viscoelastic envelope and the linear region of the extensional viscosity curves. Such observations have been previously made by Okamoto and coworkers for polypropylene clay nanocomposites [88]. To take into account such constant offsets, here method (b) was chosen to obtain the linear viscoelastic envelope and calculate the reduced strain hardening parameter χ/χ_0. A plot of χ/χ_0 versus the strain rate at a Hencky strain of 2.25 is shown in Figure 3.16. It is further evident from this plot that the level of strain hardening in PPNC B5 nanocomposite is greater than that observed for PPNC A5 nanocomposite at all given extensional strain rates. Hence a greater extent of strain hardening in the nanocomposite was obtained with the quaternary ammonium ion, 2-alkyl tail surfactant clay than with the more tightly bound primary amine ion, single alkyl tail surfactant clay. The higher amount of strain hardening in the I.44P clay nanocomposite can be explained on the basis of a higher effective aspect ratio of these nanoclay particles in the composite.

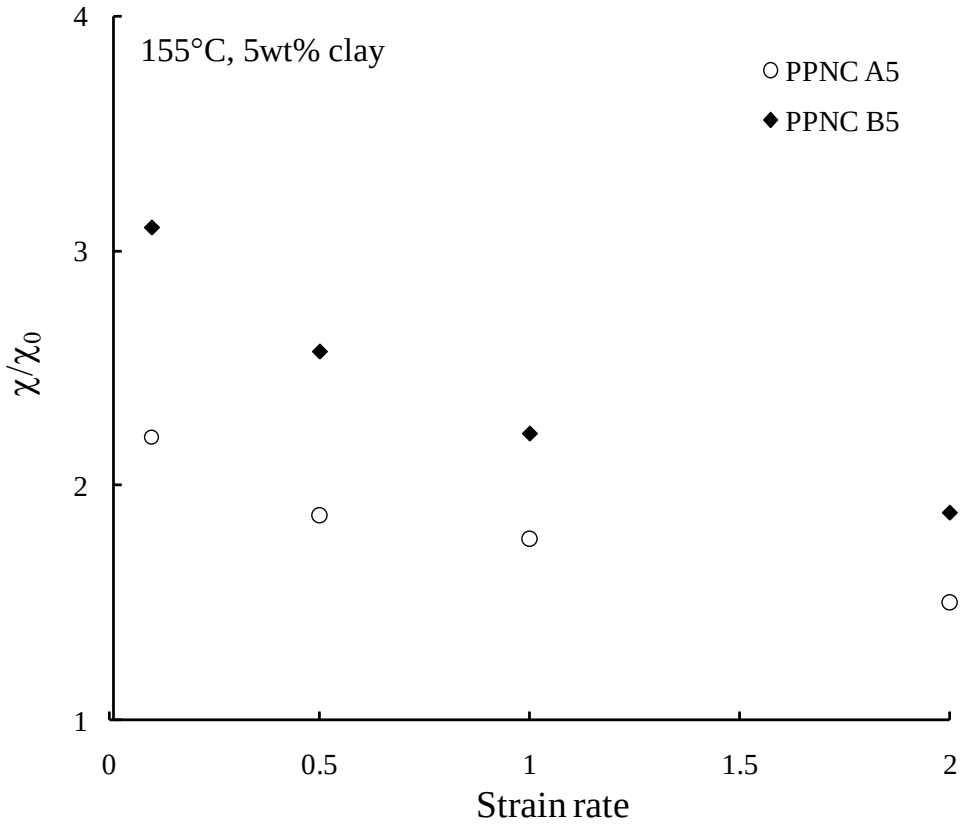

Figure 3.16. Reduced Strain hardening parameter v/s strain rate: Comparison at Hencky strain of 2.25 for PPNC –A5 and B5 at 155° C.

With higher effective aspect ratio, the number of interfacial interaction sites on the clay platelet increases thereby increasing the chance of having more physical attachments between the filler and the polymer chain as shown in figure 3.17. With an increase in the number of particle attached polymer chains the possibility of these chains forming entanglements with bulk matrix free polymer chains increases, thereby increasing the overall entanglement density. The increase in such entanglements in turn causes the overall polymer-particle entanglement network to relax slowly and have longer relaxation times.

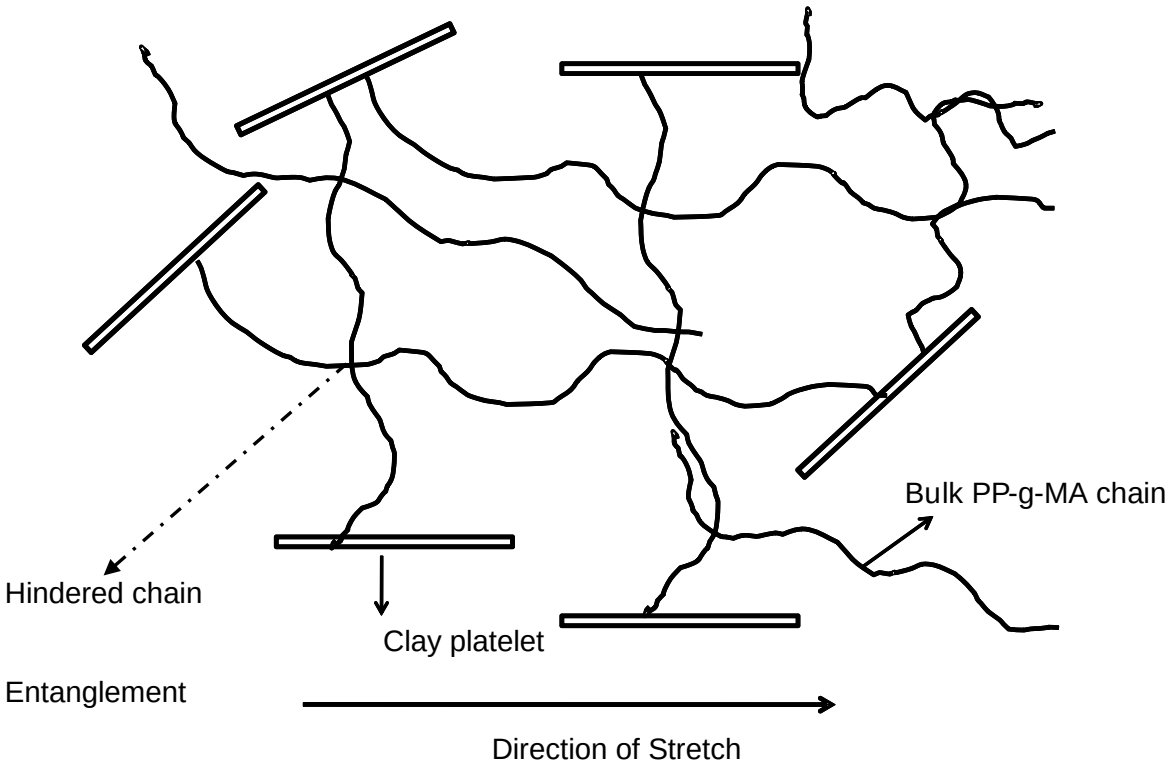

Figure 3.17. Schematic of the interaction between the PP-g-MA chains and organoclay.

This increase in the entanglement density is reflected not only in the strain hardening behavior in extension but also in the nonlinear and linear shear viscoelastic behavior for PPNC B5. Also the strain hardening observed is highest for the lowest strain rate for both nanocomposites and decreases with increasing strain rates.

3.5 CONCLUSIONS

Two different layered silicates were dispersed equally well (at about 2 vol%) in a high molecular weight (M_w=180,000) linear maleated polypropylene copolymer (with ethylene) which melts at 145°C; no other component was used. The aspect ratios (side / thickness) of the two different nanoparticles dispersed were determined to be 56 and 68 from measurements of

relative dynamic viscosity on the nanocomposite melts. The low frequency storage modulus of the nanocomposite with the higher aspect ratio nanoparticles was greater indicating a stronger filler network and/or a greater fraction of polymer chains attached to the particle surface with higher aspect ratio. Large amplitude oscillatory shear measurements on the nanocomposite melt with the higher aspect ratio particles showed a two stage drop in the storage modulus with increasing strain which highlights the breakup of two structures—the particle network followed by the hindered chain entanglement network involving attached chains. The buildup of structure during recovery is also slower for the nanocomposite with the higher aspect ratio nanoparticle system. Both nanocomposite melts display strain hardening in uniaxial extensional flow over several strain rates, unlike the matrix polymer which shows no strain hardening: the melt with the higher aspect ratio layered silicates displayed a higher extent of strain hardening at all rates. This last phenomenon may be attributed to the greater incidence of particle attached chains and entanglements involving these chains when the particle aspect ratio is greater.

EEFECT OF LOADING AND TEMPERATURE ON NON LINEAR RHEOLOGY OF MALEATED LINEAR POLYPROPYLENE-CLAY NANOCOMPOSITES

CHAPTER 4

4.1 INTRODUCTION AND BACKGROUND

Strain hardening of polymer melts in elongational flow, which in particular is a rise in polymer melt viscosity (above the linear viscoelastic limit) with increasing Hencky strain, is desirable for variety of polymer processing operations such as thermoforming, foaming and blow molding. Recently, structurally modified polymers, cross linked polymer blends and polymer composites, that show strain hardening property, have been widely developed for various applications in automotive industries, for food packaging films, etc. The study of the extensional flow behavior of these polymer nanocomposite melts is very important for the above mentioned processes and as such the measurements of transient uniaxial extensional viscosity for such polymer melts become important. Transient uniaxial extensional viscosity [69-71] and melt strength [72-74] of pure polymer melts and their blends have been measured previously to understand their stain hardening behavior.

Polypropylene (PP) is a widely used commodity polymer and linear PP does not strain harden upon melt extension. Researchers like Sugimoto have shown that strain hardening can be achieved in linear PP by introducing branched molecular structure through irradiation [75] or by adding a small amount of uhmw–PE to linear PP [76]. Extensional viscosity and strain hardening behavior of polymers with micro fillers have been investigated with different sizes, shapes and aspect ratios by Takahashi et al. [84], Le Meins et al [85] and Bhattacharya and coworkers [66,

86] and it has been shown that the strain hardening goes down with filler addition and even more so with high aspect ratio particles such as fibers. They observed that the formation of aggregates led to a decrease in strain hardening behavior. However, Seong and coworkers [87] dispersed Closite nanoclay in Polyamide 6 matrix and observed that with well dispersed systems there was an improvement in the storage modulus, viscosity as well as the strain hardening behavior in extension. Okamoto et al. [88, 89] dispersed treated montmorillonite clay in maleated polypropylene and investigated the strain hardening as well as rheopexy features of the nanocomposites.

In our previous work, we have shown that the addition of a small amount of nanoclay (5 wt%) to linear maleated polypropylene improves its strain hardening behavior significantly. We have further shown that the effective aspect ratio of dispersed nanoparticles and the nanoclay surfactant chemistry also affect the strain hardening behavior as well as the linear and nonlinear viscoelasticity of these nanocomposites. The improvements in the strain hardening behavior as well as the modulus recovery in nonlinear shear rheology were explained by considering the nanocomposite system to be similar to a blend of particle attached polymer chains and free matrix polymer chains. The polymer chains form physical cross links (-OH bonds) with the layered silicates and these chains in turn form hindered chain entanglements with other bulk polymer chains.

Yamaguchi and coworkers [79-81] made a similar observation of increase in reinforcement as well as strain hardening while working with blends of linear PP and chemically cross linked terpolymer (gEHDM) characterized as gel just beyond the sol-gel transition. They observed that the addition of a small amount of cross linked terpolymer (gEHDM) characterized as gel just beyond the sol-gel transition point to a linear polypropylene improved the strain hardening

behavior of the blend greatly. They suggested that with appropriate cross link density, the stretching of hindered chains between the crosslinking points were responsible for the strain hardening. However, an increase in the crosslinking density leads to suppression of the strain hardening behavior. Similar reports on decrease in strain hardening with increasing degree of chemical cross linking in the gel phase of the blend have been given with PMMA systems by Takahashi and Ogura [82]. These kinds of observations made with linear and chemically cross linked polymer blends leave us with a question in our work, as to whether a change in the loading of nanoclay particles to the linear maleated polypropylene affect its strain hardening behavior or not. It would be of great interest to investigate the strain hardening behavior of nanocomposites having a higher loading of nanoclay and check for the mechanisms that may or may not affect the strain hardening and reinforcement in the nanocomposites. Therefore, to answer all these questions, we varied the nanoclay loadings in the linear polypropylene matrix in this chapter and studied the linear shear, nonlinear shear and extensional rheology of the nanocomposites.

In this study, a polypropylene copolymer (with ethylene) grafted with maleic anhydride, also called as linear maleated polypropylene (PP-g-MA), is used as the matrix to which a layered silicate (Montmorillonite) was added as the filler. The montmorillonite clay is organically modified by incorporating quaternary ammonium ions in the interlayer galleries. From our previous work, this organoclay (I.44P Clay – B) shows a higher effective aspect ratio upon dispersion in the linear PP matrix as well as a better strain hardening behavior in extensional flow as compared to another clay with primary amine surfactant chemistry (I.30P Clay – A). The organoclay used in this study was melt mixed at different loadings with linear maleated polypropylene and several different nanocomposites were made. These nanocomposites were

tested for nonlinear, uniaxial extensional melt viscosity as well as low amplitude and high amplitude oscillatory shear rheology. Also, the effect of increasing the test temperature on the strain hardening behavior of these nanocomposites has been investigated.

4.2 EXPERIMENTAL TECHNIQUES

4.2.1 Materials

The matrix material is linear maleated polypropylene (PP-g-MA) (Exxelor PO1015) with 0.4 wt% maleic anhydride and a molecular weight of 180,000. (ζ =0.9 g/cc). It is important to choose a PP-g-MA having a high molecular weight and substantial polymer chain length necessary for the formation of hindered chain entanglements. Exxelor PO1015 was chosen amongst several other PP-g-MA's (Honeywell AC 950 and AC 1325) to fit the criteria for this study. The melt mass flow rate (MFR) of the neat PP-g-MA matrix is 150g /10 min at 230°C under a load of 2.16 kg and it melts at 145°C. The organoclay used for preparing the nanocomposites was Nanocor I.44P which had quaternary ammonium ion surfactant with two C-18 tails (Clay – B).

4.2.2 Compounding

PP-g-MA and the clay were dried overnight at 100°C and 20 mm Hg vacuum in a vacuum oven and then compounded with maleated polypropylene at 165° C and at 150 rpm for 10 minutes in a Banbury mixer; this was done under nitrogen to avoid thermal degradation. One batch of the mixer amounted to 47 grams of compound. The compounded material was removed from the mixer with a brass scraper and ground up with a mini granulator. The different nanocomposites and their formulation composition are given in Table 4.1. Based on the amount

of maleation on PP-g-MA and the weight of clay added to the polymer a ratio of g-mol of MA / kg of clay is also given for the different nanocomposite formulations in the table.

4.3 CHARACTERIZATION TECHNIQUES

4.3.1 DSC and TGA Measurements

The melting temperature of the nanocomposite pellets as well as the neat polymer was obtained using DSC runs on a TA DSC instrument. The melting point of neat PP-g-MA was 145°C while the nanocomposites melted around 146.5°C. Hence, the melt compounding was carried out at 165°C and compression molding was carried out at 175°C which is well above the melting points of these nanocomposites. Thermo gravimetric Analysis was carried out on the pure clay, neat matrix as well the nanocomposites on a TA Q500 TGA instrument from 4°C to 600°C through a high resolution temperature ramp of 10°C / min.

4.3.2 X ray Diffraction Measurement

All the clays and nanocomposites were analyzed using X-ray diffraction patterns. The characterization of the structure by XRD was performed on the compression-molded disks with a Rigaku Rotaflex Ru-200BH X-ray diffractometer, which is equipped with a Ni-filtered Cu K α radiation source and operated at 45 kV and 100 mA. The sample was scanned over a 2θ range of 0.5° to 10° at a rate of 0.5°/min and measurements were recorded at equal increments of 0.01°.

4.3.3 Extensional Viscosity Measurement

An extensional viscosity fixture (EVF) mounted on a TA-ARES rheometer was used to record the transient uniaxial extensional viscosity at strain rates ranging from $0.1s^{-1}$ to $2s^{-1}$ up to

a Hencky strain of 3. A 20-specimen mold was used for compression molding samples 18mm long, 10mm wide and 0.7mm thick for the EVF tests. Test specimens were molded at 175° C and the mold was cooled slowly using cooling water under a pressure of 5 tons. This ensured stress free and relaxed homogenous samples with minimum dimensional variation. The molded specimens were dried overnight before performing the extensional tests at two different test temperatures --155° C and 160° C. The test samples were examined after completion of the test and if any necking was noted in the stretched portion in the middle, the test was rejected.

4.3.4 Shear Rheology

Parallel plate geometry on a TA Instruments AR2000 rheometer was used to perform frequency sweep tests on these nanocomposites. The diameter of the parallel plates was 40 mm and a frequency range of 0.01 to 100 ω (rad/s) at 0.5% strain amplitude was chosen to perform these tests. The corresponding storage modulus and complex shear viscosity were noted over the entire frequency range. The strain amplitude was chosen such that it was in the linear viscoelastic region and this was found out by running strain sweep tests at 1 rad/s on the nanocomposites. A time sweep was also carried out on these nanocomposites on the 40 mm parallel plate geometry for about 1 hour to check for the stability of modulus for these nanocomposites with respect to time. Strain sweep tests were performed for probing into the non-linear viscoelasticity of the nanocomposites by varying the strain amplitude % from 0.1 to 100. A continuous purge of nitrogen was supplied during these tests to avoid thermal degradation.

4.4 RESULTS AND DISCUSSION

4.4.1 Dispersion of nanoclay and thermal stability of nanocomposites

The I.44P organoclay melt mixed with linear polypropylene has a quaternary onium ion surfactant with two alkyl tails in the clay interlayer galleries. Heinz et al. [29] have commented on the structure and conformation of the surfactants in the interlayer galleries. They have shown through computations that the quaternary onium ion surfactant with two C-18 tails is more mobile in the interlayer galleries and it also packs to a greater extent in these galleries. The extent of surfactant packing can be judged from the X-ray diffraction pattern of the I.44P organoclay, presented in Figure 4.1. It can be seen that the first X-ray diffraction peak for I.44P clay occurs

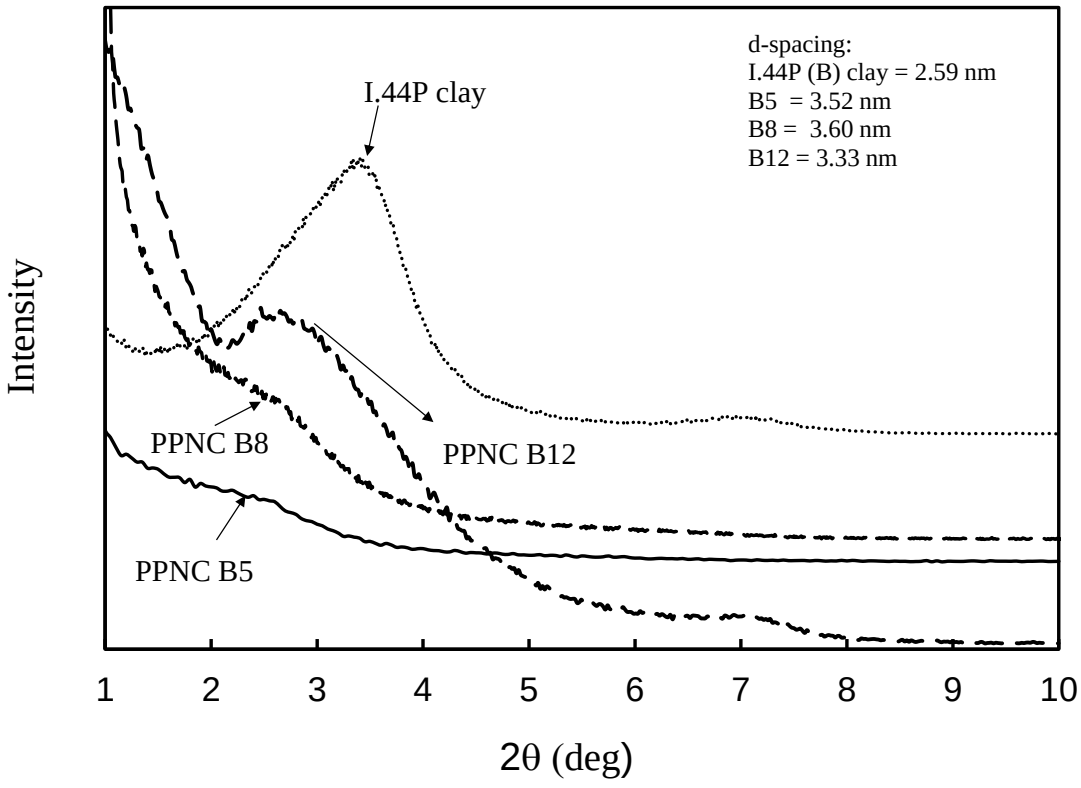

Figure 4.1. X-ray diffraction of organoclay: a) I.44 P clay, b) B5 nanocomposite (5wt% clay), c) B8 nanocomposite (8 wt% clay), d) B12 nanocomposite (12 wt% clay).

at a 2θ value of 3.4 degrees which corresponds to a basal spacing of 2.59 nm. We infer that the greater basal spacing of the I.44P clay is mainly because of the greater extent of surfactant packing in its interlayer galleries. Figure 4.1 also shows the XRD patterns for the different nanocomposites made with 5, 8 and 12 wt% of the I.44P nanoclay. The nanocomposites with 5 and 8 wt% clay do not show a prominent peak in the XRD, but a presence of a slight shoulder in the diffraction pattern. The d-spacing calculated for the nanoclay particles in these composites is around 3.5 nm (greater than that of base clay) indicating that the interlayer galleries in clay have been swelled by the polymer chains. The presence of this shoulder in XRD suggests that there must be some intercalated clay structure present in these nanocomposites. Also, the shoulder becomes more prominent and sharp in the 12 wt% filled nanocomposites with a decrease in the d-spacing to 3.33 nm. This indicates that at higher loading, the dispersion of clay is not as efficient and that there is an increase in the intercalated structure with more filler addition creating a higher probability of particle-particle interaction than that of polymer –particle interaction.

Figure 4.2 shows the %weight lost with increase in temperature for the clay, neat matrix and nanocomposites. The dispersion of clay in the matrix has increased the thermal stability of the composites by 50°C-55°C. The neat matrix decomposes completely around 400°C. The amount of clay dispersed in the nanocomposites was calculated from the char yield at 600°C and was about 5% for B5 nanocomposite and 7.9% for B8 nanocomposite.

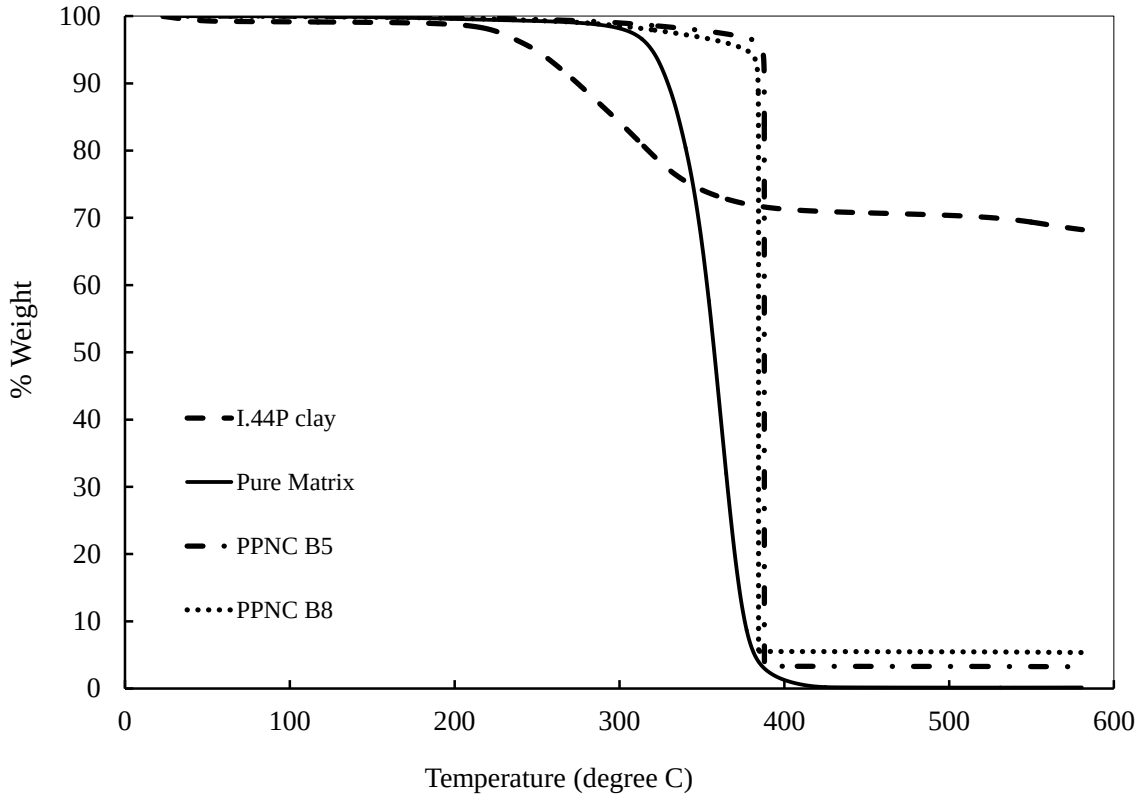

Figure 4.2. Thermo Gravimetric Analysis (TGA) curves obtained for pure clay, neat matrix, and nanocomposites at 10°C / min up to 600°C.

The stability of the modulus of maleated polypropylene matrix and the nanocomposites with the 5wt% of the I.44P organoclay was also checked with the help of a time sweep. The time sweep was carried out for about one hour and at 1 rad/s frequency and 0.5% strain amplitude. It can be seen from Figure 4.3, that the modulus of the matrix and the nanocomposite was stable and did not fluctuate over

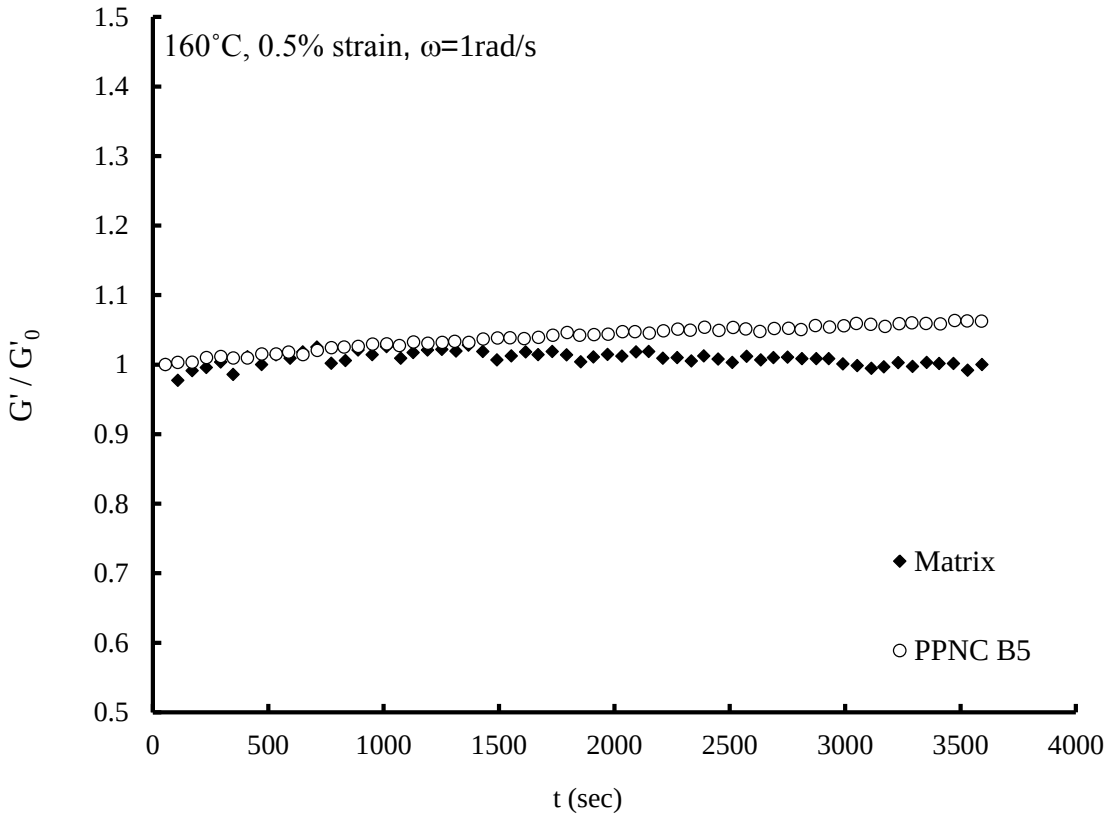

Figure 4.3. Comparison of the increase in storage modulus for the matrix and B5 nanocomposite at 160° C for 1 hour.

the time period of the test. The strain amplitude chosen was obtained by running strain sweep tests on the nanocomposites at 1 rad/s angular frequency and was found to be well within the linear viscoelastic regime.

4.4.2 Oscillatory Shear rheology

4.4.2.1 Linear Viscoelastic Measurements

The frequency sweep measurements done by parallel plate oscillatory shear rheology yielded results of the dynamic modulus and dynamic viscosity of the nanocomposites, in the linear viscoelastic regime. A comparison of the dynamic viscosities for all three composites as

well as the base polymer matrix is shown in Figure 4.4. The dynamic viscosity increases with an increase in the nanoclay loading, it being highest for composite PPNC B12 over entire frequency range.

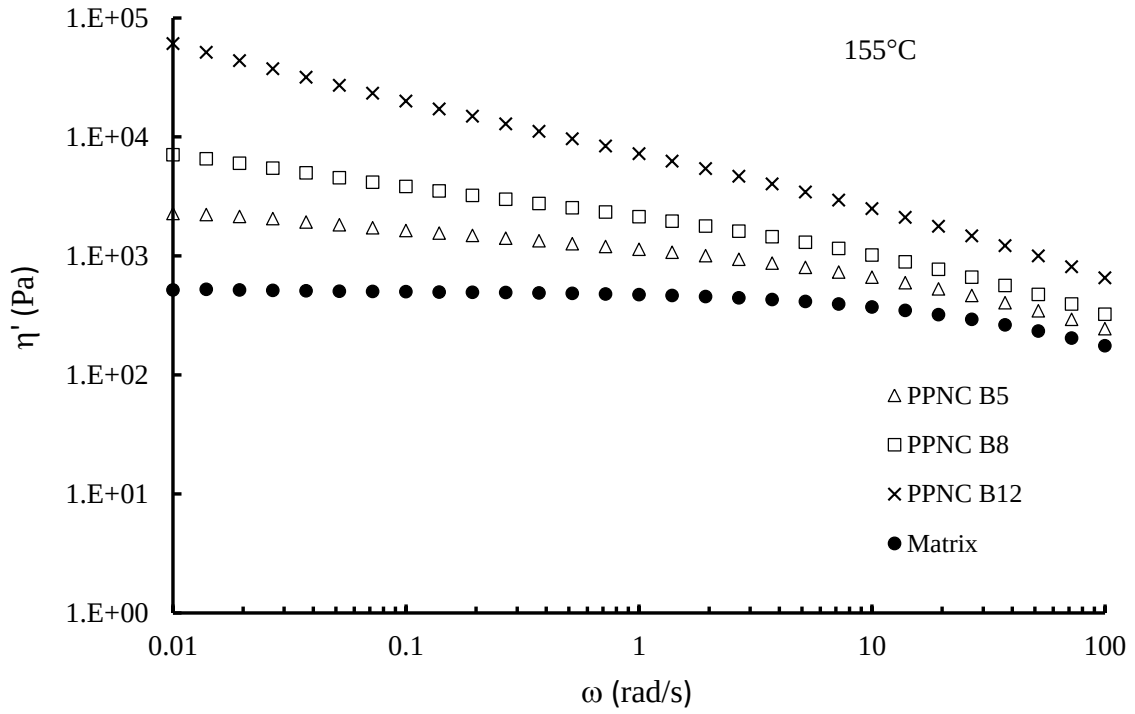

Figure 4.4. Complex viscosity curves for the neat matrix (●) and nanocomposites: PPNC B5 (Δ), PPNC B8 (□), and PPNC B12(×)

The dynamic viscosity for the pure matrix is fairly constant at lower values of the frequency. However, the dynamic viscosity for the nanocomposites does not show a complete leveling off at lower frequencies, indicating a more elastic response in these nanocomposites. The elastic or solid like response increases gradually from PPNC B5 to PPNC B8 composite and is most prominent for PPNC B12 in the low amplitude frequency region. This is further evident

from Figure 4.5, which shows a comparison of the dynamic storage moduli of these nanocomposites with the matrix.

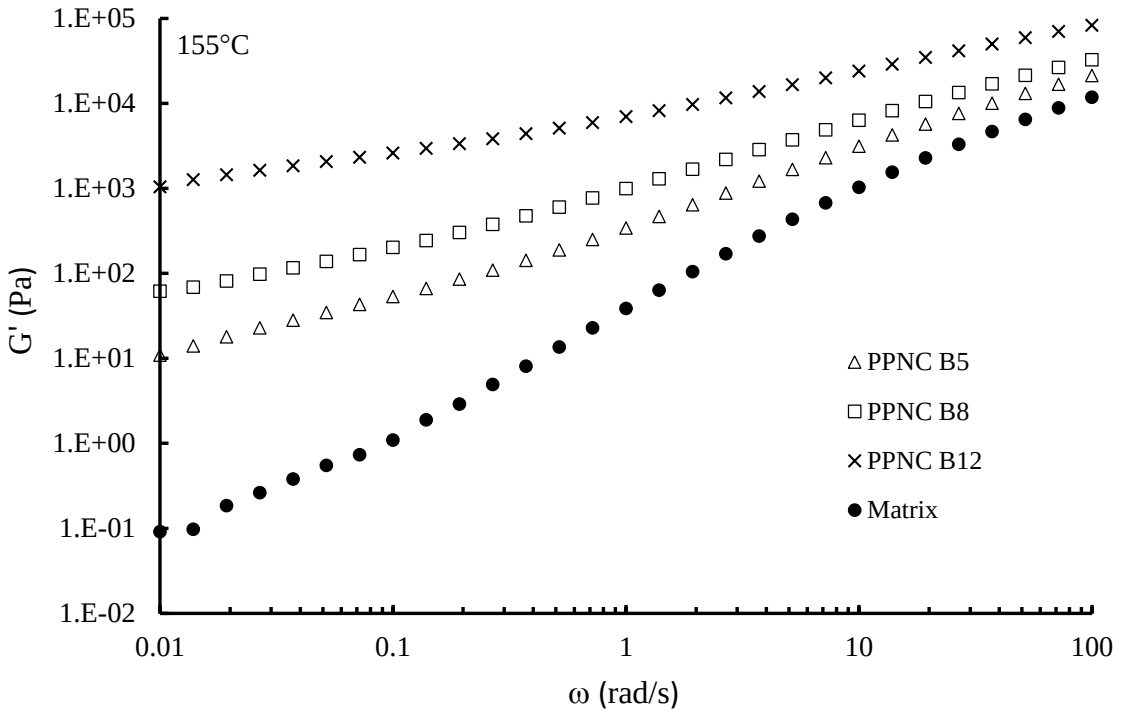

Figure 4.5. Storage Modulus (G') curves versus frequency (ω) for the neat matrix (●) and nanocomposites: PPNC B5 (Δ), PPNC B8 (□), and PPNC B12(×)

The nanocomposites show a higher modulus than the polymer matrix over the entire frequency range and a plateau like region in the low frequency range, especially for the nanocomposite with the greatest filler content. The increase in the low frequency storage modulus was about hundred fold from the melt with 5wt% to that with 12wt% loading. As discussed in chapter 3, the low frequency "plateau" in the storage modulus can be attributed to two different contributions: (1) filler particle network formed by van der Waals interactions or bridging and (2) entanglements between free chains and particle attached polymer chains. For

composites with higher filler loadings, it is seen in literature that an increase in the low frequency modulus is mainly because of the filler network formed by particle-particle interactions [97]. To understand and narrow down the actual contribution responsible for the increase in viscosity and modulus values of the nanocomposites, we further investigated the dispersion levels of the clay platelets at different nanoparticle loadings by calculating their effective aspect ratio in the nanocomposites. This was estimated with the Pierce-Maron empirical model that correlates the relative shear viscosity with the volume fraction of nanoparticles in a concentrated suspension as shown in equation 3.1 and 3.2. The relative dynamic viscosities were taken in the low frequency range. These viscosity ratios were correlated with that of volume fractions for the nanoparticles and maximum packing fraction at each weight loading and the effective aspect ratios were calculated as explained in chapter 3. The results of the effective aspect ratios are tabulated in Table 4.1.

Table 4.1. Details of Aspect Ratio Estimation for Nanoparticles in Various Composites.

PPNC	Clay loading wt %	ϕ	g-mol MA / kg clay	η'_{rel}	ϕ_M	a=D/t	ϕ a
B5	5	0.027	0.78	4.38	0.052	68	1.84
B8	8	0.044	0.47	13.7	0.060	59	2.55
B12	12	0.067	0.38	117	0.074	48	3.15

Note: Composition of Polypropylene Nanocomposites, amount of bound maleic anhydride / kg of clay, relative dynamic viscosity (η'_{rel}), particle volume fraction (ϕ), Maximum packing fraction (ϕ_M) and effective aspect ratio (a) of nanocomposite are at 155°C

It can be seen that with an increase in the weight loading of the nanoparticles the maximum packing fraction of the particles goes up and the effective aspect ratio decreases. This can indicate that with more nanoparticles the dispersion level goes down progressively and there is presence of more stacked particles in the nanocomposite. This was further evident in the XRD patterns of the 5wt%, 8wt% and 12 wt% I.44P filled nanocomposites as discussed earlier. The evidence from the XRD patterns and the decrease in effective aspect ratio with increase in filler loading does suggest that the actual contribution responsible for the higher viscosity and modulus values, especially in B12 nanocomposite, are mainly due to the filler network formed by particle-particle interactions.

4.4.2.2 Non-Linear Viscoelastic Measurements

Non-Linear viscoelasticity in composites can be observed both in large amplitude oscillatory shear and in extensional flow. In dynamic shear rheology, higher levels of strain amplitude lead to strain softening of the dynamic moduli and the critical strain at which this begins, scales with the loading level of filler particles. It has been discussed in chapter 3, that higher levels of reinforcement for the linear PP and layered silicate nanocomposites is associated with the formation of hindered chain entanglements between the free PP matrix chains and the particle attached chains. It was also shown that at large strain amplitudes, the dynamic moduli begin to drop at a critical strain. This drop was attributed to the breaking up of two structures—the particle network followed by the hindered chain entanglement network involving attached

chains. Cassagnau [97] also has showed the effect of non-linearity in silica filled composites of different polymeric materials. He investigated the effect of filler particles and their loadings on the subsequent strain sweeps in nonlinear shear and pointed out that the degree of non-linearity increases with filler concentrations. He established this occurrence as a result of the "Payne effect" and also developed a correlation between the critical strain and the volume fraction of the fumed silica particles.

In the present work, the nanocomposites having different nanoclay loading were tested for their nonlinear viscoelastic behavior by performing strain sweep tests at a test temperature of 155°C and a frequency of 1 Hz.

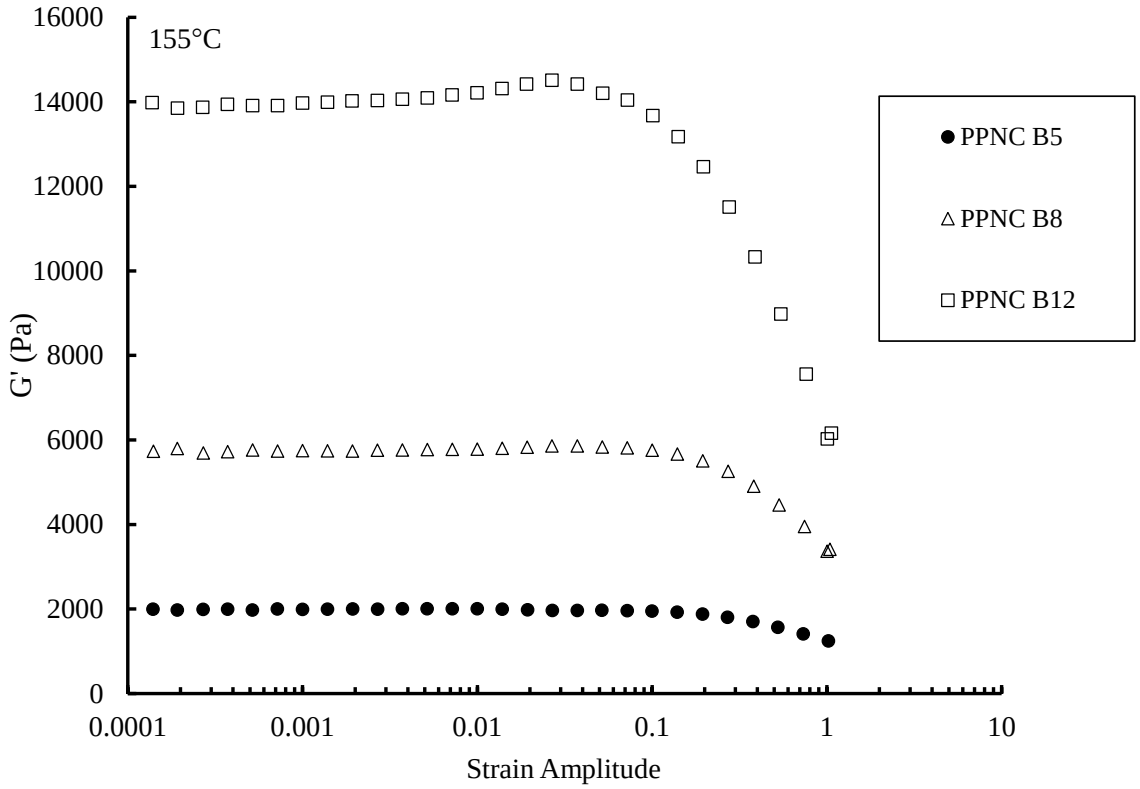

Figure 4.6. Strain sweep tests. Variation of storage modulus with strain amplitude for PPNC B5 (●), PPNC B8 (Δ), and PPNC B12(□) at 155°C and 1 Hz

The strain amplitude varied from 0.1% to 100% and the consequent storage and loss moduli were recorded. Figure 4.6 shows the strain sweep measurements on PPNC B5, PPNC B8 and PPNC B12. It was observed that the storage moduli increased with an increase in the filler loading for all strain amplitudes. The modulus, however showed a sharp drop as the strain increased and this was most evident in the highest filled composite – PPNC B12.

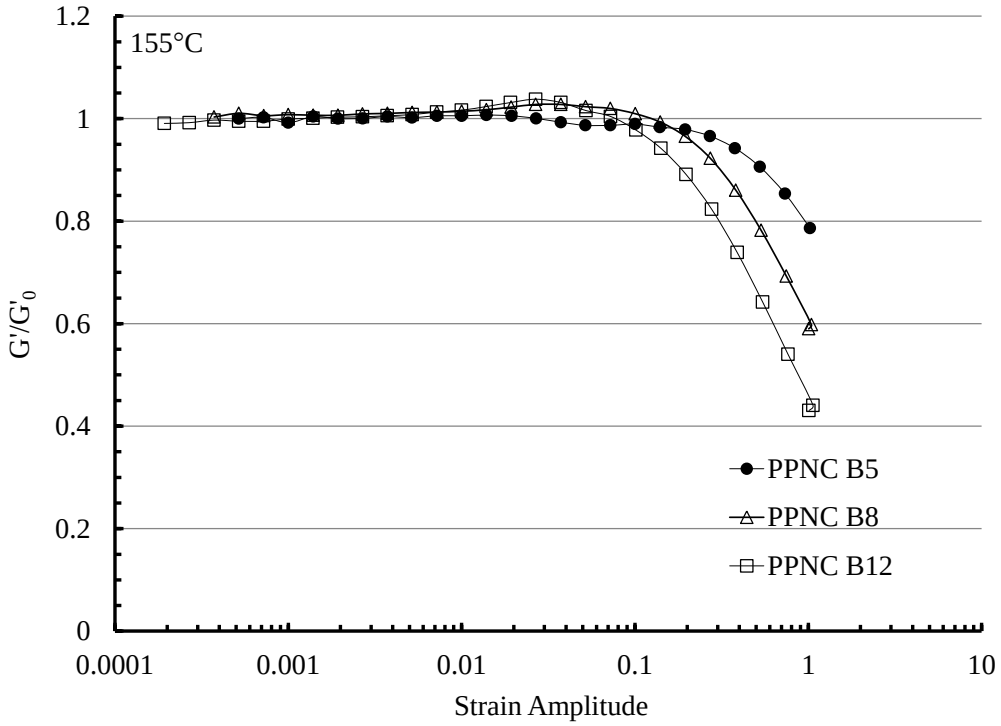

Figure 4.7. Strain sweep tests. Reduced Storage Modulus versus strain amplitude for PPNC B5 (●), PPNC B8 (Δ), and PPNC B12(□) at 155°C and 1 Hz.

Such a drop in the moduli values with increasing strain is a result of the strain softening mechanism which is generally observed as the" Payne effect". The causes of a drop in the modulus or strain softening are, in order of importance (i) Breaking of particle-particle network, (ii) Breaking of hindered chain entanglement network. Furthermore, it can be seen that the

"critical strain" at which the storage modulus begins to drop is lower for the higher filled loadings. It is the lowest for PPNC B12, indicating that the non-linearity sets earliest in this composite. This is more evident from Figure 4.7, which is a plot of the reduced shear modulus v/s the strain. Also a maximum is observed in the storage as well as loss modulus for PPNC B12 nanocomposite just before the critical strain. This could suggest that with increasing strain perturbations the filler network gets rearranged in the B12 composite such that it increases the moduli values just before the critical strain. At the critical strain, the perturbation is large enough to break down this filler network and causes a sudden drop in the moduli values. The loss moduli of these nanocomposites, as shown in figure 4.8, also show a trend similar to that of the storage moduli.

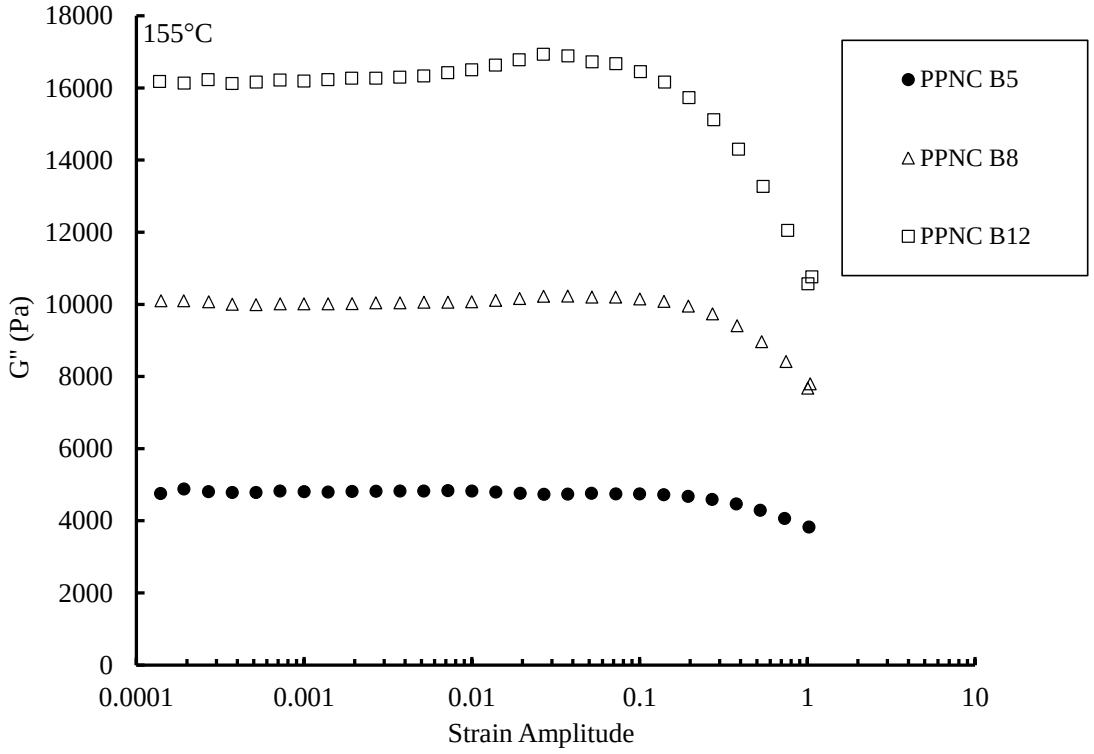

Figure 4.8. Strain sweep tests. Variation of loss modulus with strain amplitude for PPNC B5 (●), PPNC B8 (Δ), and PPNC B12(□) at 155°C and 1 Hz

To understand the effect of aspect ratio on non-linearity of these nanocomposites, we calculated the specific surface area (A_{sp}) of particles / g clay as shown in Table 4.2. It can be seen that as the aspect ratio goes down with increasing filler loading, the overall specific surface area available for interaction with the polymer chains also goes down. This area was then correlated to the critical strain at which the storage modulus shows a sharp drop in strain sweep experiments for each nanocomposite. Figure 4.9 shows such a correlation and it can be seen that the critical strain decreases along with a decrease in the specific surface area (A_{sp}).

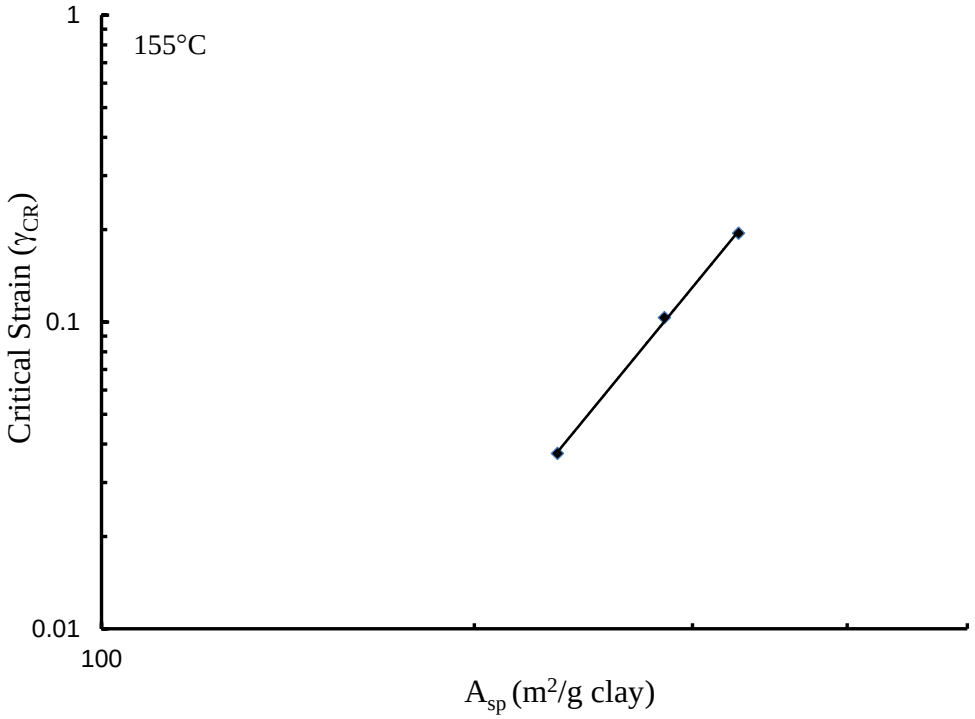

Figure 4.9. Critical Strain Plot: Variation of critical strain with respect to Specific Surface Area (A_{sp}) per gram of clay.

In the case of PPNC B12 it is seen from the linear viscoelastic data and the XRD patterns that there is a higher probability of particle-particle interaction which is consistent with a lower effective aspect ratio and a lower critical strain. As compared to that, PPNC B5 and PPNC B8 have much higher effective aspect ratios and greater specific surface area per gram of clay that is available for interaction with polymer chains which lead to more chances of particle-polymer interactions than particle-particle interactions. In order to break down the combination of these two interactions, it requires slightly higher strain amplitude and as such the critical strain is higher in the case of PPNC B8 and highest in the case of PPNC B5.

4.4.2.3 Modulus recovery after strain sweep

Another significant aspect of understanding the mechanisms of non-linear viscoelasticity in filled polymer systems is the recovery of modulus following the breakdown of the filler network caused by a large strain perturbation. Hence, similar to the work shown in previous chapter between two different clays, we investigated the complex modulus recovery kinetics from nonlinearity for the nanocomposites with different loadings. For this purpose, a time sweep experiment was run at lower strain amplitude (in linear viscoelastic region) immediately after a strain sweep experiment. Figure 4.10 shows the recovery kinetics of the storage modulus for all three nanocomposites. It can be clearly seen here that PPNC B5 shows a much faster recovery as compared to PPNC B8, whereas PPNC B12 does not show complete recovery in the given time range of the experiment. Also it can be seen from the time sweep experiment that the storage modulus keeps increasing even beyond the initial modulus that was measured before the strain sweep experiment for PPNC B5 and PPNC B8. This could imply that the strain sweep experiment acts as a trigger in rearranging the entanglement structure such that it requires much more time to reach an equilibrium state and have a leveled out modulus value.

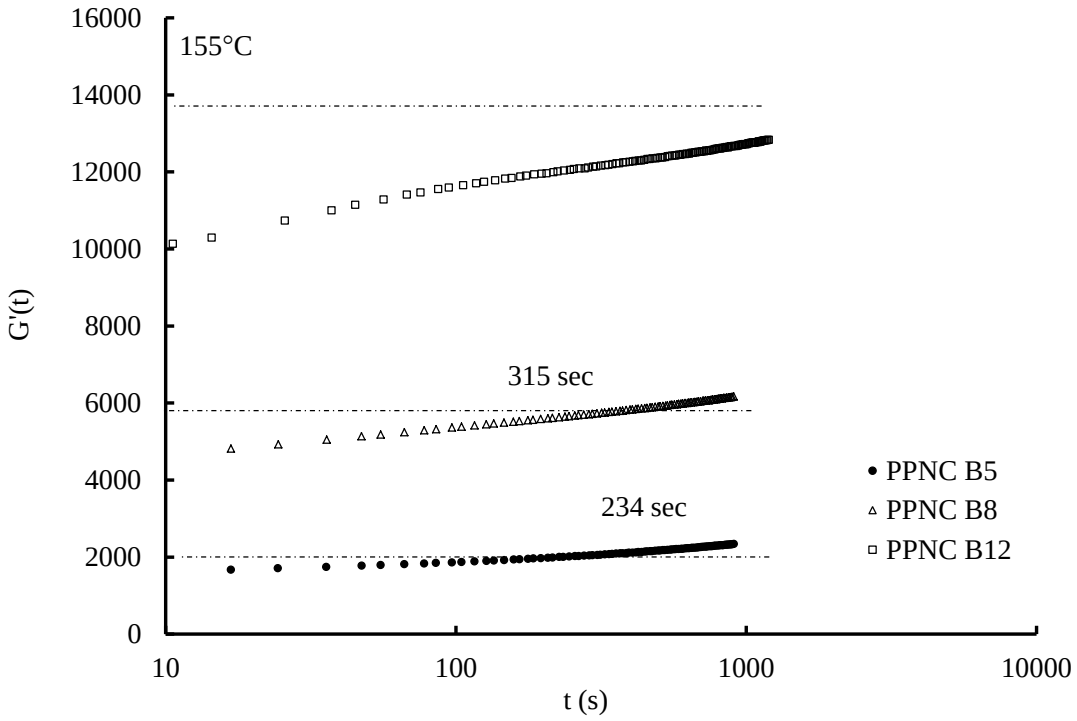

Figure 4.10. Storage modulus recovery versus time ($\omega = 1$Hz and $\gamma = 0.5\%$). PPNC B5, PPNC B8 and PPNC B12 nanocomposites at 155°C. G' (t) is the storage modulus value as obtained from time sweep test which is done immediately after one strain sweep.

The rate of recovery can also be compared between the nanocomposites by plotting the ratio of loss factor observed during the recovery time sweep to that observed in the linear viscoelastic region of the strain sweep experiment. Such a plot is shown in Figure 4.11. It can be seen through this plot that the loss factor value for PPNC B12 is much greater than that of PPNC B8 and PPNC B5. Also, since the drop in the storage modulus value after first time sweep was greater in case of PPNC B8, it takes slightly more time to reach that initial value as compared to PPNC B5. In case of PPNC B12 the time range of experiment is not sufficient to recover the drop in modulus completely.

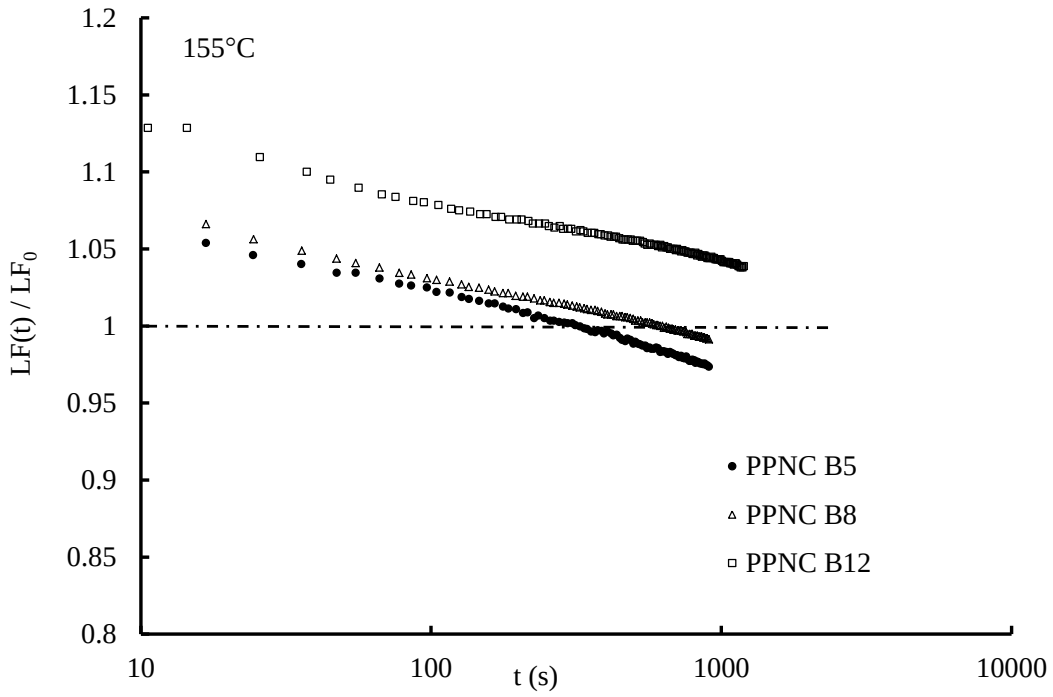

Figure 4.11. Rate of Recovery of the loss factor after initial strain sweep for PPNC B5, PPNC B8 and PPNC B12. The Loss Factor LF (t) is that obtained from the time sweep test and LF_0 is the plateau value of loss factor obtained from initial strain sweep test.

This could indicate that in PPNC B12 the non-linearity causes a much greater breakdown of the filler network and possibly disentanglement of the polymer chains, which hinders the recovery of the composite modulus.

4.4.3 Uniaxial Extensional rheology

4.4.3.1 Effect of filler addition and test temperature

It was established in the previous chapter, that neat matrix doesn't show any strain hardening for the different extensional strain rates measured in the uniaxial extensional flow

(Figure3.15). Also, by the addition of just 5 wt% of nanoclay in the polymer matrix significant amount of strain hardening is observed for the nanocomposites as seen in Figure 4.12.

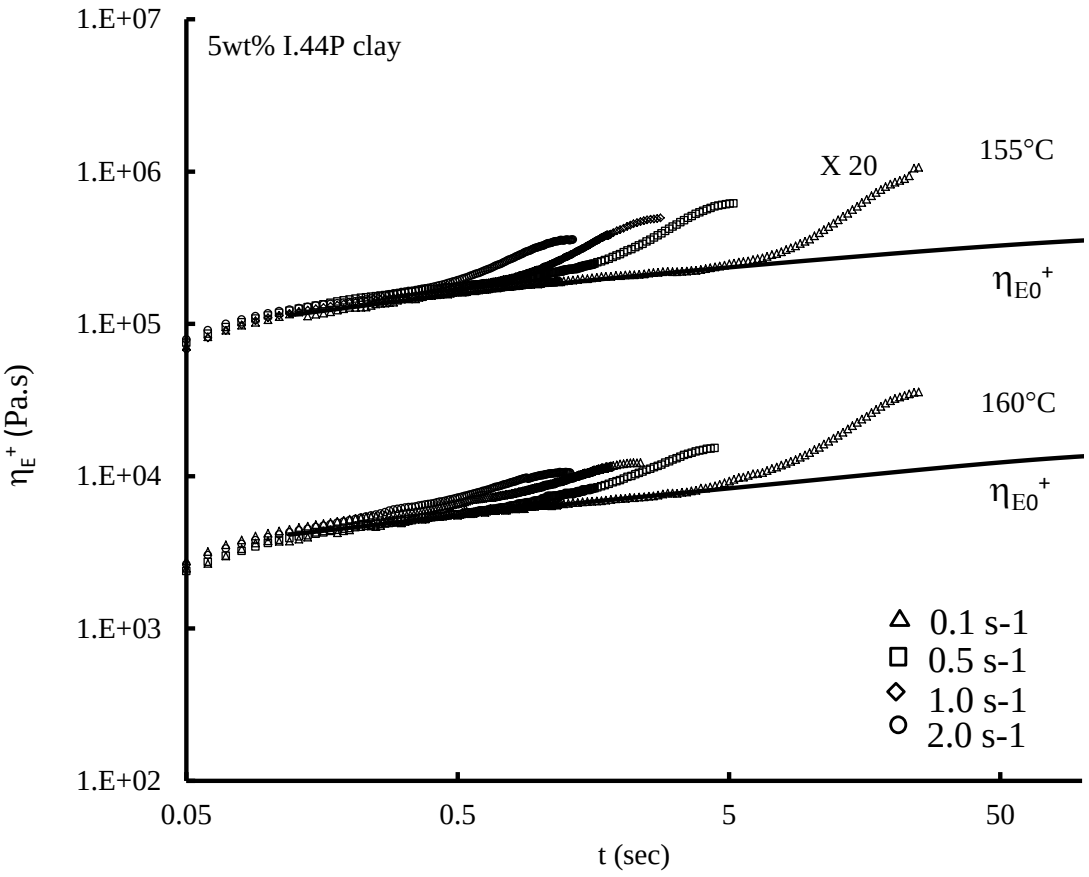

Figure 4.12. Transient extensional viscosity curve for nanocomposite B5 at 155° C and 160° C at four extensional strain rates: $0.1s^{-1}$ (Δ), $0.5s^{-1}$(□), $1s^{-1}$(◊) and $2s^{-1}$(○).

The addition of nanoclay provides the necessary interaction sites or cross link points on the edges and faces of the clay for the functional groups on the maleated polypropylene chains. The polymer chains form physical cross links with clay via hydrogen bonds and in turn entangle with the surrounding free matrix chains. These kind of entanglements that are formed between the particle attached polymer chains and free polymer chains are termed as hindered chain

entanglements and the increase in entanglements would in turn cause the polymer chains to relax slowly upon stretching thereby increasing the relaxation times. Figure 4.12 shows the transient extensional viscosity curves η_E^+ (t) for the nanocomposite with 5wt% I.44P clay at four different strain rates and at two different test temperatures: 155˚C and 160° C. The test temperatures chosen were well above the melting point of the nanocomposites. While doing the EVF tests care was taken such that the test sample does not sag or neck during the test. The samples that sagged were discarded. Also, a relatively lower molecular weight, a low melting point and a high melt flow rate (150 g/10min @ 230°C/2.16 kg) of the maleated polypropylene matrix did not allow us to go to higher test temperatures on the extensional viscosity fixture.

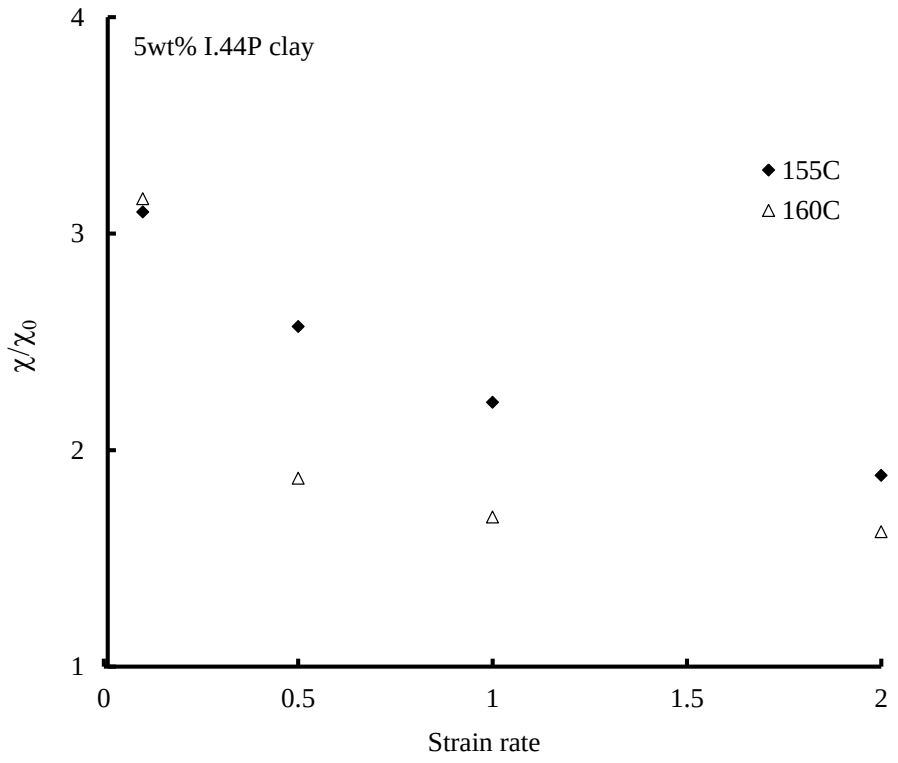

Figure 4.13. Reduced Strain hardening parameter v/s strain rate: Comparison at Hencky strain of 2.25, for PPNC B5 at 155° C (Δ) and 160° C (♦)

The comparison of the extensional viscosity transients show that the viscosity curve rose sharply from the base viscoelastic envelope $3\eta_0^+$ (t) for nanocomposite B5 at each strain rate for both the test temperatures. It can also be seen that temperature does affect the strain hardening behavior slightly, especially at higher strain rates. This is evident from a plot of χ/χ_0 versus the strain rate at a Hencky strain of 2.25 (Figure 4.13). A possible explanation for the decrease in the strain hardening parameter is that the convective constraint release of the polymer chains becomes more dominant at higher test temperatures as well as higher strain rates. The convective constraint release leads to loss of the trapped entanglements and as such relaxes the overall matrix from the applied extensional force. This reflects in a steeper drop of the strain hardening parameter at 160°C and at higher strain rates. As explained in the previous chapter the reduced strain hardening parameter was calculated by taking a ratio of the transient extensional viscosity η_E^+ to the viscosity obtained from linear viscoelastic measurements η_{E0}^+. The base linear viscoelastic envelope was obtained by multiplying the viscosity obtained from linear viscoelastic measurements with the offset value between the base curve and linear portion of the transient extensional viscosity.

4.4.3.2 Effect of clay loading on the extensional viscosity of nanocomposites

The effect of filler loading on the strain hardening behavior of the nanocomposites was studied by comparing the extensional viscosities of nanocomposites with three different loadings of I.44 P clay. As mentioned earlier, nanocomposites PPNC B5, PPNC B8 and PPNC B12 were made with 5, 8 and 12 wt% of nanoclay loading respectively. A lower loading of nanoclay (3%) was used in formulating a nanocomposite, however due to lower viscosity of the sample at 155°C; it was extremely difficult to measure its extensional viscosity transient because of its

sagging. Figure 4.14 shows a comparison of the extensional viscosities for the nanocomposites with different loadings at 155° C.

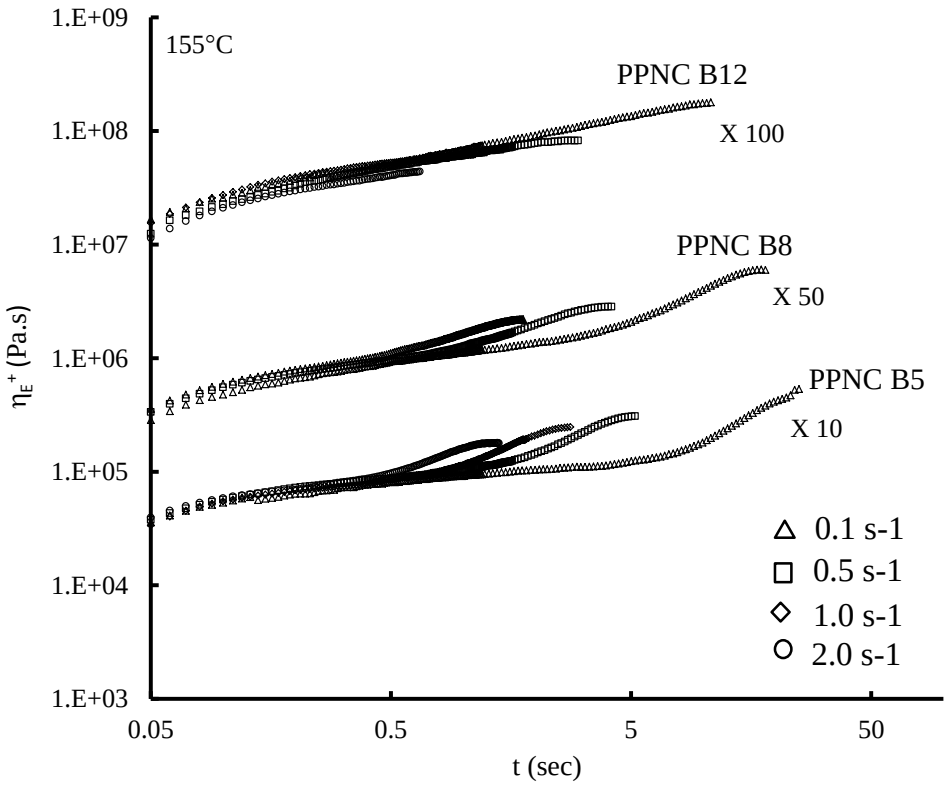

Figure 4.14. Transient extensional viscosity curve for nanocomposite PPNC B5, PPNC B8, and PPNC B12 at 155° C and four extensional strain rates: $0.1s^{-1}$ (Δ), $0.5s^{-1}$(□), $1s^{-1}$(◊) and $2s^{-1}$(○).

It is observed that PPNC B8 shows a slight reduction in the lift off of the extensional viscosity curve, at higher rates as compared to the PPNC B5 nanocomposite. In case of PPNC B12, the strain hardening is completely lost as no lift off in the extensional viscosity is observed at all possible extensional strain rates. To quantify this effect, the strain hardening parameter was calculated and compared at a Hencky strain of 2.25 at the different strain rates for only the

composites - PPNC B5 and PPNC B8. It was evident from Figure 4.14 that the strain hardening parameter for PPNC B12 at all measured rates would be 1, as there is no strain hardening. The strain hardening parameter comparison for PPNC B5 and PPNC B8 is shown in Figure 4.15 at 155°C. The reduced strain hardening parameter is clearly higher for PPNC B5 as compared to PPNC B8 nanocomposite, especially at higher extensional strain rates.

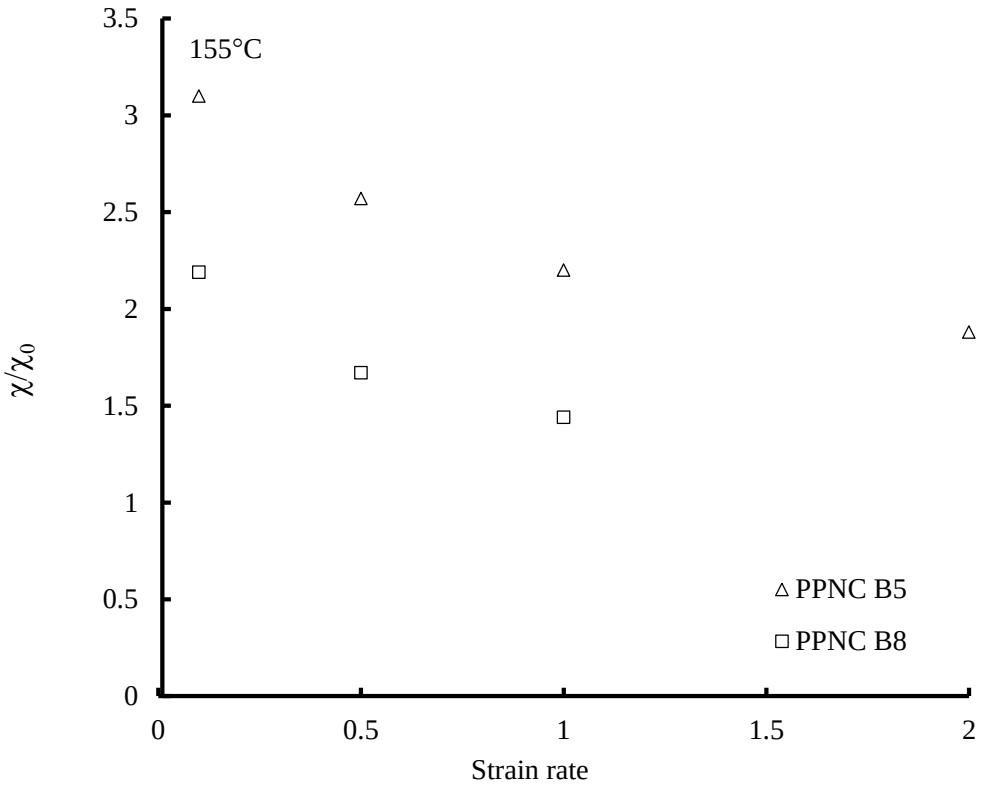

Figure 4.15. Reduced Strain hardening parameter v/s strain rate: Comparison at Hencky strain of 2.25, for PPNC B5 (Δ) and PPNC B8 (□) at 155° C.

The progressive decrease in strain hardening observed for the nanocomposites with increasing loading is mainly be due to the decrease in the overall hindered chain entanglements. With a decrease in the number of hindered chain entanglements, the overall relaxation of the melt happens much faster and as such the strain hardening behavior starts diminishing. In the

nanocomposite melts, the hindered chain entanglements are mainly formed between the particle attached polymer chains and the free polymer chains. With a decrease in the effective aspect ratio of the particles with increasing filler loading, even the specific surface area of the particles that is available for interaction with the polymer chains decreases. This in turn lowers the probability of forming an entanglement network between the particle attached polymer chains and the free matrix polymer chains, thereby reducing the strain hardening behavior in extensional rheology. In order to understand the strain hardening trends with increasing filler loading, we quantitatively estimated the particle statistics and the particle dimensions; discussed in the following section.

4.4.3.3 Estimate of particle dimensions and inter-particle spacing

In the previous sections, we discussed that an increase in filler loading leads to greater reinforcement levels in the linear viscoelastic regime. However in the non – linear viscoelastic regime, an increase in filler loading causes strain softening or drop in the modulus as well as suppression of the strain hardening behavior in extensional flow. This can be attributed to a decrease in the effective aspect ratio of the particles as well as the specific surface area available for polymer particle interactions which in turn reduces the probability of forming hindered chain entanglements. In order to understand this hypothesis better, we evaluated the particle statistics to obtain quantitative comparisons between the different nanocomposites. The effective aspect ratio (a) has already been calculated earlier from the linear viscoelastic data (Table 4.1). In order to obtain the particle thickness, we assumed an average particle length (L_p) in nm based on some TEM analysis done in our research group on polypropylene –I.44P nanoclay composites. Taking in account the aspect ratio and the average lengths of I.44P clay particles observed in TEM, the

average particle length was assumed to be 306 nm. The average particle length was then multiplied with the effective aspect ratio for respective nanocomposites and the average particle thickness (t_p) was found. It can be seen from Table 4.2 that as the filler loading increases, the effective aspect ratio goes down and the particle thickness increases.

Table 4.2. Estimates of Particle Dimensions and Packing.

PPNCs	a=D/t	(L_p) nm	(t_p) nm	(A_{sp}) m^2/g clay	(V_p) micron^3	(ϕ)	(n/V_p)	(δ) nm
B5	68	306	4.5	327	4.21E-04	0.027	64	1329
B8	59	306	5.2	285	4.86E-04	0.044	91	1086
B12	48	306	6.4	233	5.97E-04	0.067	113	944

Note: Effective aspect ratio (a), Length of particle (L_p), Thickness of particle (t_p), Specific surface area (A_{sp}), Particle volume (V_p), Number of particles (n) and Average lateral spacing between particles (δ) of nanocomposite are at 155°C.

For a single platelet thickness of 1 nm and an average d-spacing of 3.5 nm for the composites, we can conclude that with an increase in filler loading and particle thickness, the number of clay platelets in a particle stack also increases. This indicates that for the higher loading composites like PPNC B12, there are more clay platelets aggregated in a stack and as

such there is more particle-particle kind of interaction. This is further verified by calculating the specific area (A_{sp}) of the particles that is available for interaction. The specific area for the particles was calculated in m^2/g of clay using the following equation:

$$A_{sp} = \left(\frac{1}{\rho_{clay}}\right)\frac{Total\ Particle\ Surface\ Area}{Paricle\ Volume} \ldots\ldots\ldots (4.1)$$

Where, ρ_{clay} is the density of I.44P clay in this case. For a particle with length (L_p) and thickness (t_p), equation 4.1 becomes

$$A_{sp} = \left(\frac{1}{\rho_{clay}}\right)\left(\frac{4}{L_p} + \frac{2}{t_p}\right) \ldots\ldots\ldots\ldots\ldots\ldots (4.2)$$

Equation 4.2 gives the specific surface area of the particles at different loadings and It can be seen in Table 4.2, that as the filler loading increases from 5wt% to 12wt%, the specific area of the particles available for interactions reduces by almost 30%. As such the chances of polymer-particle interaction goes down in the case of PPNC B12 composite which in necessary for creating hindered entanglements between the particle attached polymer chains and the free polymer chains. Besides this, if the particles are spaced very close to each other, there are more chances of particle-particle kind of interactions which is observed from the linear and non-linear viscoelastic data trends in the case of composites with higher filler loadings. In order to verify this and get an estimate of the particle spacing, we first calculated the particle volume (V_p) in $micron^3$ using the average particle length and thickness as shown in Table 4.2. The total number of particles per unit volume were then calculated by taking the ratio of particle volume (V_p) to

that of the volume fraction of the filler particles (ϕ) inclusive of the surfactant between them. It can be seen in Table 4.2 that the number of particle per unit volume increases as the filler loading increases from 5 wt% to 12 wt%. With an increase in the number of particles in a given volume, the lateral spacing between them decreases. To calculate the average lateral spacing between the particles, we used the mean chord length formula as used in the work done by Olson and co-workers [123-124]. They have shown that in a binary medium the discs can be arranged either in a tightly packed manner with a coordination number of 4 or in a hexagonal pattern with a coordination number of 6. In our case we first assumed the filler particles to be disc shaped and used the mean chord length formula for discs in a tightly packed pattern to calculate the average lateral spacing between the nanoparticles. According to Olson, the area or volume fraction of the discs also gives the probability (p_1) that a given point is inside a disk or sphere as shown in equation (4.3). For a tightly packed pattern

$$p_1 = \pi (r/\delta)^2 \ldots\ldots\ldots\ldots (4.3),$$

Where, r is the radii of the disc (i.e. $L/2*\sqrt{2}$) and δ is the lateral spacing between the adjacent discs. In order to obtain δ, we first calculated the area fraction values from the respective volume fraction of the fillers in the different composites. These area fraction values are the same as p_1, as stated in the work done by Olson. We then used equation 4.3 and calculated the lateral spacing (δ) for each composite shown in Table 4.2. It can be seen that with an increase in filler loading the lateral spacing between the particles decreases which is also consistent with an increase in the number of particles in a given volume. The lateral spacing between particle stacks for all nanocomposites are however too large to cause any kind of bridging effect between them and as such it can be concluded that bridging doesn't contribute to

any kind of filler network formation; it is mainly formed due to direct particle-particle interaction. The estimation of particle statistics gives a quantitative analysis of the level of dispersion of the filler particles in the different nanocomposites as well as an insight of the possible mechanisms responsible for their shear and extensional flow behavior.

4.5 CONCLUSIONS

The quality of dispersion is lowered with increasing volume fraction (from 2.7% to 6.7% vol.) of the same layered silicates in a high molecular weight (M_w=180,000) linear maleated polypropylene copolymer (with ethylene) which melts at 145°C; no other component was used. This was confirmed with both XRD and estimates of effective particle aspect ratio from relative dynamic viscosity. The low frequency storage modulus was increased a hundred fold from the melt with lowest to that with the highest loading and this may be attributed largely to the stronger filler network with the highest loading. Observations with a strain sweep (large amplitude oscillatory shear) on the nanocomposite with the highest loading revealed a maximum in both dynamic moduli with increasing strain for the nanocomposite melt before they dropped in magnitude. The strain sweep on the nanocomposite with the best dispersion (and the lowest loading) showed a two-stage drop. The critical strain decreased with increasing loading and decreasing effective aspect ratio.

Two nanocomposite melts (B5 and B8) with lower loading of nanoparticles and better dispersion showed significant strain hardening in uniaxial extensional flow tests over a range of strain rates while the matrix polymer melt did not show any strain hardening. In the case of B12, with highest filler loading, the strain hardening was completely lost. The specific surface area (A_{sp}) of particles that is available for interaction with the polymer chains decreases by almost

30% for the highest filled composite as compared to the lowest filled one. With a progressive decrease in specific surface area, there is a progressively lower probability of forming a network of hindered chain entanglements between the particle-attached polymer chains and free polymer chains that is necessary to achieve strain hardening.

CONCLUSIONS AND RECOMMENDATIONS

CHAPTER 5

5.1 CONCLUSIONS

The research work in the present study was focused on achieving strain hardening in linear polypropylene matrix that was functionalized at ends with maleic anhydride. Although, there have been several methods of achieving strain hardening in linear polymeric systems by either modifying the polymer molecular structure or by incorporating other components like high molecular weight fractions, cross-linked polymers etc., here , we have taken the approach of adding a very small amount of an inorganic nano-sized filler to a linear maleated polyproypelene copolymer. In doing this we have addressed several issues that are necessary to understand the effect of nano filler addition into linear polymers based on shear and extensional rheology:

5.1.1 Addition of nanoclay and its effect on viscoelastic properties and strain hardening

Linear polypropylene, which is a widely used commodity polymer, does not exhibit any strain hardening upon stretching it in uniaxial extensional melt flow. In order to verify if the addition of nanoclay provided the necessary strengthening of PP melt upon stretching, we added different nanoclays to the linear maleated polypropylene matrix. The primary objective in choosing just the functionalized (maleated) polypropylene as the complete matrix was to understand the kind of interactions taking place between the maleic anhydride group on the polymer chains and the -OH groups on the clay edges, which would lead to any kind of strain hardening in the nanocomposites. The addition of linear bulk polypropylene would add a third phase making the system more complex. Hence a linear maleated polypropylene (PP-g-MA)

(M_W = 180,000, 0.4% maleic anhydride) was chosen as the matrix to which layered silicates (Montmorillonite) having different surfactant treatments were added as the filler. The X-ray diffraction patterns suggested that the nanoclays dispersed well in the polypropylene matrix at 2 vol%. The additions of nanoclay lead to a substantial increase in the dynamic moduli and viscosity values as compared to the base matrix in the linear viscoelastic region. The nanocomposites also showed greater degree of non-linearity in large amplitude oscillatory shear measurements as compared to the base polymer with a steep drop in the moduli values beyond a critical strain. But the most striking result was the marked improvement in strain hardening behavior in melt extensional flow for the nanocomposites. The study showed that by addition of just 5 wt% of nanoclay to linear polypropylene matrix, the extensional viscosity as well as the strain hardening behavior of the linear matrix improves as seen for the nanocomposites. The improvement in strain hardening behavior is mainly because of the formation of hindered chain entanglements between the free matrix chains and the PP chains that are physically cross linked to the clay sites. Upon stretching, the polymer chains try to relax to regain their original state, however, the formation of the hindered chain entanglement structure slows down this polymer chain relaxation and this reflects in a lift off of the extensional viscosity curve from the base linear viscoelastic curve for the composites. This lift off is the observed strain hardening in nanoclay filled polypropylene composites.

5.1.2 Effect of surfactant head group and effective aspect ratio

To further investigate the effect of nanoclay addition, two different grades of nanoclay were added in the linear polymer matrix to check for their effects on the viscoelastic and extensional flow properties. One of the clay was organically modified by incorporating

primary amine surfactant (I.30P clay) and other had a quaternary ammonium ion surfactant (I.44P clay) in the interlayer galleries. The amount of surfactant packing in the interlayer galleries of the clays was verified by X-ray diffraction and Thermo gravimetric Analysis and was concluded that the I.44P organoclay having quaternary ammonium surfactant was packed more with the surfactant and had a higher d-spacing. The dispersion of these clays in the matrix PP was fairly intercalated as seen from a shoulder in the XRD pattern of the nanocomposites. The addition of both these clays improved the dynamic modulus and viscosity values in linear shear, with I.44P clay nanocomposite (PPNC B5) showing a greater value than the I.30P clay nanocomposite (PPNC A5). The aspect ratios (side / thickness) of the two different nanoparticles dispersed were determined to be 56 and 68 from measurements of relative dynamic viscosity on the nanocomposite melts. The low frequency storage modulus of the nanocomposite with the higher aspect ratio nanoparticles was greater indicating a stronger filler network and/or a greater fraction of polymer chains attached to the particle surface with higher aspect ratio. Large amplitude oscillatory shear measurements on the nanocomposite melt with the higher aspect ratio particles showed a two stage drop in the storage modulus with increasing strain which highlights the breakup of two structures—the particle network followed by the hindered chain entanglement network involving attached chains. The buildup of structure is also slower for the nanocomposite with the higher aspect ratio nanoparticle system. Both nanocomposite melts display strain hardening in uniaxial extensional flow over several strain rates, unlike the matrix polymer which shows no strain hardening: the melt with the higher aspect ratio layered silicates displayed a higher extent of strain hardening at all rates. This last phenomenon may be attributed to the greater incidence of particle attached chains and entanglements involving these chains when the particle aspect ratio is greater.

5.1.3 Effect of test temperature and nanoclay loading

The second part of the research work was focused on investigating the effects of different loadings of the nanoclay and the test temperature on the strain hardening behavior of these nanocomposites. From the first part of the research work, it was concluded that the organoclay with higher effective aspect ratio and quaternary ammonium surfactant with 2 alkyl tails showed better rheological properties. The same clay was used at different loadings in the linear PP matrix in second part of the research and the linear shear, non-linear shear and uniaxial extensional flow properties were investigated. With respect to different test temperatures in uniaxial extensional flow, the nanocomposite with a loading of 5wt% (PPNC B5) was used. It was found that the strain hardening of the nanocomposites decreased with an increase in temperature from 155°C to 160°C especially at higher strain rates which is due to the dominant convective constraint release at those higher test temperatures as well as higher strain rates.

The loading of filler particles also significantly affects the linear and non-linear viscoelastic properties as well as the strain hardening behavior of the nanocomposites. A lower loading of nanoclay (3%) was used in formulating a nanocomposite, however due to lower viscosity of the sample at 155°C; it was extremely difficult to measure its extensional viscosity transient because of its sagging. The other loadings were at 5wt% (2.7 vol%), 8wt% (4.4 vol%) and 12wt% (6.7 vol%) of the nanoclay. It was seen that the quality of dispersion is lowered with increasing volume fraction (from 2.7% to 6.7% vol.) of the same layered silicates in a high molecular weight maleated linear polypropylene copolymer (with ethylene). This was confirmed with both XRD and estimates of effective particle aspect ratio from relative dynamic viscosity. The low frequency storage modulus was increased a hundred fold from the melt with lowest to that with the highest loading and this may be attributed largely to the stronger filler network with

the highest loading. Observations with a strain sweep (large amplitude oscillatory shear) on the nanocomposite with the highest loading revealed a maximum in both dynamic moduli with increasing strain for the nanocomposite melt before they dropped in magnitude. The strain sweep on the nanocomposite with the best dispersion (and the lowest loading) showed a two-stage drop. The critical strain decreased with increasing loading and decreasing effective aspect ratio.

Two nanocomposite melts (B5 and B8) with lower loading of nanoparticles and better dispersion showed significant strain hardening in uniaxial extensional flow tests over a range of strain rates while the matrix polymer melt did not show any strain hardening. In the case of B12, with highest filler loading, the strain hardening was completely lost. The specific surface area (A_{sp}) of particles that is available for interaction with the polymer chains decreases by almost 30% for the highest filled composite as compared to the lowest filled one. With a progressive decrease in specific surface area, there is a progressively lower probability of forming a network of hindered chain entanglements between the particle-attached polymer chains and free polymer chains that is necessary to achieve strain hardening.

5.2 RECOMMENDATIONS

The research done in this study still has a wide scope and provides further opportunities to explore other aspects that were not covered in here. The following recommendations are therefore made:

1. One of the main goals of this study was to study the effect of nanoclay addition on the strain hardening behavior of linear polypropylene nanocomposites and understand the interaction between the nanoclay platelets and the functional groups on maleated polypropylene. It was conclusive that a higher effective aspect ratio and better interaction via hydrogen bonding, led to greater loose reversible attachments between the polymer

chains and clay particles. This in turn helped in increasing the entanglement density of the nanocomposites and also the strain hardening improved, however it still remains to find out the exact nature of these interactions and also if possible to quantify the hydrogen bonding interactions between different composites. This can also be related to the entanglement density of the nanocomposites and the strain hardening parameters.

2. Also in this study we had prepared nanocomposites using two different types of organoclays. One of the clay had a primary amine surfactant with a single alkyl tail and other a quaternary ammonium surfactant with 2 alkyl tails. In future a study on the extensional behavior of the nanocomposites can be made wherein the clay surfactant head group is same and the numbers of alkyl tails vary. Also, one can have different surfactant head groups with the same number of alkyl tails dangling. Heinz and coworkers [38, 39] have worked and simulated the conformations of the different surfactants in interlayer galleries with increasing number of C (C_4 to C_{22}) atoms in the alkyl tails as well with increasing number of alkyl tails. Such organoclays can be incorporated into the polymer matrix and investigated for their effects on the dispersion levels, linear and non-linear viscoelastic properties as well the extensional flow properties for the nanocomposites.
3. The non-linearity in shear and extension can be further explored using a combination of different molecular weight polymer matrices as well as different clays. Also the modulus recovery kinetics can be studied with respect to differences in the molecular weight of the polymer matrix and different clay loadings.
4. The effects of using additional coupling agents such as silanes on nanoclay can be investigated for the non-linear shear and extensional behavior. Silane functional groups in

general provide additional interaction sites as has been shown by research work done previously in our group [100] and significantly improve the linear viscoelastic properties.

5. The non-linear viscoelastic and extensional behavior of these nanocomposites can be modeled by identifying the shear and extensional damping functions as was done by Wagner and Fulchiron for polymer melts. As has been shown by Fulchiron [121] for PP melts the transient shear data can be used to identify the elongation behavior using Wagner's time integral constitutive model. A similar modeling can be done with shear viscoelastic data of the nanocomposites and the transient extensional viscosity may be predicted.

BIBLIOGRAPHY

BIBLIOGRAPHY

1. Manias, E., Touny, A., Wu, L., Strawhecker, K., Lu, B., and Chung, T., "Polypropylene/Montmorillonite nanocomposites. Review of the synthetic routes and materials properties." *Chem. Mater.*, **13**, (10), (2001), 3516-3523.

2. Qian, G., Cho, J.W. and Lan, T., "Preparation and Properties of Polyolefin Nanocomposites." Polyolefins 2001, Houston, TX, (2001).

3. Bartholmai, M. and Schartel, B., "Layered silicate polymer nanocomposites: new approach or illusion for fire retardancy? Investigations of the potentials and the tasks using a model system." *Polym. Advan Technol.*, **15**, (7), (2004), 355-364.

4. Gilman, J., Jackson, C., Morgan, A., Harris, R., Manias, E., Giannelis, E., Wuthenow, M., Hilton, D., and Phillips, S., "Flammability properties of polymer - Layered-silicate nanocomposites. Polypropylene and polystyrene nanocomposites." *Chem. Mater.*, **12**, (7), (2000), 1866-1873.

5. Tang, Y., Hu, Y., Li, B., Liu, L., Wang, Z., Chen, Z., and Fan, W., "Polypropylene/montmorillonite nanocomposites and intumescent, flame-retardant montmorillonite synergism in polypropylene nanocomposites." *J. Poly. Sci. Poly. Chem.*, **42** (23), (2004), 6163-6173.

6. Tang, Y., Hu, Y., Wang, S., Gui, Z., Chen, Z., and Fan, W., "Intumescent flame retardant-montmorillonite synergism in polypropylene-layered silicate nanocomposites." *Poly. Int.*, **52** (8), (2003), 1396-1400.

7. Usuki,A., Kojima,Y., Kawasumi,M., Okada,A., Fukushima,Y., Kurauchi,T., and Kamigaito,O., Synthesis of Nylon 6 - clay Hybrid, *J. Mater. Res*, **8**, (1993), 1179-1184.

8. Kojima, Y., Usuki, A., Kawasumi, M., Okada, A., Kurauchi, T., and Kamigaito, O., Synthesis of Nylon-6-Clay Hybrid by Montmorillonite Intercalated with Epsilon-Caprolactam, *J. Polym. Sci., Part A: Polym. Chem*., **31**, (1993), 983-986.

9. Giannelis, E.P., Polymer Layered Silicate Nanocomposites, *Adv. Mater*., **8**, (1996), 29-35.

10. Giannelis, E.P., Polymer Layered Silicate Nanocomposites: Synthesis, Properties, and Applications, *Appl. Organomet. Chem*., **12**, (1998), 675-680.

11. Ray, S. and Okamoto, M., Polymer/layered silicate nanocomposites: a review from preparation to processing, *Prog. Polym. Sci*., **28**, (2003), 1539-1641.

12. Vaia, R. and Giannelis, E., Polymer melt intercalation in organically-modified layered silicates: Model predictions and experiment, *Macromolecules*, **30**, (25), (1997), 8000-8009.

13. Kawasumi, M., Hasegawa, N., Kato, M., Usuki, A. and Okada, A. Preparation and mechanical properties of polypropylene-clay hybrids, *Macromolecules*, **30**, (1997), 6333-6338.

14. Kato, M., Usuki, A. and Okada, A., Synthesis of polypropylene oligomer-clay intercalation compounds, *J. Appl. Poly. Sci*., **66**, (1997), 1781-1785.

15. Hasegawa, N., Kawasumi, M., Kato, M., Usuki, A., and Okada, A., Preparation and mechanical properties of polypropylene-clay hybrids using a maleic anhydride-modified polypropylene oligomer, *J. Appl. Poly. Sci.*, **67**, (1998), 87-92.

16. Usuki, A., Kato, M., Okada, A., and Kurauchi, T., "Synthesis of polypropylene-clay hybrid." *J. Appl. Polym. Sci.*, **63**, (1), (1997), 137-139.

17. Ginzburg, V. and Balazs, A., "Calculating phase diagrams of polymer-platelet mixtures using density functional theory: Implications for polymer/clay composites." *Macromolecules*, **32**, (17), (1999), 5681-5688.

18. Hasegawa, N., Okamoto, H., Kawasumi, M., Kato, M., Tsukigase, A., and Usuki, A., "Polyolefin-clay hybrids based on modified polyolefins and organophilic clay." *Macromol. Mater. Eng.*, **280**, (7-8), (2000), 76-79.

19. Hasegawa, N. and Usuki, A., "Silicate layer exfoliation in polvolefin/clay nanocomposites based on maleic anhydride modified polyolefins and organophilic clay." *J. Appl. Polym. Sci.*, **93**, (1), (2004), 464-470.

20. Gopakumar, T., Lee, J., Kontopoulou, M., and Parent, J., "Influence of clay exfoliation on the physical properties of montmorillonite/polyethylene composites." *Polymer*, **43**, (20), (2002), 5483-5491.

21. Ishida, H., Campbell, S., and Blackwell, J., "General approach to nanocomposite preparation." *Chem. Mater.*, **12**, (5), (2000), 1260-1267.

22. Marchant, D. and Jayaraman, K., "Strategies for optimizing polypropylene-clay nanocomposite structure." *Ind. Eng. Chem. Res.*, **41**, (25), (2002), 6402-6408.

23. Minoura, Y., Ueda, M., Mizunuma, S., and Oba, M., "The Reaction of Polypropylene with Maleic Anhydride." *J. Appl. Polym. Sci.*, **13**, (1969),1625.

24. Van Olphen, H., An Introduction to Clay Colloid Chemistry; Interscience Publishers: New York, (1962).

25. Theng, B.K.G., Soils with Variable Charge., New Zealand: Offset Publications (1980).

26. Greenwell, H.C., Harvey, M.J., Boulet, P., Bowden, A., Coveney, P.V., Whiting, A., Interlayer structure and bonding in nonswelling primary amine intercalated clays, *Macromolecules*, **38**, (2005), 6189-6200.

27. Osman, MA; Seyfang, G; Suter, UW.. Two-dimensional melting of alkane monolayers ionically bonded to mica, *Journal of Physical Chemistry B*, **104** (18), (2000), 4433-4439.

28. Osman, MA; Ernst, M; Meier, BH; Suter, UW., Structure and molecular dynamics of alkane monolayers self-assembled on mica platelets, *Journal of Physical Chemistry B*, **106** (3), (2002), 653-662.

29. Heinz, H; Castelijns, HJ; Suter, UW, Structure and phase transitions of alkyl chains on mica. *Journal of American Chemical Society*, **125** (31), (2003), 9500-9510.

30. Osman, MA; Ploetze, M; Skrabal, P, Structure and properties of alkylammonium monolayers self-assembled on montmorillonite platelets, *Journal of Physical Chemistry B*, **108** (8), (2004), 2580-2588.

31. Zhu, JX; He, HP; Zhu, LZ; Wen, XY; Deng, F. Characterization of organic phases in the interlayer of montmorillonite using FTIR and C-13 NMR, *Journal of Colloid and Interface Science,* **286** (1), (2005), 239-244.

32. Vaia, RA; Teukolsky, RK; Giannelis, EP., Interlayer Structure and Molecular Environment of Alkylammonium Layered Silicates, *Chemistry of Materials,* **6** (7), (1994), 1017-1022.

33. Vaia, R. and Giannelis, E., "Lattice model of polymer melt intercalation in organically-modified layered silicates." *Macromolecules*, **30**, (25), (1997), 7990-7999.

34. Vaia, R. and Giannelis, E., "Polymer melt intercalation in organically-modified layered silicates: Model predictions and experiment." *Macromolecules*, **30**, (25), (1997), 8000-8009.

35. Osman, MA; Rupp, JEP; Suter, UW, Gas permeation properties of polyethylene-layered silicate nanocomposites, *Journal of Material Chemistry,* **15** (12), (2005), 1298-1304.

36. Yalcin, B; Cakmak, M., Superstructural hierarchy developed in coupled high shear/high thermal gradient conditions of injection molding in nylon 6 nanocomposites, *Polymer,* **45** (8), (2004), 2691-2710.

37. Jacobs, JD; Koerner, H; Heinz, H; Farmer, BL; Mirau, P; Garrett, PH; Vaia, RA., Dynamics of alkyl ammonium intercalants within organically modified montmorillonite: Dielectric relaxation and ionic conductivity, *Journal of Physical Chemistry:B,* **110** (41), (2006), 20143-20157.

38. Heinz, H., Vaia, R.A. Krishnamoorti, R. and Farmer, B.L., Self-assembly of alkylammonium chains on montmorillonite: Effect of chain length, head group structure, and cation exchange capacity, *Chem. Mater.*, **19**, (2007), 59-68.

39. Fu, YT; Heinz, H., Cleavage Energy of Alkylammonium-Modified Montmorillonite and Relation to Exfoliation in Nanocomposites: Influence of Cation Density, Head Group Structure, and Chain Length, *Chemistry of Materials,* **22** (4), (2010), 1595-1605.

40. Agrawal, PK; Lee, WK; Lornston, JM; RIichardson, CI; Wissburn, KF; Metzner, AB., Rheological behavior of molten polymer in shear and in extensional flows, *Transactions of the Society of Rheology,* **21** (3), (1977), 355-379.

41. Wagner, MH, The Nonlinear Strain Measure of Polyisobutylene Melt in General Biaxial Flow & its Comparison to the Doi-Edwards Model., *Rheologica Acta,* **29** (6), (1990), 594-603.

42. Sridhar, T; Gupta, RK., Material Properties of Viscoelastic Liquids in Uniaxial Extension, *Journal of Rheology,* **35** (3), (1991), 363-377.

43. Wilson, TS, Baird, DG, Transient Elongational Flow Behavior of Thermotropic Liquid Crystalline Polymer, *Journal of Non-Newtonian Fluid Mechanics,* **44**,(1992), 85-112.

44. Kim.HC, Pendse.A., Collier JR., Polymer Melt Lubricated Elongational Flow, *Journal of Rheology,* **38** (4), (1994), 831-845.

45. PADMANABHAN, R.. Measurement of Extensional Viscosity of Viscoelastic Liquid Foods, *Journal of Food Eng.,* **25** (3), (1995), 311-327.

46. Kelly, J; Graessley, WW.. Some tests of constitutive equations for entangled polymers based on planar-extension flow histories in a periodically constricted channel, *Rheologica Acta,* **35** (1), (1996), 24-38.

47. Micic, P; Bhattacharya, SN; Field, G., Melt strength and elastic behaviour of LLDPE/LDPE blends. *International Polymer Processing,* **11** (1), (1996), 14-20.

48. Takahashi, T; Wu, WG; Toda, H; Takimoto, J; Akatsuka, T; Koyama, K., Elongational viscosity of ABS polymer melts with soft or hard butadiene particles.*Journal of Non-Newtonian Fluid Mechanics,* **68** (2-3), (1997), 259-269.

49. Levitt, L; Macosko, CW; Schweizer, T; Meissner, J, Extensional rheometry of polymer multilayers: A sensitive probe of interfaces, *Journal of Rheology,* **41** (3), (1997), 671-685.

50. Lin, GG; Hu, MC, Measurement of elongation viscosity for polymer melts by fiber spinning. *Advances in Polymer Technology,* **16** (3), (1997), 199-207.

51. Greener, J; Evans, JRG, Measurement of elongational flows in ceramic processing – Review, *Journal of the European Ceramic Society*, **17** (10), (1997), 1173-1183.

52. Kasehagen, LJ; Macosko, CW, Nonlinear shear and extensional rheology of long-chain randomly branched polybutadiene. *Journal of Rheology*, **42** (6), (1998), 1303-1327.

53. Kapoor, B; Bhattacharya, M., Transient shear and extensional properties of biodegradable polycaprolactone, *Polymer Eng. And Science*, **39** (4), (1999), 676-687.

54. Haworth, B; Jumpa, S; Miller, NA, Melt-state elongational rheometry of mineral-filled polyethylene, *Polymer Testing*, **19** (4), (2000), 459-477.

55. Micic, P; Bhattacharya, SN, Rheology of LLDPE, LDPE and LLDPE/LDPE blends and its relevance to the film blowing process, *Polymer International*, **49** (12), (2000), 1580-1589.

56. Minegishi, A; Nishioka, A; Takahashi, T; Masubuchi, Y; Takimoto, J; Koyama, K., Uniaxial elongational viscosity of PS/a small amount of UHMW-PS blends, *Rheologica Acta*, **40** (4), (2001), 329-338.

57. Sugimoto, M; Masubuchi, Y; Takimoto, J; Koyama, K., Melt rheology of polypropylene containing small amounts of high-molecular-weight chain. 2. Uniaxial and biaxial extensional flow, *Macromolecules*, **34** (17), (2001), 6056-6063.

58. Muke, S; Ivanov, I; Kao, N; Bhattacharya, SN, Extensional rheology of polypropylene melts from the Rheotens test, *Journal of Non-Newtonian Fluid Mechanics*, **101** (1-3), (2001), 77-93.

59. Malmberg, A; Gabriel, C; Steffl, T; Munstedt, H; Lofgren, B., Long-chain branching in metallocene-catalyzed polyethylenes investigated by low oscillatory shear and uniaxial extensional rheometry, *Macromolecules*, **35** (3), (2002), 1038-1048.

60. Huang, JC; Leong, KS, Shear viscosity, extensional viscosity, and die swell of polypropylene in capillary flow with pressure dependency, *Journal of Applied Polymer Science*, **84** (6), (2002), 1269-1276.

61. Kao, N; Chandra, A; Bhattacharya, S, Melt strength of calcium carbonate filled polypropylene melts, *Polymer International*, **51** (12), (2002), 1385-1389.

62. Hachmann, P; Meissner, J.. Rheometer for equibiaxial and planar elongations of polymer melts. *Journal of Rheology,* **47** (4), (2003), 989-1010.

63. Sentmanat, ML, Miniature universal testing platform: from extensional melt rheology to solid-state deformation behavior, *Rheologica Acta*, **43** (6), (2004), 657-669.

64. Hong, JS; Ahn, KH; Lee, SJ., Strain hardening behavior of linear polymer melts, *Korea-Australia Rheology Journal*, **16** (4), (2004), 213-218.

65. Sentmanat, M; Muliawan, EB; Hatzikiriakos, SG, Fingerprinting the processing behavior of polyethylenes from transient extensional flow and peel experiments in the melt state. *Rheologica Acta*, **44** (1), (2004), 1-15.

66. Gupta, RK; Pasanovic-Zujo, V; Bhattacharya, SN, Shear and extensional rheology of EVA/layered silicate-nanocomposites. *Journal of Non Newtonian Mechanics,* **128** (2-3), (2005), 116-125.

67. Bhattacharya, S; Gupta, RK; Jollands, M; Battacharya, SN., Foaming Behavior of High-Melt Strength Polypropylene/Clay Nanocomposites, *Polymer Eng. And Sci.,* **49** (10), (2009), 2070-2084.

68. Chaudhary, A.K.; Jayaraman, K., "Extrusion of Linear Polypropylene-Clay Nanocomposite Foams," *Polym. Eng. Sci*., **51**, (2011).

69. Spitael, P. and C.W. Macosko, Strain hardening in polypropylenes and its role in extrusion foaming, *Polym. Eng. Sci*., **44**, (2004), 2090–2100.

70. Stange, J. and H. Munstedt, Rheological properties and foaming behavior of polypropylenes with different molecular structures, *J. Rheol.,* **50**, (2006), 907-923.

71. Kurzbeck, S., F. Oster, H. Münstedt, T. Q. Ngyuen, and R. Gensler, Rheological properties of two polypropylenes with different molecular structure, *J. Rheol*., **43**, (1999), 359–374.

72. Gotsis AD, BLF Zeevenhoven, AH Hogt, The effect of long chain branching on the processability of polypropylene in thermoforming, *Polym. Eng. Sci*., **44**, (2004), 973-982.

73. Wollecke F, Altstadt V, Sandler J, Rakutt D, The influence of melt elongational properties on the morphology of PES cellular materials, *Cellular Polymers*, **21**, (2002), 445-453.

74. McInerney, L. N. Kao and S.N. Bhattacharya, Melt strength and extensibility of talc-filled polypropylene, *Polym. Eng. Sci*., **43**, (2003), 1821-1829.

75. Sugimoto, M., Tanaka, T., Y. Masubuchi, J. Takimoto and K. Koyama, Effect of chain structure on the melt rheology of modified polypropylene, *Journal of Applied Polymer Science*, **73**, (1999), 1493-1500.

76. Sugimoto, M., Y. Masubuchi, J. Takimoto and K. Koyama, Melt rheology of polypropylene containing small amounts of high-molecular-weight chain. 2. Uniaxial and biaxial extensional flow, *Macromolecules*, **34**, (2001), 6056-6063.

77. Minegishi, A; Naka, Y; Takahashi, T; Masubuchi, Y; Takimoto, J; Koyama, K, The effect of ultrahigh molecular weight polymers on the nonlinear response in uniaxial elongational viscosity, *Nihon Reorji Gakkaishi* ,**25** (4), (1997), 215-216.

78. Berger.L, Meissner, J., Linear Viscoelasticity, Simple and Planar Melt Extension of Linear Polybutadienes with Bimodal Molar Mass Distributions, *Rheologica Acta* ,**31** (1), (1992), 63-74.

79. Yamaguchi.M and Miyata.H., Strain hardening behavior in elongational viscosity for binary blends of linear polymer and crosslinked polymer, *Polymer Journal*, **32**, (2000), 164-170.

80. Yamaguchi.M, Rheological Properties of linear and crosslinked polymer blends: Relation between crosslink density and enhancement of elongational viscosity, *Journal of Polymer Science: Part B: Polymer Physics*, **39**, (2001), 228-235.

81. Yamaguchi.M, Suzuki.K, Rheological Properties and foam process ability for blends of linear and crosslinked polyethylenes, *Journal of Polymer Science: Part B: Polymer Physics*, **39**, (2001), 2159-2167.

82. Ogura.K, Takahashi.M., Uniaxial extension behavior of cross-linked Poly(methyl methacryalte)s with various degrees of cross linking, *J. Soc. Rheol.*, **31**, (2003), 85-89.

83. Takahashi, H; Ishimuro, Y; Watanabe, H. 2008. Nonlinear mechanical Behavior of scarcely crosslinked poly(dimethyl siloxane) gel: Effect of strand length polydispersity. *Polymer*, **40** (5): 465-474

84. Takahashi.T., Takimoto.J, and Koyama.K, Uniaxial elongational viscosity of various molten polymer composites, *Polymer Composites*, **20**, (1999), 357-¬366.

85. Le Meins, J-F., P. Moldenaers and J. Mewis, Suspensions of monodisperse spheres in polymer melts: particle size effects in extensional flow, *Rheol. Acta*, **42**, (2002), 184-190.

86. Prasad, R., Pasanovic-Zujo, V., Gupta, R.K., Cser, F. and Bhattacharya, S.N., Morphology of EVA based nanocomposites under shear and extensional flow, *Polymer Engineering and Science*, **44**, (2004), 1220-1230.

87. Seong. D., Kang. T., Young. J., Rheological characterization of polymer-based nanocomposites with different nanoscale dispersions, *e-Polymers*, (2005).

88. Okamoto.M, Nam.P, Maiti.P, Kotaka.T, Hasegawa.N, Usuki.A, A house of card structures in polypropylene/clay nanocomposites under elongational flow, *Nano Letters*, **1**, (2001), 295-298.

89. Okamoto, M; Nam, PH; Maiti, P; Kotaka, T; Nakayama, T; Takada, M; Ohshima, M; Usuki, A; Hasegawa, N; Okamoto, H. 2001. Biaxial flow-induced alignment of silicate layers in polypropylene/clay nanocomposite foam. *Nano Letters*, **1** (9): 503-505.

90. Ray, SS; Okamoto, M.., New polylactide/layered silicate nanocomposites- Melt rheology and foam processing, *Macromolecular Materials and Engineering*, **288** (12), (2003), 936-944.

91. Wagner, M.H., S. Kheirandish, J. Stange and H. Munstedt, Modeling elongational viscosity of linear and long-chain branched polypropylenes, *Rheol. Acta*, **46**, (2006), 211-221.

92. Payne.A.R, *J. Appl. Polym. Sci.*, **6**, (1962), 57.

93. Kraus.G.J., Mechanical losses in carbon-black-filled rubbers, J. Appl. Polym. Sci.: Appl. *Polym. Symp*., **39**, (1984), 75.

94. Heinrich.G, Kluppel.M., Recent advances in the theory of filler networking in elastomers, *Adv. Polym. Sci*., **160**, (2002), 1-44.

95. Sternstein.S.S and Zhu.A.J., Reinforcement mechanism of nanofilled polymer melts as elucidated by non-linear viscoelastic behavior, *Macromolecules*, **35**, (2002), 7262-7232.

96. Sternstein.S.S and Zhu.A.J., Nonlinear viscoelasticity of nanofilled polymers: interfaces, chain statistics and properties recovery kinetics, *Composites Science and Technology*, **63**, (2003), 1113-1126.

97. Cassagnau.Ph, Melis.F, Non-linear viscoelastic behavior and modulus recovery in silica filled polymers, *Polymer*, **44**, (2003), 6607-6615.

98. Shariatpanahi.H., Sarabi.F., Mirrali.M., Hemmati.M., and Mahadavi.F., "Polypropylene Organoclay Nanocomposite: Preparation, Microstructure, Mechanical Properties." *Journal of Applied Polymer Science*, **113**, (2009), 922-926.

99. Gianelli.W., Camino.G., Dintcheva.N.T., Verso.S.L., Mantia. F.P., "EVA-Montmorillonite Nanocomposites: Effect Of Processing Conditions." *Macromol. Mater. Eng*., **289**, (2004), 238-244.

100. Kumar.S., "Effects of grafting from edges of nanoclayers on flow induced structure in Polypropylene/Clay nanocomposites" PhD Dissertation, Michigan State University, (2005).

101. Gopakumar, T. and Page, D., "Compounding of nanocomposites by thermokinetic mixing." *J Appl Polym Sci*, **96,** (5), (2005), 1557-1563.

102. Lee, J., Lim, Y., and Park, O., "Thermal characteristics of organoclay and their effects upon the formation of polypropylene/organoclay nanocomposites." *Polymer Bullet*, **45,** (2), (2000), 191-198.

103. Cullity, B.D., Elements of X-ray Diffraction. 2nd ed., Massachusetts: Addison-Wesley, (1978).

104. Theng, B.K.G., Formation and Properties of Clay-Polymer Complexes, Amsterdam: Elsevier, (1979).

105. Macosko, C.W. Rheology: Principles, Measurements and Applications, New York: Wiley, (1994).

106. Krishnamoorti, R. and Giannelis, E., "Rheology of end-tethered polymer layered silicate nanocomposites." *Macromolecules*, **30,** (14), 4097-4102 (1997).

107. Krishnamoorti, R. and Giannelis, E., "Strain hardening in model polymer brushes under shear." *LANGMUIR*, **17,** (5), 1448-1452 (2001).

108. Meissner.J., *Rheologica Acta*, **8**, 78, (1969).

109. Meissner.J., *Rheologica Acta*, **10**, 230, (1971).

110. Meissner.J., Raible.T., Stephenson.S.E., "Addendum: Rotary Clamp in Uniaxial and Biaxial Extensional Rheometry of Polymer Melts." *J.Rheol.*, **25**, 1, 673, (1981).

111. Li.L, Masuda.T., Takahasi.M., "Elongational Flow Behavior of ABS Polymer Melts.", *J. Rheol*., **34**, 103, (1990)

112. Macosko.C.W., Lornston.J.M., *SPE Tech. Pap*., **19**, 461, (1973).

113. Everage.A.E., ballma.R.L., "Extensional Viscosity of Amorphous Polypstyrene.", *J. Appl. Polym. Sci*., **20**, 1137, (1976)

114. Ide.Y., White.J.L., "The Spinnability of Polymer Fluid Filaments", *J. Appl. Polym. Sci*., **20**, 2511, (1976)

115. Ide.Y., White.J.L., "Experimental Study of Elongational Flow and Failure of Polymer Melts", *J. Appl. Polym. Sci*., **22**, 1061, (1978)

116. Munstedt.H., "New Universal Extensional Rheometer for Polymer Melts. Measurements on a Polystyrene Sample." *J. Rheol*., **23**, 412, (1979)

117. Connelly.R.W., Garfield.L.J., Pearson.G.H., "Notes: Local Stretch history of Fixed-End-Constant Length-Polymer-Melt Stretching Experiment." *J.Rheol.*, **23**, 651, (1979)

118. Ishizuka.O., Koyama.K., "Elongational Viscosity at a constant Elongational strain rate of Polypropylene Melt." *Polymer*, **21**, 164, (1980).

119. Aranguren MI, Mora EM, DeGroot JV, Macosko CW, Effect of reinforcing fillers on the rheology of polymer melts, *Journal of Rheology*, **36**, (1992), 1165-1182.

120. Lee.K., Han.C., Linear dynamic viscoelastic properties of functionalized block copolymer/organoclay nanocomposites, *Maromolecules*, **36**, (2003) , 804-815.

121. Fulchiron. R, Verney.V, Determination of the elongational behavior of polypropylene melts from transient shear experiments using Wagners model, *Jounral of Non- Newtonian Fluid Mechanics*, **48**, (1992), 49-61.

122. Lertwimolnum.W, Vergnes.B, Influence of compatibilizer and processing conditions on the dispersion of nanoclay in a polypropylene matrix, *Polymer*, **46**, (2008), 3462-3471.

123. Olson.G.L, Miller.D.S, Larsen.E.W, Morel.J.E, Chord length distributions in binary stochastic media in two and three dimensions, *Journal Of Quantitative Spectroscopy and Radiative Transfer*, **101**, (2006), 269-283.

124. Olson.G.L, Chord length distributions between hard disks and spheres in regular, semi-regular, and quasi-random structures, *Annals of Nuclear Energy*, **35**, (2008), 2150-2155.

125. Carreau.P.J, Ghanbari.A, Heuzey.M.C, Ton-That.M, Morphological and rheological properties of PET/clay nanocomposites, *Rheol Acta*, **52**, (2013), 59-74.

126. Sun.L, Boo.W., etal., Effect of Nanoplatelets on the Rheological Behavior of Epoxy Monomers, *Macromol Mater Eng.*, **294**, (2009), 103-113.

127. Wan.T, Wang.B., Liao.S, Clifford.M, Rheological investigation on the interaction of polyamide 6 with clay., *J Appl Polym Sci.*, **125**, (2012), E27-E33.